Estimating a Social Cost of Carbon for Global Energy Consumption*

Ashwin Rode[1], Tamma Carleton[2,3], Michael Delgado[4], Michael Greenstone[5,3], Trevor Houser[4], Solomon Hsiang[6,3], Andrew Hultgren[1,5], Amir Jina[7,3], Robert Kopp[8], Kelly E. McCusker[4], Ishan Nath[9], James Rising[10], and Jiacan Yuan [11]

[1]Energy Policy Institute, University of Chicago

[2]Bren School of Environmental Science and Management, University of California, Santa Barbara

[3]National Bureau of Economic Research

[4]Rhodium Group

[5]Department of Economics, University of Chicago

[6]Global Policy Laboratory, Goldman School of Public Policy, University of California, Berkeley

[7]Harris School of Public Policy, University of Chicago

[8]Department of Earth & Planetary Sciences and Rutgers Institute of Earth, Ocean, and Atmospheric Sciences, Rutgers University

[9]Department of Economics, Princeton University

[10]School of Marine Science and Policy, University of Delaware

[11]Department of Atmospheric and Oceanic Sciences, Institute of Atmospheric Sciences, IRDR ICoE-RIG-WECEIPHE, and Big Data Institute for Carbon Emission and Environmental Pollution, Fudan University

This is a post-print of an article published in Nature.
https://doi.org/10.1038/s41586-021-03883-8

*This version: Friday 4th February, 2022.

Abstract

Estimates of global economic damage caused by carbon dioxide (CO_2) emissions can inform climate policy.[1–3] The social cost of carbon (SCC) quantifies these damages by characterizing how additional CO_2 emissions today impact future economic outcomes through altering the climate.[4–6] Previous estimates suggest that large, warming-driven increases in energy expenditures could dominate the SCC,[7,8] but they rely on models[9–11] that are spatially coarse and not tightly linked to data.[2,3,6,7,12,13] Here we show that the release of 1t CO_2 today is projected to reduce total future energy expenditures, with most estimates valued between -$3 and -$1, depending on discount rates. Our results are based on a new architecture that integrates global data, econometrics, and climate science to estimate local damages worldwide. Notably, we project that emerging economies in the tropics will dramatically increase electricity consumption due to warming, requiring critical infrastructure planning. However, heating reductions in colder countries offset this increase globally. We estimate that 2099 global electricity consumption rises $\sim$ 4.5 EJ/yr (7% current global consumption) while direct consumption of other fuels declines $\sim$ 11.3 EJ/yr (7% current consumption) per +1°C increase in global mean temperature. Our finding of net savings contradicts previous research,[7,8] because global data indicate that many populations will remain too poor for most of the 21st century to substantially increase energy consumption in response to warming. Importantly, damage estimates would differ if poorer populations were given greater weight.[14]

Assessing damages from climate change

Quantifying the benefits of greenhouse gas mitigation is a topic of considerable importance to researchers and policy makers alike. The "social cost of carbon" (SCC)—defined as the dollar value of climate change damages imposed globally by an additional (i.e. "marginal") ton of CO_2 emissions (or its equivalent)—provides a means to determine the global social benefits of mitigation policies.[6] To date, our understanding of the SCC has been informed by theoretical-numerical integrated assessment models[9–11] (IAMs). These pioneering models have produced numerous valuable insights and guided research and policy for decades.[1,5] For instance, SCC estimates derived from these models have been used by the US federal government to assess over 80 policies to date, with a combined value of $1 trillion in estimated benefits.[15] Yet as research has progressed with advances in data and computing, new challenges and opportunities have emerged.[3,13]

Recent assessments[2,3,6,7] have raised the concerns that the category of current IAMs used to perform aggregate benefit-cost analyses related to climate change[16] are not tightly constrained by data. They also do not utilize best-available Earth System models, do not capture many known linkages between climate change and society, and only resolve damages at the geographic scale of large regions (e.g. continents). We address these concerns by designing a fully modular "bottom-up" architecture[17] to develop "partial" SCC estimates for individual sub-sectors of the global economy (e.g. agriculture, health, labor), using representative data and detailed climate models.[7,18–25] Each global partial SCC is built up from econometrically derived, probabilistic, local damage estimates for thousands of geographic regions. In ongoing work, we are integrating these partial SCC estimates[17] to compute a total SCC, taking into account inter-sector linkages . "Top down" econometric results describing Gross Domestic Product (GDP) impacts of warming[26,27] have been previously translated into SCC values;.[28,29] However, to our knowledge, no existing IAM transparently assembles a bottom-up and globally-representative SCC based on local econometric-based projections of damage.[6]

Climate-driven energy expenditures

Here we develop the first empirically-derived estimates of the net change in global energy expenditures associated with an additional ton of CO_2 emissions, i.e. a *partial SCC for energy expenditure*. IAM developers have themselves argued that uncertainty over this number is the most important uncertainty to resolve in the total SCC,[8] in part because some models predict that rising energy expenditures will be the single largest global cost from warming.[16] Prior econometric studies have measured the effect of local temperatures on local electricity consumption,[30–34] although they often omit non-electric energy consumption (e.g. natural gas used for heating) because the data are difficult to obtain. Moreover, these studies generally focus on residential end uses in regions that are wealthy

and thus not globally representative (e.g. California). In contrast, an appealing feature of non-econometric studies using process-based models is that they simulate how climate change will affect all aspects of the production, conversion, delivery, and use of energy.[35–38] However, similar to IAMs, their drawback is that they are not generally constrained by plausibly causal econometric estimates of consumption behavior in response to warming. This analysis is the first to recover globally representative measurements of total energy consumption in response to rising temperatures, accounting for economic development and adaptive behavior, and to use these results to compute a partial SCC for energy expenditure.

Because there remains debate on how best to aggregate costs across populations over time[39,40] (i.e. discounting), here we present results using multiple approaches and a range of parameter values.[6] When aggregating costs between different populations within a time period, we treat all individuals equally, consistent with guidance to US federal agencies,[6] although alternative approaches that upweight costs to poor populations have been proposed.[14]

Computing a social cost of carbon

Our modular approach to computing partial-SCC values has five steps, each of which can be implemented for each sector of the global economy. Here we apply these steps to compute the energy expenditure component of the SCC.

First, we match globally representative, longitudinal data on energy consumption with $0.25° \times 0.25°$ globally harmonized historical climate data.[41] This represents, to our knowledge, the most comprehensive global dataset compiled on energy consumption and temperature (*Methods Step 1*; *Supplementary Section* A). Energy consumption data are derived from International Energy Agency (IEA) data files[42] that describe electricity and direct fuel consumption across residential, commercial, industrial, and agricultural end-uses (excluding transportation) in 146 countries during 1971-2010. To make these data usable for global analysis, we harmonize data across diverse reporting systems and use econometric methods that minimize the influence of errors in record keeping (*Methods Step 1*; *Supplementary Section* A.1).

Second, we econometrically estimate the effect of historical temperature distributions on national annual per capita energy consumption using random year-to-year variation,[24] and measure how this *energy-temperature response* differs across energy types (*electricity* and *other fuels*), income levels, and climate zones.[17] This allows us to observe the effects of adaptive behaviors that populations undertake as they become richer[31] and/or are exposed to warmer climates[34] (e.g. AC adoption). Our approach accounts for all permanent differences between countries in energy consumption (e.g. due to geography or history) and all common trends in energy consumption (e.g. due to macroeconomic

fluctuations, price changes, or technological innovations) to identify a plausibly causal effect[30] of temperature distributions on energy consumption. We then use variation in income level and climate zone to predict how the temperature-energy relationship may change in association with these two factors. (*Methods Step 2*; *Supplementary Section* B).

Third, we project impacts of climate change in 24,378 globally comprehensive geographic regions (roughly the size of US counties, See Extended Data Figure 1) through 2099 (the final year high-resolution climate simulations are available) by combining the econometric results above with a probabilistic ensemble of downscaled climate projections (Extended Data Figure 2)[43] based on CMIP5 models.[19] When projecting these impacts, we account for how the energy-temperature response will evolve as populations become richer and exposed to warmer climates (*Methods Step 3*). Standard socioeconomic scenarios[22] forecast that over 90% of the end-of-century population will still remain within the range of historical temperatures and incomes that we currently observe around the world (See Extended Data Figure 3). In isolating the impact of future climate change on energy consumption, we hold constant the current energy supply mix, an assumption that should be relaxed in future work.

Fourth, we monetize and pool the empirically-derived damage estimates from the last step and fit *global energy expenditure damage functions* by aggregating impacts across locations and indexing them against the global mean surface temperature anomaly (ΔGMST) expressed in each climate model realization.[18] These functions describe the full distribution of global damage conditional on ΔGMST. We estimate damage functions up to 2100 that evolve over time to reflect expected changes in socioeconomics and adaptation, and extrapolate their continuing evolution forward to 2300 (*Methods Step 4*; *Supplementary Section* D).[17]

Fifth, we adapt a probabilistic, simple climate-carbon cycle model[25] to project the distribution of annual ΔGMST up to 2300 that results from the release of 1 additional GtC of CO_2 (*Methods Step 5*; *Supplementary Section* E). Applying the distribution of impulse-responses of ΔGMST to damage functions from the last step generates a probability distribution for the stream of total global damages that result from the emission of a marginal ton of CO_2 today. This probability distribution accounts for uncertainty in our econometric estimates at all stages of the analysis as well as climatological uncertainty. Finally, the value of the flow of damage is discounted[6] to capture the partial SCC for global energy expenditure.

Results

Energy consumption and temperature

The role of income

Empirically, we find that a population's average income per capita is a key determinant of how its end-use energy consumption responds to temperature. Electricity-temperature responses (Figure 1a) are "U"-shaped (i.e. increasing with hot and cold temperatures), but only in the seventh decile or higher of the global income distribution (annual per-capita income≥$11,258, 2019 USD PPP), while the other fuels-temperature response is "L-shaped" (i.e. increasing with cold temperatures) in the third decile or higher (annual per-capita income≥$2,849, 2019 USD PPP). Above these thresholds, rising incomes appear to amplify both responses, such that in the top decile, electricity consumption rises 0.017 GJ-per-capita (4.6 kWh-per-capita, 66% of 2010 global average per capita daily consumption) on a 35°C day (relative to a 20°C day) and 0.0068 GJ-per-capita (1.9 kWh-per-capita, 27% of 2010 global average per capita daily consumption) on a 0°C day, on average, while direct consumption of other fuels increases 0.034 GJ per-capita (50% of 2010 global average per capita daily consumption) on a 0°C day. These differing responses likely reflect the use of electricity for cooling and heating, compared to the use of other fuels (e.g. natural gas, oil, and coal) for heating. Prior research has documented similarly "U"-shaped electricity-temperature responses in the top decile[30,32–34] (See *Supplementary Section* H for comparisons), but our data reveal that such responses do not generalize to other income levels nor do they capture the substantial other fuels-temperature response, which dominates on cold days (Figure 1b). To our knowledge, these findings represent the first empirical demonstration of how economic development shapes energy-temperature responses on a global, macroeconomic scale. The differing income thresholds at which electricity and other fuels consumption starts to respond to temperature are consistent with microeconomic evidence that air-conditioning is widely adopted only at very high income levels,[31,44] while solid fuels are burned for heating even in lower income settings.[45,46]

Adaptation to local long-run climate

While income per capita is the dominant driver of the energy-temperature response, long-run climate also plays a smaller role in how populations adapt. For instance, higher AC adoption in hot locations may increase electricity use on hot days.[31,34] We empirically recover how income and long-run climate continuously and jointly shape the energy-temperature response (*Methods*, Equation 3; *Supplementary Section* B.3), thereby accounting simultaneously for effects of economic development and climate (Figure 1c). We find evidence that populations adapt to their long-run climate in ways that change their energy consumption during hot and cold periods, conditional on their income level.

For instance, on a 35°C day, per capita electricity consumption is 0.004 GJ (16% of 2010 global average per capita daily consumption) greater in the hottest climate tercile relative to the coldest. Conversely, on a 0°C day, per capita consumption of electricity and other fuels are respectively 0.0002 GJ (1% of 2010 global average per capita daily consumption) and 0.027 GJ (40% of 2010 global average per capita daily consumption) greater in the coldest tercile relative to the hottest. These results are consistent with populations adopting more heating or cooling technologies when their climate is cooler or hotter, respectively.

Impacts of future climate change

Accounting for local adaptation globally

Combining the measured relationships estimated using country-by-year energy consumption observations (Figure 1c) with projections for how incomes and climate will change over the next century in each of 24,378 globally comprehensive geographic units, we project how the structure of energy-temperature responses will evolve (See *Methods Step 3*, and *Supplementary Section* B.3). This spatial granularity contrasts with existing IAMs used to develop SCC estimates, which partitioned the world into at most 16 units[10] (Extended Data Figure 1). Prior analysis[18] demonstrated that accounting for this spatial granularity is crucial in order to capture the unequal impacts of climate change within countries. Applying the ensemble of downscaled climate models and surrogates (*Methods Step 1*; *Supplementary Section* A.2.2) to our evolving projections of local energy-temperature responses, we isolate the *additional* energy consumption in each region caused by changes in the temperature distribution, over and above any changes to consumption that would occur without climate change, such as those increases associated with economic development (*Methods*, Equation 4).

Impacts on energy consumption

In a high emissions scenario (RCP8.5), we project that by end-of-century, most of the world is expected to increase net annual per-capita electricity consumption and decrease consumption of other fuels due to climate change (Figure 2a). The amplitude of these effects reflects differences in incomes and climates across locations. Hot and wealthy locations exhibit large net increases in electricity consumption, although very cold locations exhibit net declines where warming does not increase the number of hot days enough to offset the loss of cold days. Low income regions, such as much of Sub-Saharan Africa, do not increase electricity consumption as dramatically because they are projected to still have relatively low incomes at end-of-century (e.g. see Ethiopia in Figure 1a). Declines in consumption of other fuels are projected throughout the world, consistent with the use of these fuels for heating across a wider range of incomes.

To understand the scale of these impacts, they can be compared to current levels of energy consumption (Figure 2b). In many of today's rich countries, impacts at end-of-century are projected to be modest relative to current consumption, e.g. a +2.7% relative increase in annual US electricity consumption. This small magnitude is both due to high current consumption levels in conjunction with the fact that many rich countries are in temperate climates, where large projected increases and decreases in electricity consumption – from more hot and fewer cold days, respectively – offset one another. In contrast, in many of the poorest and/or most populous countries, the additional consumption imposed by climate change is projected to be substantial relative to current consumption, e.g. a +2000% relative increase in annual Nigerian electricity consumption. This is due both to uniformly hot temperatures and very low levels of current energy use.

Aggregating energy impacts globally, we project that in a high emissions scenario, annual electricity consumption will increase due to climate change by 1.21 GJ per capita (90% C.I. = $[0.54, 2.43]$, $p<0.001$) in 2099 (RCP8.5), while consumption of other fuels will decline 2.94 GJ per capita ($[6.15, 1.02]$, $p<0.01$) (Figure 2c). Estimates in a moderate emissions scenario (RCP4.5) are 0.44 and 1.16 GJ per capita, respectively. (Electricity impacts do not include the primary energy lost in conversion to electricity.) It is notable that ignoring the effects of income growth and climate adaptation on the energy-temperature response would have resulted in dramatic underestimation of projected changes to global energy consumption due to warming (green lines, Figure 2c; *Supplementary Section* D).

Impacts on total energy expenditures

We monetize the climate-change induced changes in total energy consumption (electricity and other fuels combined) to develop a measure of the economic *damages* from climate change, i.e. all economic resources that would be available for other purposes in the absence of warming. In a baseline scenario of future real energy price growth of 1.4% per year (the historical growth rate of US energy prices), we project that end-of-century warming will cause net energy expenditure declines in much of the world, although there are net increases in many tropical and subtropical middle-income regions, such as portions of India, China, Indonesia and Mexico (Figure 3a). This pattern occurs because currently low income countries will likely be rich enough by end-of-century to consume other fuels on cold days but not rich enough to consume electricity on hot days, thus they experience savings from warming because it reduces other fuel costs (e.g. Ethiopia in Figure 1a). Hot middle income countries will be rich enough to spend on electricity for cooling in the future, so in some regions the additional spending on electricity during hot days outweighs the savings on cold days (e.g. India in Figure 1a). The largest overall savings are projected to occur among today's richest countries, however net savings are projected across most of the present-day income distribution (Extended Data Figure 4).

Aggregating costs globally, we project modest net savings at end-of-century due to cli-

mate change, amounting to 0.17 % ([−0.1%, 0.53%], p<0.3) and 0.08 % ([−0.03%, 0.21%], p<0.25) of 2099 world GDP in RCP 8.5 and RCP 4.5, respectively (Figure 3b). The magnitude of net global savings is similar across alternative pricing scenarios (Extended Data Figure 5; *Supplementary Section* C). This result differs qualitatively from the increased energy spending reported in prior studies[16,18,30,32–34] that focused on electricity consumption in wealthy regions. Because low and middle-income populations spend little on electricity to cool and other fuels are consumed everywhere almost exclusively for heating, projections that use only electricity-temperature responses from high-income populations will overestimate new cooling expenditures and underestimate savings from reduced heating, leading to systematic overestimation of the total energy damages from climate change.

Future damages from CO_2 emissions today

Damage functions describe the relationship between ΔGMST and global aggregate costs in a sector or the economy as a whole—they are at the heart of all IAMs used to develop SCC estimates,[4,9–11] informing mitigation policy implications by summarizing the costs of additional warming. We construct the first empirically-based global damage functions for energy consumption using the method in refs. [18] and [17], organizing global aggregate costs into functions of realized ΔGMST across 33,000 simulations (Figure 3c). These damage functions evolve over time, thereby capturing the influence of changing demographics, rising incomes, and warming local climates (See *Methods Step 4*). Damages are slightly quadratic in GMST anomaly, although essentially linear, with an additional +1° ΔGMST warming at end-of-century (relative to 2001-2010 average) increasing annual consumption of electricity 4.54 EJ ([4.50, 4.59], p<0.001) and decreasing consumption of other fuels 11.28 EJ ([11.12, 11.44], p<0.001), causing a net reduction in energy expenditures by $176 billion ([169, 183], p<0.001). Earlier and later damage functions are less and more steep, respectively, primarily due to trends in income and population (Figure 3d; *Methods Step 4*; *Supplementary Section* D).

Since CO_2 is long-lived in the atmosphere, the US National Academy of Sciences recommends computing SCC values that capture damages through to the year 2300.[6] To do this, we combine our empirically-derived damage functions with the Finite Amplitude Impulse Response (FAIR) climate model[25] to project through to 2300 the distribution of ΔGMST responses to the emission of a marginal 1 GtC of CO_2 (*Supplementary Section* E) (The high-resolution CMIP5 model runs used above to project spatially granular impacts end in 2100.) A CO_2 pulse emitted today perturbs the future trajectory of atmospheric CO_2 concentrations nonlinearly, affected by the half life of CO_2 in the atmosphere as it is stored and released in the oceans and biosphere (Figure 4a-b). This results in future ΔGMST that deviates from the baseline scenario, which in turn causes a stream of energy damages in future years (Figure 4c-d). The partial SCC from energy expenditure is the

net present value (NPV) of these annual damages. Because there are multiple views on how best to discount future damages into an NPV (see refs. [39,40]), we present multiple estimates using both constant discount rates and rates that evolve with economic growth[6] ("Ramsey" discounting,[47] see *Methods Step 5*).

We find that one ton of CO_2 emitted today generates a total energy expenditure burden valued at -$13.93 to -$0.69 in net present value under the high-emissions RCP8.5 scenario and -$4.16 to -$0.76 under a moderate-emissions RCP4.5 scenario (central estimates, 1.4% price growth scenario, Figure 4e, Subpanel I), with most estimates between -$3 and -$1.

Our finding that the partial SCC from energy expenditure is negative and small in magnitude is broadly robust across multiple pricing scenarios (Figure 4e, Subpanel II; Extended Data Tables 1 and 2).

Discussion

Our estimates are the first, to our knowledge, to make use of globally comprehensive data and empirical relationships to compute a global partial SCC for energy expenditure. This approach reveals the critical role of economic development in shaping how energy consumption patterns respond to climate change, as we find that much of the world will remain too poor in coming decades to spend substantially on energy-intensive cooling technologies. Our approach also demonstrates the importance of accounting for non-electricity energy consumption since global populations use other fuels to cope with cold temperatures even at low income levels. Together, these two factors explain why our analysis indicates that total global energy expenditures are not likely to increase dramatically in response to warming, and why marginal emissions today may in fact produce savings in global energy expenditures.

The modest magnitude of the aggregate global impacts, however, masks substantial important shifts in projected energy consumption. Most notably, projected impacts of warming in many of today's emerging economies may impose substantial costs and represent a large fraction of current consumption. For instance, we project that climate change will increase end-of-century electricity consumption in India by over 100% of its current consumption (Figure 2b). Future work should explore alternative approaches to valuing global damages across space and time when costs are distributed unequally, as we find.[14]

Our approach is designed to isolate the effect of future climate change on energy consumption under given emissions and socioeconomic pathways. However, a natural area for future exploration is to account for feedback effects that climate change and climate policy may introduce via changes in the energy supply mix, the trajectory of global CO_2 and local air pollutant emissions, and technological innovation.[48,49] While future work should explore the potential for these factors to alter the partial SCC for energy consumption, we believe at least the CO_2 emissions feedbacks are likely immaterial, given

the small size of our aggregate estimated impacts (Extended Data Table 3).

Another extension to this analysis would be to account for additional types of future technological advancements that may affect the energy consumption response to climate change (e.g. changes in the relative cost of cooling technologies). Because we allow energy-temperature responses to evolve with rising incomes and temperatures in our projection, our estimates reflect historical trends in advancement and diffusion of technology that occur with changes in these two factors. Theoretically, larger values of the partial SCC for energy consumption can arise if the price of cooling technology falls indefinitely relative to other goods and services without a corresponding trend in efficiency. However, these assumptions are unlikely to hold and we do not observe evidence of such a trend historically. The difficulty of predicting the direction and magnitude of unprecedented technological innovation under climate change underscores the critical need for further research in this area.

The results of our analysis contrast with estimates derived from alternative approaches. For example, the numerical-theoretical FUND IAM[10] — the only modeling framework where direct comparison is possible — estimates a partial SCC for energy expenditure[16] of \$10 per ton of CO_2, which constitutes 90% of that model's total SCC estimate (high emissions scenario, 3% discount rate) and is considered uncertain by its developers.[8] Our findings differ from this estimate, in part, because FUND projects very large increases in energy expenditures due to warming across many middle and low income regions, such as China, North Africa, Southeast Asia and Sub-Saharan Africa; in contrast we project small or negative changes in these regions (*Supplementary Section* I). This divergence can be explained by the data used to inform these projections. In FUND, these regional projections are driven by parameters (e.g. the income elasticity of cooling and heating energy demand) that are calibrated using data from a single high-income country (the United Kingdom),[10] which we found exhibits energy consumption behavior fundamentally different from these regions (Figure 1a). Our findings thus underscore the importance of employing a representative empirical approach when estimating global impacts of climate change.

We demonstrate the feasibility of combining global data, econometrics, detailed climate models, and modern computing to estimate a partial SCC for energy expenditure. Although implementing such an approach substantially reduces the energy expenditure partial SCC relative to prior estimates, this does not necessarily hold for all sectors of the economy. While focusing on data from only wealthy locations can lead to large estimates of certain climate change damages (e.g. energy expenditures), a similarly limited data focus has been shown to severely underestimate damages in other areas (e.g. human health[17]). A total SCC, composed of many partial SCCs for different sectors of the economy, would be required to determine the full social cost of warming to global society. Our approach can be extended to the full range of outcomes potentially affected

by climate (e.g. mortality,[17] agriculture, labor), thereby providing an empirically-based characterization of the total SCC.

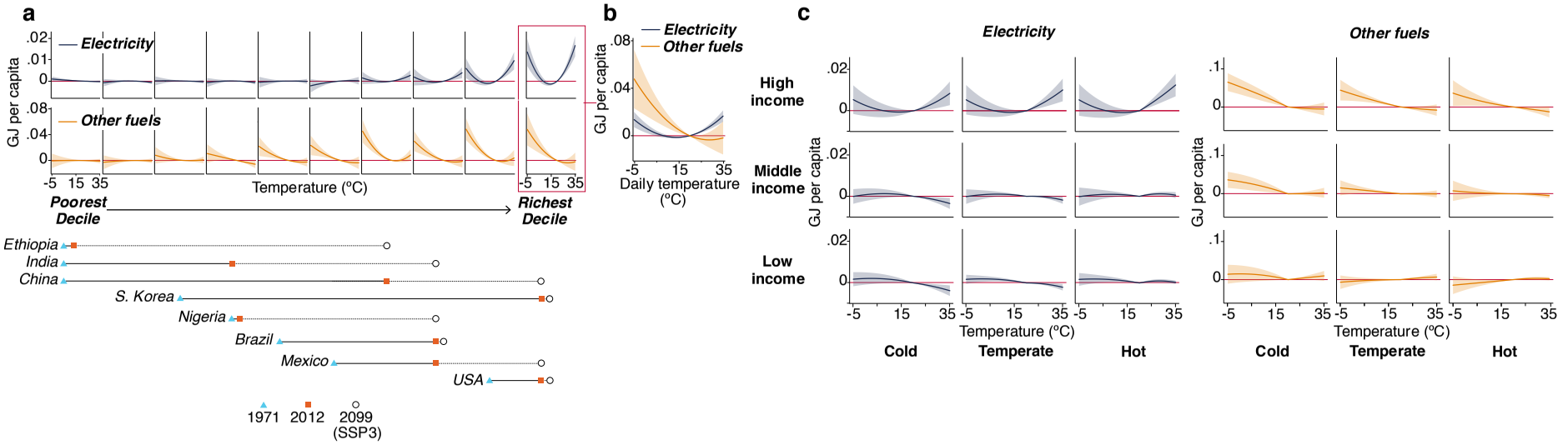

Figure 1: Estimated effect of temperature on energy consumption is mediated by income and climate. Additional daily electricity (blue) or other fuels (orange) consumption per-capita (GJ) in response to daily average temperature, relative to a reference temperature of 20°C. Solid lines depict point estimates, and shading is 95% confidence interval. **(a)** Seperate energy-temperature relationships for global deciles of income (sample is 146 countries over 1971-2010, see *Supplementary* Equation B.3), based on 15-year moving-average annual GDP per-capita. Income decile boundaries are held fixed through time, and incomes of selected country-years are indicated. Future income is drawn from the Shared Socioeconomic Pathway 3 (SSP3) scenario.[22] **(b)** Overlay of fuel-specific responses for the richest decile on a common scale. **(c)** Estimated energy-temperature relationship as simultaneously influenced by income and local long-run climate (see *Methods*, Equation 3). Each cell within a matrix illustrates a predicted energy-temperature relationship for a level of income and long-run climate. Rows separate income terciles (increasing income from bottom to top), columns separate climate terciles based on annual cooling degree-days (increasingly warm climate from left to right, see *Methods Step 2* and *Supplementary Section* B.3).

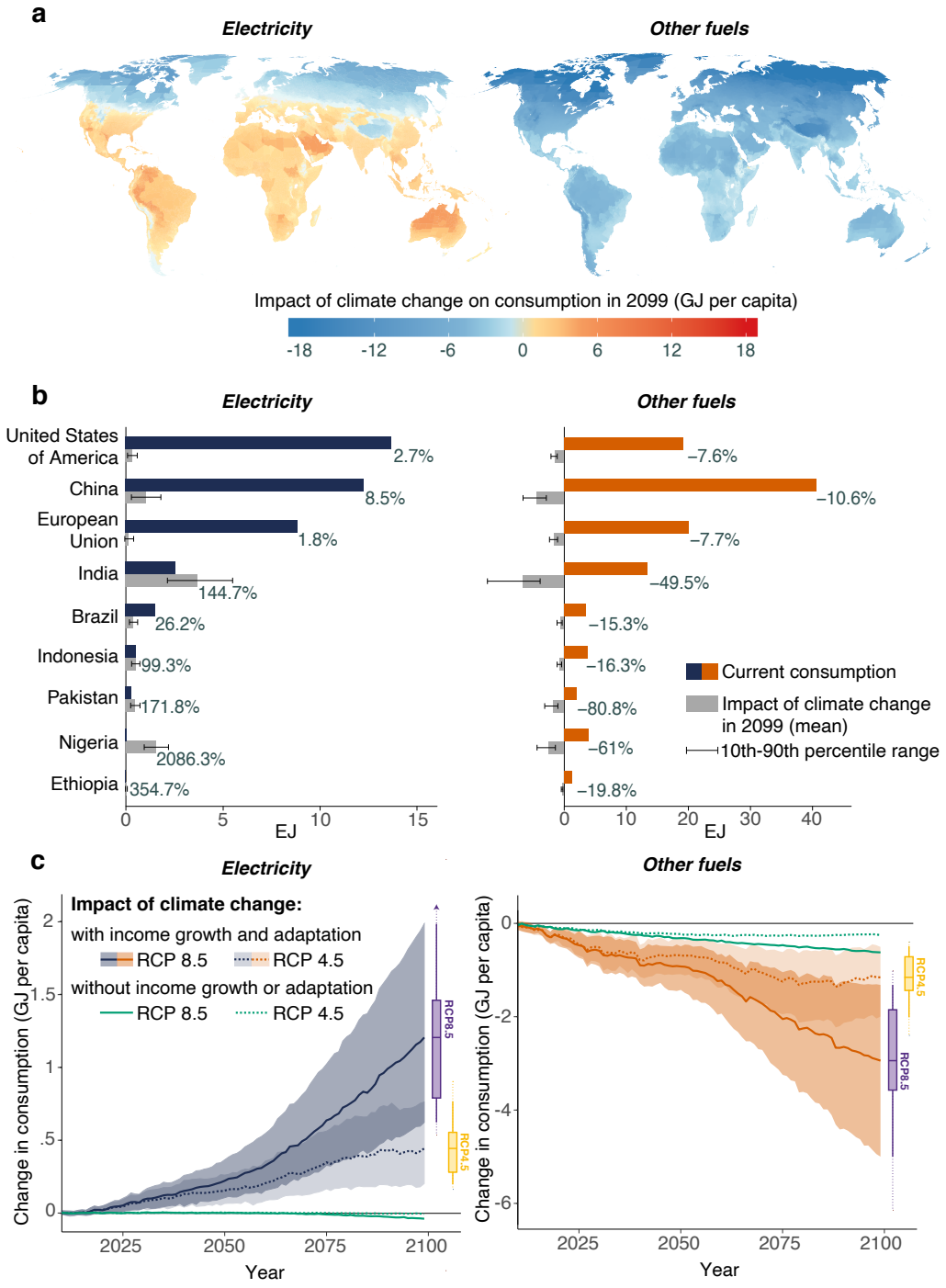

Figure 2: Projected impact of climate change on energy consumption in the twenty-first century. Projected impacts of climate change under high (RCP8.5) or moderate (RCP4.5) emissions scenarios (SSP3 socioeconomic scenario). **(a)** The spatial distribution of projected consumption impacts across 24,378 subnational geographic regions in 2099 (RCP8.5), accounting for the effect of income growth and adaptation on energy-temperature responses in each region. Map (produced with R software, ggplot2 package, using GADM basemap[50]) displays mean impacts across 33 climate models and model surrogates. **(b)** Aggregating to countries, grey bars show total impacts in 2099 (RCP8.5) alongside current consumption levels for selected countries (blue=electricity; orange=other fuels). Percentages are ratios of grey bars relative to colored bars. Intervals indicate 10^{th}-90^{th} percentiles of projected distributions, accounting for climate model and econometric uncertainty (*Supplementary Section* B.5). **(c)** Aggregating globally, time series of total global impacts. Shading indicates 10^{th}-90^{th} percentile range of projected distributions, accounting for climate model and econometric uncertainty. Boxplots show full distribution in 2099 (boxes=inter-quartile range; solid whiskers=10^{th}-90^{th} percentiles; dashed whiskers=5^{th}-95^{th} percentiles). Green lines illustrate projected impacts if present-day energy-temperature responses are held fixed and do not respond to rising incomes and changing temperatures.

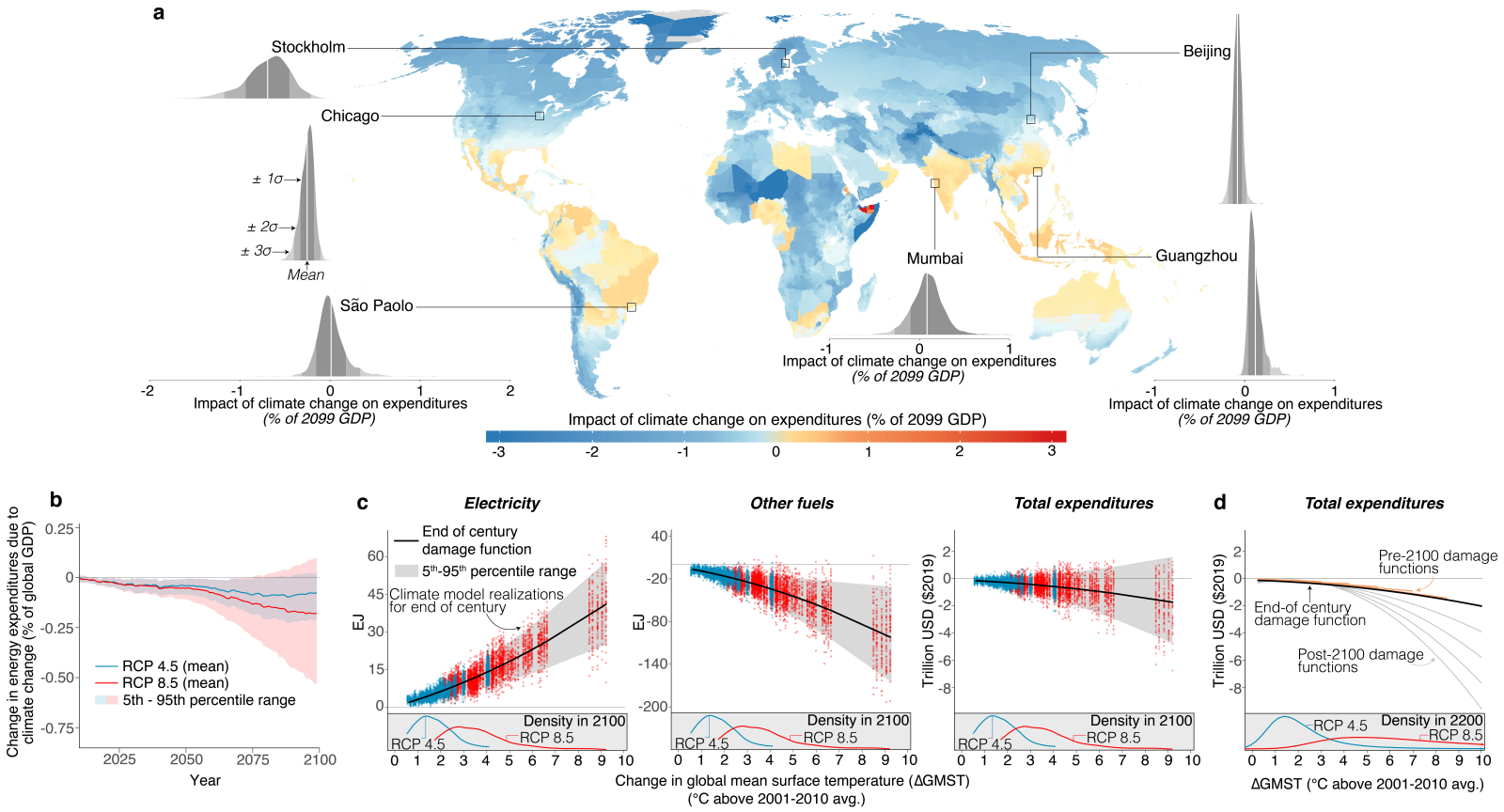

Figure 3: Economic costs from energy consumption impact of climate change. **(a)** Change in 2099 total annual energy expenditures (electricity + other fuels) due to warming in a high emissions scenario (RCP8.5), SSP3 socioeconomic scenario, 1.4% annual price growth scenario, expressed as a percent of 2099 local GDP for 24,378 geographic regions. Map (produced with R software, ggplot2 package, using GADM basemap[50]) depicts mean; probability density functions for selected cities plot distribution of projected impacts accounting for climate model and econometric uncertainty (*Supplementary Section* B.5). **(b)** Time series of globally aggregated change in total energy expenditures under both high (RCP8.5) and moderate (RCP4.5) emissions scenarios, expressed as a percent of global GDP in each year. **(c)** Global energy damage functions. Total global electricity consumption impacts, other fuels consumption impacts, and total energy expenditure impacts at end-of-century, indexed against ΔGMST realized in each climate model simulation (blue dots=RCP 4.5; red dots=RCP 8.5; see *Methods Step 4*). Probability density functions display the distribution of ΔGMST at end-of-century in each emissions scenario. **(d)** Damage functions evolve over time. Estimated using high resolution projections pre-2100 (e.g. orange curves, every 10 years) and extrapolated post-2100 (e.g. grey curves, every 50 years; *Supplementary Section* D).

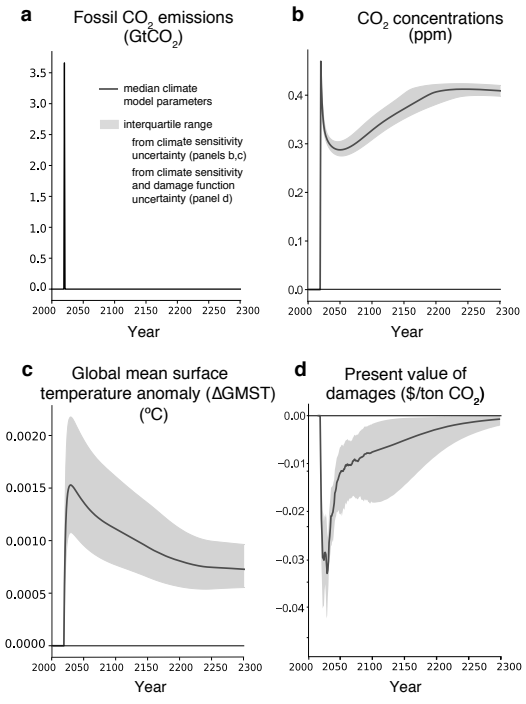

e

Discount rate	RCP 8.5	RCP 4.5	RCP 8.5	RCP 4.5
	I: 1.4% price growth		II: Min-max range across price scenarios	
Constant 2%	-2.27 (-9.42, 0.84)	-1.73 (-8.49, 0.50)	[-7.45,-0.99]	[-6.24,-0.88]
Constant 2.5%	-1.61 (-5.64, 0.24)	-1.43 (-5.31, 0.00)	[-4.53,-0.81]	[-4.58,-0.81]
Constant 3%	-1.25 (-3.70,-0.04)	-1.21 (-3.67,-0.17)	[-3.44,-0.70]	[-3.60,-0.73]
Constant 5%	-0.69 (-1.27,-0.22)	-0.76 (-1.50,-0.27)	[-1.80,-0.43]	[-1.96,-0.49]
Ramsey δ = 0%, η = 1	-13.93 (-81.41,13.56)	-4.16 (-71.19,14.08)	[-67.08,-3.44]	[-30.56,-0.40]
Ramsey δ = 0%, η = 2	-6.00 (-33.28,5.17)	-2.46 (-28.86,4.99)	[-26.86,-1.72]	[-14.11,-0.66]
Ramsey δ = 1%, η = 1	-3.35 (-16.46,2.13)	-1.97 (-14.37,1.77)	[-13.03,-1.20]	[-8.61,-0.82]
Ramsey δ = 1%, η = 2	-1.90 (-8.20,0.81)	-1.38 (-7.32,0.54)	[-6.48,-0.80]	[-5.13,-0.68]

Figure 4: Social cost of carbon for global energy consumption. (a)-(d) Effects of CO_2 pulse using FAIR simple climate model[25] (RCP8.5). Black line is default configuration. Shading is interquartile range sampling from constrained joint distribution of climate parameters (b-c), and also damage function quantiles (d) (*Supplementary Section* E.2, E.4). **(a)** 1GtC (3.67 $GtCO_2$) pulse released in 2020. **(b)** Response of atmospheric CO_2 concentrations, relative to baseline. **(c)** Impact on ΔGMST. **(d)** Change in discounted flow of energy expenditures (2%/yr discount rate) using damage functions in Figure 3d. Integral of this flow is the partial social cost of carbon (SCC) for energy consumption. **(e)** Estimates of partial SCC for energy consumption under high (RCP8.5) and moderate (RCP4.5) emissions scenarios. Rows apply different constant or Ramsey discount rates (δ=pure rate of time preference, η=elasticity of marginal utility of consumption; see *Methods Step 5*). Subpanel I assumes future energy prices reflect historical average US price growth (1.4%/yr). Parentheses contain 5^{th}-95^{th} percentile ranges, accounting for damage function and climate model uncertainty. Subpanel II shows range of central estimates across alternative energy price scenarios, including those from other models (Extended Data Tables 1-2). All estimates use socioeconomic scenario SSP3 (Supplementary Section F contains alternative scenarios).

Extended Data Figure 1: Map of the 24,378 "impact regions" for which location-specific projections are calculated. Map is produced with R software, ggplot2 package, using Global Administrative Region dataset (GADM) basemap.[50] A clustering algorithm[17] is used to form these impact regions from the full set of GADM administrative regions,[50] such that they are roughly similar in total population, and so that they are approximately internally homogenous with respect to mean temperature, diurnal temperature range, and mean precipitation.

a **Global mean surface temperature anomaly under RCP8.5: Distribution across future climate projections**

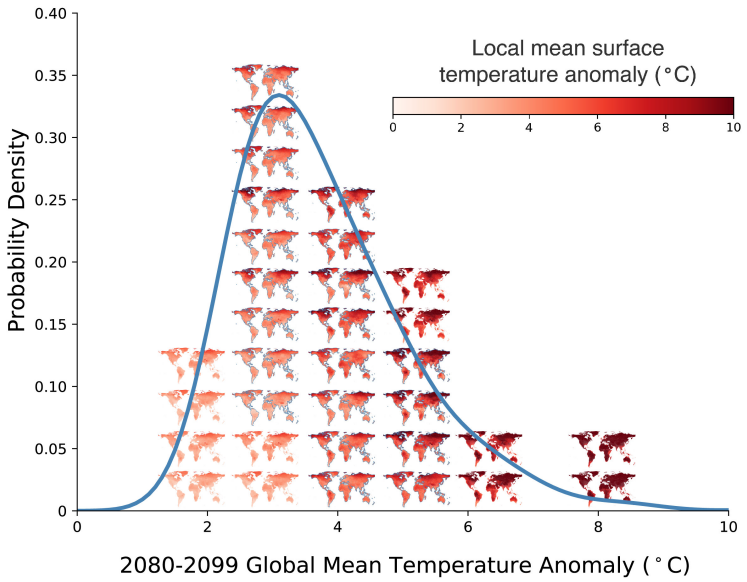

b **Model weights by emissions scenario**

Model or model surrogate name	Weight in RCP4.5	Weight in RCP8.5
ACCESS1-0	3.12%	3.00%
bcc-csm1-1	2.38%	2.29%
BNU-ESM	3.12%	3.00%
CanESM2	3.12%	3.00%
CCSM4	2.38%	2.29%
CESM1-BGC	2.38%	2.29%
CNRM-CM5	2.38%	2.29%
CSIRO-Mk3-6-0	3.12%	3.00%
GFDL-CM3	4.17%	4.00%
GFDL-ESM2G	4.17%	4.00%
GFDL-ESM2M	4.17%	4.00%
inmcm4	4.17%	4.00%
IPSL-CM5A-LR	3.12%	3.00%
IPSL-CM5A-MR	3.12%	3.00%
MIROC5	2.38%	2.29%
MIROC-ESM	4.17%	4.00%
MIROC-ESM-CHEM	4.17%	4.00%
MPI-ESM-LR	2.38%	2.29%
MPI-ESM-MR	2.38%	2.29%
MRI-CGCM3	9.37%	9.00%
NorESM1-M	9.37%	9.00%
surrogate_CanESM2_89	1.04%	1.00%
surrogate_CanESM2_94	4.17%	4.00%
surrogate_CanESM2_99	1.04%	1.00%
surrogate_GFDL-CM3_89	1.04%	1.00%
surrogate_GFDL-CM3_94	4.17%	4.00%
surrogate_GFDL-CM3_99	1.04%	1.00%
surrogate_GFDL-ESM2G_01	1.04%	1.00%
surrogate_GFDL-ESM2G_06	-	4.00%
surrogate_GFDL-ESM2G_11	1.04%	1.00%
surrogate_MRI-CGCM3_01	1.04%	1.00%
surrogate_MRI-CGCM3_06	4.17%	4.00%
surrogate_MRI-CGCM3_11	1.04%	1.00%

Extended Data Figure 2: Future climate projections used in generating probabilistic, empirically-based climate change impact projections. Panel **(a)** shows local climate distributions under the 21 climate models (outlined maps) and 12 model surrogates (dimmed maps) (*Methods Step 1*, Supplementary Section A.2.2, A.2.3) that are weighted in climate change impact projections so that the weighted distribution of the 2080 to 2099 global mean surface temperature anomaly (ΔGMST) exhibited by the 33 total models matches the probability distribution of estimated ΔGMST responses (blue-grey line) under a high (RCP8.5) emissions scenario. For this construction, the anomaly is relative to values in 1986-2005. Maps are produced with Python programming language, using data from ref. [43] and Global Administrative Region dataset (GADM) basemap.[50] Panel **(b)** lists all 33 models and model surrogates, and their corresponding model weights for both high (RCP8.5) and moderate (RCP4.5) emissions scenarios.[43] These are used to capture climate model uncertainty when generating climate change impact projections under a given emissions scenario (Supplementary Section B.5).

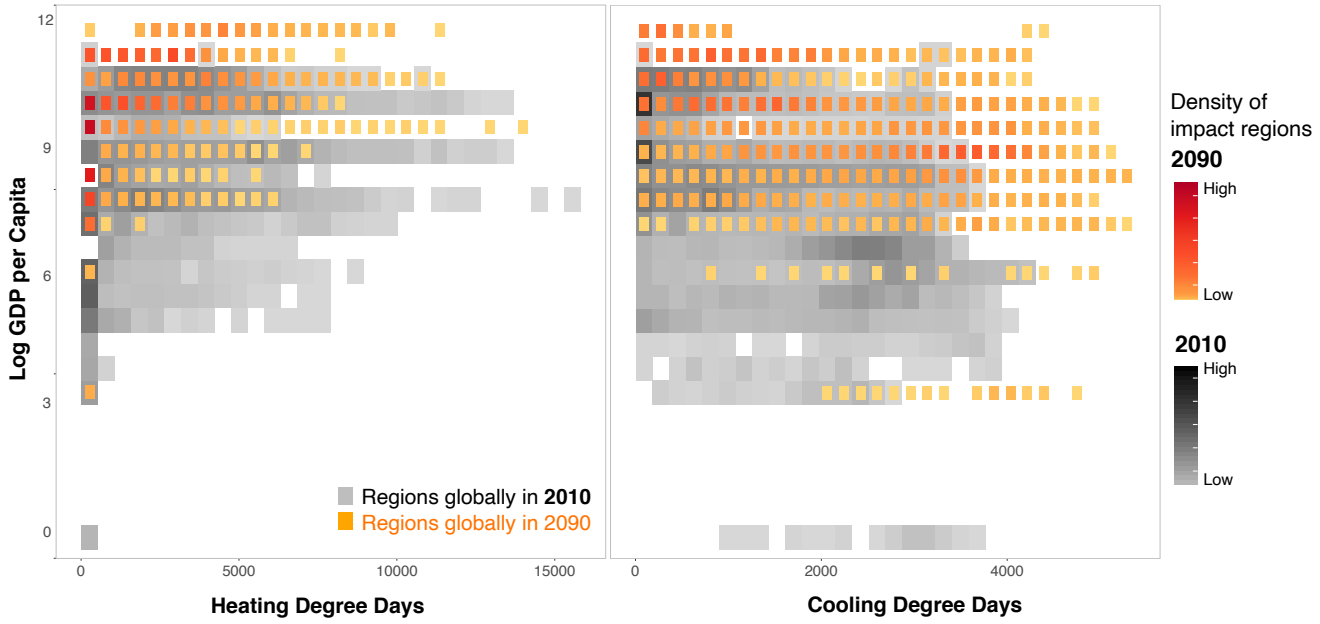

Extended Data Figure 3: Sample overlap between present and future. The density plots demonstrate the overlap in the joint income × long-run climate distributions at 2010 and 2090. Long-run climate is measured by heating degree days (**a**) and cooling degree days (**b**). Distributions are for 24,378 impact regions, in 2010 (grey-black) and 2090 under the RCP8.5 emissions scenario and SSP3 socioeconomic scenario (red-orange). All impact regions within a country are assigned the national per capita income. Although the future distribution is shifted towards higher incomes, greater cooling degree days, and fewer heating degree days, the substantial overlap in the two distributions allows for credible extrapolation of energy-temperature responses into the future (*Methods Step 3*).

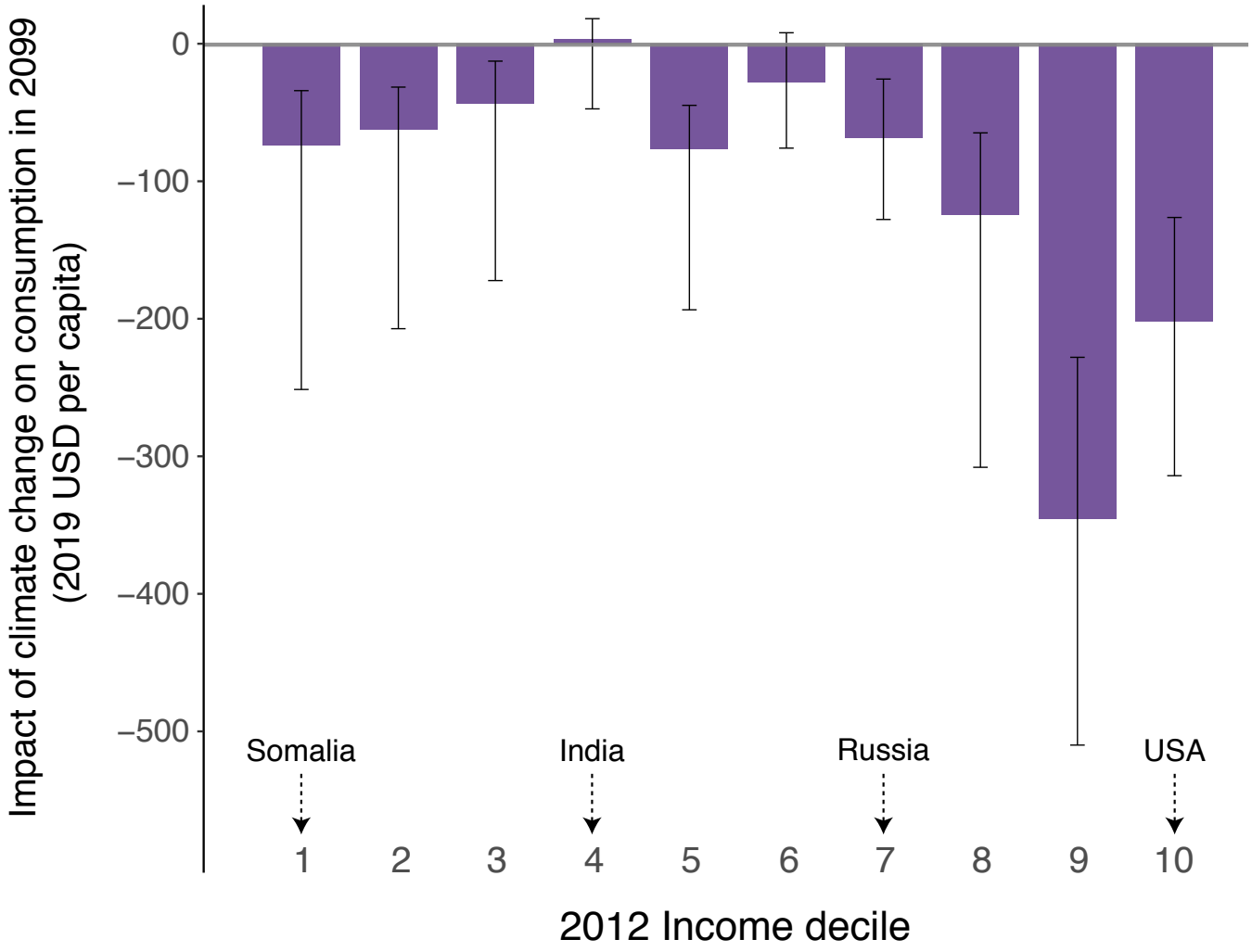

Extended Data Figure 4: Climate-change induced changes in total energy expenditures at end-of-century, by present-day income deciles. The bar chart above depicts annual climate-change induced changes in total energy expenditures at 2099 under a high emissions scenario (RCP8.5) and the SSP3 socioeconomic scenario, separately for each decile of 2012 national per capita income. Income deciles are calculated across all countries at 2012; representative countries in selected deciles are indicated. Expenditures are calculated under a 1.4% annual price growth scenario and are expressed in 2019 USD per capita based on each decile's projected 2099 population. Bars represent mean estimates across an ensemble of 33 climate models. Intervals indicate 5^{th}-95^{th} percentiles of projected distributions, accounting for climate model and econometric uncertainty (*Supplementary Section* B.5). The chart demonstrates that heterogeneity in expenditure changes at end-of-century (Figure 2A) is systematically correlated with present-day national income per capita. Over the upper half of the present-day income distribution, we find that countries with higher incomes today are generally projected to experience larger overall net savings at end-of-century. This partly reflects the fact that today's richest countries tend to be in temperate climates, where energy savings from fewer cold days will more than offset increases in costs from more hot days. The smallest savings at end-of-century are projected to occur in middle deciles of the present-day income distribution, which is consistent with many of these countries being situated in the tropics and also attaining sufficiently high income levels at end-of-century to increase electricity consumption due to more hot days. The positive correlation between present-day income and net savings at end-of-century does not hold in the lower ranges of today's income distribution. Net savings in today's poorest deciles (i.e. first and second) are actually higher than in the third and fourth deciles, as many of the poorest countries are projected to remain too poor at end-of-century to increase electricity consumption on hot days.

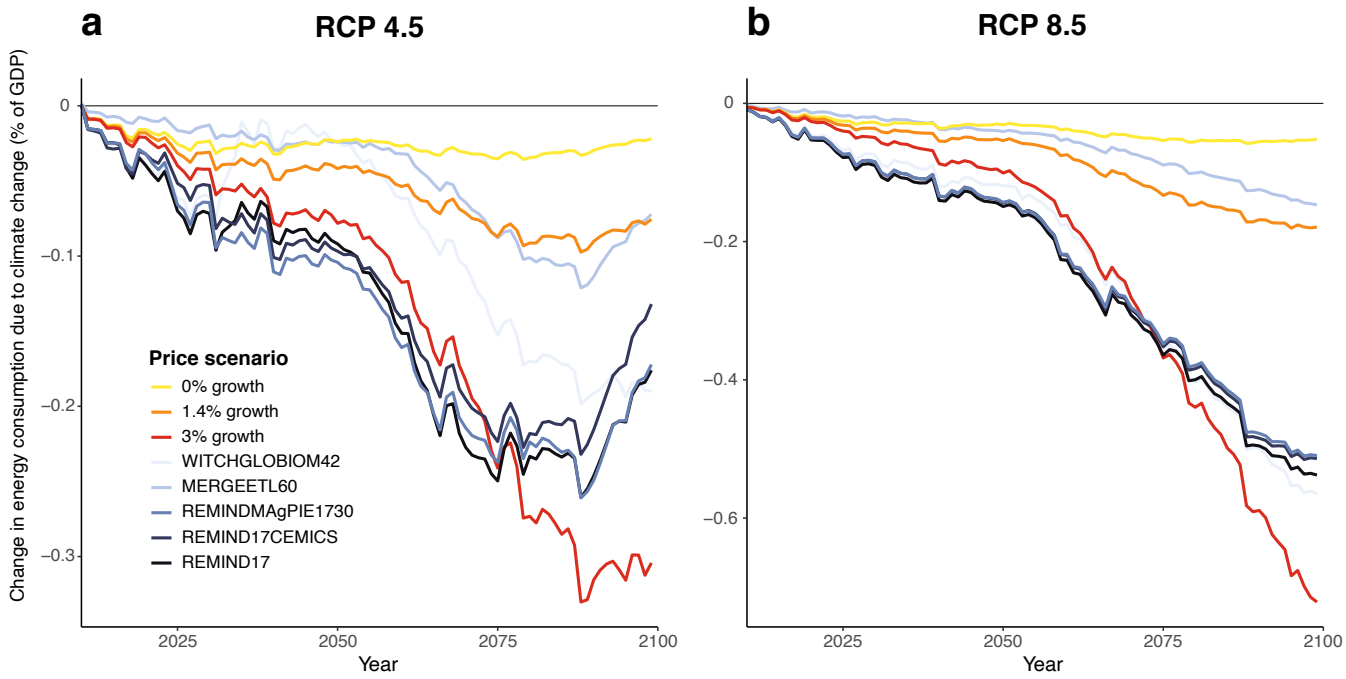

Extended Data Figure 5: The impacts of climate change on energy expenditures. Time series of changes in total global energy expenditures under the SSP3 socioeconomic scenario for moderate (RCP4.5; Panel **a**) and high (RCP8.5; Panel **b**) emissions scenarios, assuming various energy price trajectories. Three of these trajectories are based on direct extrapolation of present-day price statistics at either moderate (1.4%), stagnant (0%), or high (3%) annual growth rates (*Supplementary Section* C.1), while five are based on price projections from integrated assessment models (*Supplementary Section* C.2) named in the legend. Expenditure changes in a given year are expressed as a percent of global GDP in that year. Aggregate global expenditure changes are obtained by monetizing and summing over the spatially disaggregated impacts across both electricity and other fuels. Regardless of the emissions scenario or assumed price trajectory, end-of-century changes (i.e. net savings) represent a minute fraction of the US $353 trillion end-of-century global GDP projected under SSP3.

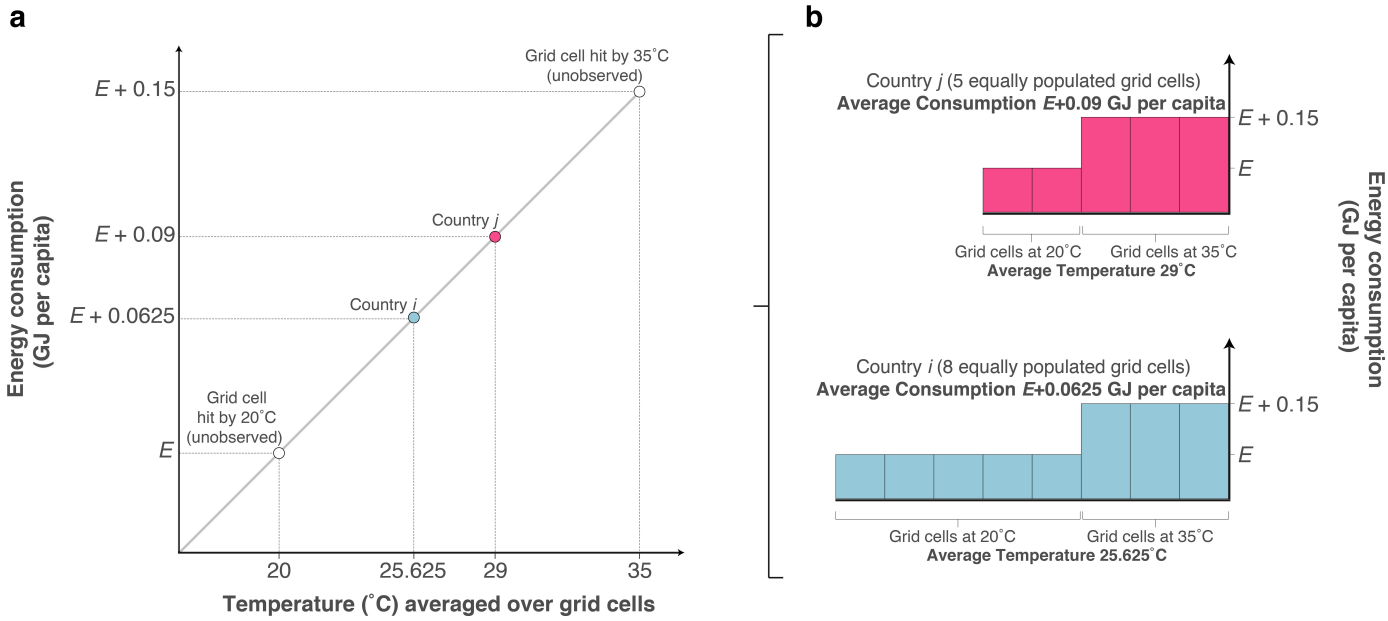

Extended Data Figure 6: Recovering local temperature-energy consumption relationships using aggregate energy consumption data. An illustration demonstrating how the effect of local temperature on local per capita energy consumption can be recovered from observations of local temperatures and national per capita energy consumption. **a:** Let a hypothetical, linear response of daily temperature and energy consumption exist at a local (i.e. grid cell) level, depicted by the diagonal grey line. Let E denote baseline daily energy consumption on a 20°C day. Average per capita energy consumption is observed on day d in countries i (blue circle) and j (pink circle), respectively consisting of 8 and 5 equally populated grid cells experiencing different temperatures. While the temperature is observed in each grid cell, only the national average per capita energy consumption is observed. **b:** Height of each bar represents unobserved energy consumption on day d within each grid cell. Pink bars are grid cells in country j and blue bars are grid cells in country i. Energy consumption within each grid cell responds to temperature within that grid cell. Averaging temperature and per capita energy consumption across grid cells within each country produces the country-level observations in Panel **a**. A regression using these observations recovers the grid cell-level response. Note that this illustration depicts a linear energy-temperature response for illustrative purposes, however a nonlinear temperature-energy consumption response can be recovered as well, if nonlinear transformations of temperature are computed at the grid-cell-level before being aggregated to the national level (See *Methods Step 2* and Equation 2).

Discount rate:	Constant 2%	Constant 2.5%	Constant 3%	Constant 5%
		1.4% price growth		
RCP 8.5	-2.27 (-9.42,0.84)	-1.61 (-5.64,0.24)	-1.25 (-3.70,-0.04)	-0.69 (-1.27,-0.22)
RCP 4.5	-1.73 (-8.49,0.50)	-1.43 (-5.31,0.00)	-1.21 (-3.67,-0.17)	-0.76 (-1.50,-0.27)
		0% price growth		
RCP 8.5	-0.99 (-2.97,-0.04)	-0.81 (-1.99,-0.13)	-0.70 (-1.46,-0.17)	-0.47 (-0.72,-0.17)
RCP 4.5	-0.88 (-2.87,-0.11)	-0.81 (-2.08,-0.19)	-0.73 (-1.63,-0.22)	-0.52 (-0.90,-0.20)
		3% price growth		
RCP 8.5	-7.45 (-38.77,5.26)	-4.53 (-21.35,2.39)	-3.06 (-12.76,1.04)	-1.20 (-3.04,-0.21)
RCP 4.5	-5.04 (-34.53,3.61)	-3.50 (-19.16,1.36)	-2.63 (-11.68,0.38)	-1.27 (-3.22,-0.33)
		MERGE-ETL 6.0 prices		
RCP 8.5	-1.77 (-5.85,-0.34)	-1.18 (-3.36,-0.27)	-0.87 (-2.13,-0.23)	-0.43 (-0.71,-0.14)
RCP 4.5	-1.83 (-6.18,-0.62)	-1.26 (-3.67,-0.43)	-0.95 (-2.43,-0.32)	-0.49 (-0.93,-0.17)
		REMIND 1.7 (ADVANCE) prices		
RCP 8.5	-6.40 (-22.19,-1.55)	-4.50 (-13.66,-1.29)	-3.44 (-9.20,-1.10)	-1.80 (-3.38,-0.69)
RCP 4.5	-6.24 (-22.18,-1.88)	-4.58 (-14.00,-1.50)	-3.60 (-9.74,-1.25)	-1.96 (-4.04,-0.75)
		REMIND 1.7 (CEMICS) prices		
RCP 8.5	-6.15 (-22.52,-1.45)	-4.32 (-13.73,-1.19)	-3.30 (-9.17,-1.01)	-1.70 (-3.30,-0.63)
RCP 4.5	-6.09 (-21.92,-1.50)	-4.44 (-13.78,-1.28)	-3.47 (-9.55,-1.10)	-1.86 (-3.93,-0.68)
		REMIND-MAgPIE 1.7-3.0 prices		
RCP 8.5	-6.04 (-20.53,-1.36)	-4.27 (-12.56,-1.18)	-3.27 (-8.38,-1.03)	-1.72 (-3.00,-0.66)
RCP 4.5	-5.95 (-20.81,-1.80)	-4.39 (-13.09,-1.46)	-3.47 (-9.08,-1.22)	-1.90 (-3.72,-0.73)
		WITCH-GLOBIOM 4.2 prices		
RCP 8.5	-6.30 (-23.55,-0.38)	-4.31 (-14.65,-0.49)	-3.22 (-9.88,-0.53)	-1.58 (-3.41,-0.41)
RCP 4.5	-5.58 (-22.81,-0.96)	-4.05 (-14.39,-0.78)	-3.14 (-9.95,-0.66)	-1.65 (-3.95,-0.41)

Extended Data Table 1: Social cost of energy consumption due to climate change under alternative future price scenarios. This table displays estimates of a partial Social Cost of Carbon for excess energy expenditure, under the socioeconomic scenario SSP3. Parentheses contain 5^{th}-95^{th} percentile ranges, accounting for damage function and climate model uncertainty (*Supplementary Section* E.4). Costs are valued under various projected energy price trajectories. Three of these trajectories are based on direct extrapolation of present-day price statistics at either moderate (1.4%), stagnant (0%), or high (3%) annual growth rates (*Supplementary Section* C.1), while five are based on price projections from integrated assessment models (*Supplementary Section* C.2) named in the table. Costs are discounted to the present using a constant annual discount rate (2%, 2.5%, 3%, or 5%). Estimates using Ramsey discounting are displayed in Extended Data Table 2.

Discount rate:	Ramsey $\delta = 0\%, \eta = 1$	Ramsey $\delta = 0\%, \eta = 2$	Ramsey $\delta = 0\%, \eta = 3$	Ramsey $\delta = 1\%, \eta = 1$	Ramsey $\delta = 1\%, \eta = 2$	Ramsey $\delta = 1\%, \eta = 3$
			1.4% price growth			
RCP 8.5	-13.93 (-81.41,13.56)	-6.00 (-33.28,5.17)	-2.93 (-14.87,2.02)	-3.35 (-16.46,2.13)	-1.90 (-8.20,0.81)	-1.20 (-4.45,0.25)
RCP 4.5	-4.16 (-71.19,14.08)	-2.46 (-28.86,4.99)	-1.60 (-12.93,1.76)	-1.97 (-14.37,1.77)	-1.38 (-7.32,0.54)	-1.01 (-4.11,0.09)
			0% price growth			
RCP 8.5	-3.44 (-20.04,2.55)	-1.72 (-8.59,0.87)	-1.00 (-4.10,0.25)	-1.20 (-4.64,0.24)	-0.80 (-2.52,0.00)	-0.58 (-1.51,-0.08)
RCP 4.5	-0.40 (-15.76,2.89)	-0.66 (-6.99,0.89)	-0.63 (-3.53,0.21)	-0.82 (-4.08,0.16)	-0.68 (-2.39,-0.06)	-0.56 (-1.54,-0.12)
			3% price growth			
RCP 8.5	-67.08 (-396.41,66.96)	-26.86 (-157.24,25.86)	-11.81 (-67.35,10.56)	-13.03 (-73.36,11.28)	-6.48 (-34.51,4.84)	-3.55 (-17.45,2.11)
RCP 4.5	-29.87 (-374.36,59.47)	-13.14 (-144.86,21.91)	-6.49 (-60.82,8.41)	-7.46 (-65.96,8.78)	-4.21 (-30.71,3.45)	-2.60 (-15.56,1.32)
			MERGE-ETL 6.0 prices			
RCP 8.5	-13.02 (-57.46,-1.38)	-5.41 (-22.82,-0.66)	-2.51 (-9.85,-0.36)	-2.82 (-10.77,-0.43)	-1.51 (-5.16,-0.27)	-0.89 (-2.70,-0.19)
RCP 4.5	-12.32 (-60.50,-3.71)	-5.21 (-23.75,-1.64)	-2.47 (-10.20,-0.81)	-2.81 (-11.17,-0.93)	-1.54 (-5.42,-0.52)	-0.94 (-2.90,-0.31)
			REMIND 1.7 (ADVANCE) prices			
RCP 8.5	-37.64 (-180.18,-3.60)	-16.55 (-74.59,-2.14)	-8.19 (-33.90,-1.41)	-9.40 (-37.72,-1.74)	-5.34 (-19.21,-1.23)	-3.34 (-10.66,-0.91)
RCP 4.5	-30.56 (-181.99,-5.18)	-14.11 (-74.14,-2.94)	-7.37 (-33.41,-1.82)	-8.61 (-37.22,-2.23)	-5.13 (-19.08,-1.50)	-3.34 (-10.79,-1.06)
			REMIND 1.7 (CEMICS) prices			
RCP 8.5	-35.77 (-187.73,-4.09)	-15.79 (-77.19,-2.22)	-7.84 (-34.85,-1.37)	-9.01 (-38.70,-1.68)	-5.13 (-19.55,-1.15)	-3.20 (-10.78,-0.83)
RCP 4.5	-30.33 (-181.98,-0.89)	-13.96 (-73.98,-1.31)	-7.25 (-33.23,-1.14)	-8.46 (-36.97,-1.50)	-5.01 (-18.89,-1.15)	-3.24 (-10.64,-0.87)
			REMIND-MAgPIE 1.7-3.0 prices			
RCP 8.5	-35.03 (-168.48,-1.83)	-15.46 (-69.72,-1.38)	-7.68 (-31.61,-1.07)	-8.83 (-35.13,-1.37)	-5.04 (-17.82,-1.06)	-3.16 (-9.85,-0.82)
RCP 4.5	-28.45 (-171.20,-4.30)	-13.22 (-69.76,-2.61)	-6.95 (-31.44,-1.68)	-8.14 (-34.99,-2.08)	-4.88 (-17.92,-1.43)	-3.19 (-10.12,-1.02)
			WITCH-GLOBIOM 4.2 prices			
RCP 8.5	-39.88 (-179.02,2.48)	-17.28 (-75.55,0.53)	-8.39 (-34.98,-0.07)	-9.56 (-39.20,-0.17)	-5.30 (-20.27,-0.29)	-3.24 (-11.36,-0.33)
RCP 4.5	-27.64 (-181.90,-2.71)	-12.82 (-74.87,-1.48)	-6.69 (-34.04,-0.94)	-7.79 (-38.04,-1.11)	-4.62 (-19.59,-0.79)	-2.98 (-11.07,-0.59)

Extended Data Table 2: Social cost of energy consumption due to climate change under alternative future price scenarios. This table displays estimates of a partial Social Cost of Carbon for excess energy expenditure, under the socioeconomic scenario SSP3. Parentheses contain 5^{th}-95^{th} percentile ranges, accounting for damage function and climate model uncertainty (*Supplementary Section* E.4). Costs are valued under various projected energy price trajectories. Three of these trajectories are based on direct extrapolation of present-day price statistics at either moderate (1.4%), stagnant (0%), or high (3%) annual growth rates (*Supplementary Section* C.1), while five are based on price projections from integrated assessment models (*Supplementary Section* C.2) named in the table. Costs are discounted to the present using Ramsey discount rates under various values of the pure rate of time preference, δ, and elasticity of marginal utility of consumption, η (*Methods Step 5*). Estimates using constant annual discount rates are displayed in Extended Data Table 1.

	Electricity	Other Fuels
Per capita impact (GJ)	1.2	-2.9
Total impact (billion GJ)	15.0	-36.6
Emissions factor (t CO_2e per GJ)	0.11	0.05
Additional emissions (Gt CO_2e)	1.6	-1.8

Extended Data Table 3: Feedback effects of climate change-induced energy consumption on CO_2 emissions. This table provides a calculation of additional CO_2 emissions in 2099 resulting from projected impacts of climate change on energy consumption under the RCP8.5 emissions scenario and SSP3 socioeconomic scenario. The calculation assumes that all climate change impacts to electricity consumption are powered by a combined cycle natural gas plant with 46 % efficiency (i.e. the average 2015 efficiency of US natural gas-fired combined-cycle technology),[51] and all climate change impacts to other fuels consumption are due to changes in natural gas consumption. Global average per capita impacts at 2099 to electricity and other fuels consumption (Row 1) are taken from projections displayed in Figure 2C (main text), and are converted to global total impacts (Row 2) by multiplying by the projected world population in 2099 under SSP3. Multiplying total electricity impacts by the emissions factor for natural gas[52] scaled by 46% efficiency, and multiplying total other fuels impacts by the emissions factor for natural gas (Row 3) yields additional emissions from projected climate change-induced electricity and other fuels consumption (Row 4). While assuming all impacts occur through natural gas likely leads to an upper bound in the magnitude of CO_2 emissions feedbacks, the magnitude is nonetheless small when compared to total 2099 global emissions of 100 Gt CO_2 under RCP 8.5.[53] While global CO_2 emissions feedbacks are likely negligible, it is possible that climate change-induced energy consumption will result in substantial changes to local air pollutant emissions in certain locations. The extent of these changes will depend heavily on the shape of the future global energy system, including for example, the location and emissions trajectory of individual electricity generation plants throughout the world and the populations who will be exposed to the air pollution from each. Future research should explore the local air pollution implications of climate change-induced energy consumption.

Methods

Here we provide an overview of the data and methods used to complete each of the five stages of analysis that compose our modular approach to constructing a partial SCC. Details on each stage can be found in the online Supplementary Information.

Step 1: Data assembly

We compile a comprehensive dataset on historical energy consumption, climate, and income, as well as future projections of climate, income, populations, and energy prices (*Supplementary Section* A). Historical data are used to econometrically estimate the energy-temperature response, and how it differs by energy type (electricity and other fuels), income, and climate. Future projection data are used to generate high-resolution projected impacts of climate change, accounting for the effects of income growth and warming on the shape of the energy-temperature response.

Historical datasets Annual data on final consumption of electricity and other fuels for 146 countries from 1971 to 2010 were obtained from the International Energy Agency's (IEA) *World Energy Balances* dataset.[42] We take electricity consumption directly from the dataset, while other fuels consumption is constructed by aggregating over coal, peat, oil shale and oil sands, oil products, natural gas, solar, wind, goethermal, biofuels and waste, heat, and heat production from non-specified combustible fuels. For both electricity and other fuels, we aggregate over the industrial, commercial/public services, residential, agricultural, forestry, fishing, and non-specified sectors. Data inconsistencies and quality issues in the IEA's records are extensively documented.[42] We classify every such change in record-keeping methodology and employ specific data preparation and econometric techniques to address each individually (*Supplementary Section* A.1).

Historical data on daily average temperature and precipitation, as well as historical climatologies, are obtained from the Global Meteorological Forcing Dataset, v1 (GMFD),[41] a global gridded ($0.25^\circ \times 0.25^\circ$) daily climate record available from 1948 to 2010.[20] We link high-resolution daily climate data to country-level annual energy consumption data using a procedure detailed in Supplementary Section A.2.4 that preserves nonlinearity in the energy consumption response to daily temperature.

We obtain historical values of country-level annual income per capita (constant dollar PPP) from within the International Energy Agency's *World Energy Balances* dataset, which in turn sources these data from the World Bank.

Datasets of future projections We use a set of 21 high-resolution ($0.25^\circ \times 0.25^\circ$) bias-corrected global climate projections that provide daily temperature and precipitation through the year 2099 from the NASA Earth Exchange (NEX) Global Daily Downscaled Projections (GDDP) dataset.[54] We obtain climate projections based on two standardized emissions scenarios: Representative Concentration Pathways 4.5 (RCP4.5, an emissions

stabilization scenario) and 8.5 (RCP8.5, a scenario with intensive growth in fossil fuel emissions).[55–57] Because this set of 21 climate models systematically underestimates tail risks of future climate change,[43,58] we assign probabilistic weights to climate projections and use 12 surrogate models that describe local climate outcomes in the tails of the climate sensitivity distribution.[43] The 21 models and 12 surrogate models are treated identically in our calculations and are referred to as the surrogate/model mixed ensemble (SMME). We utilize the probabilistic weights when calculating and reporting summary statistics of impact estimates across the 33 models and surrogates (Extended Data Figure 2, Supplementary Section B.5). Full details on the SMME climate projections are in Supplementary Section A.2.3. Gridded output from these projections is aggregated to 24,378 globally comprehensive agglomerated political units we call *impact regions* using the same method applied to historical climate data (*Supplementary Section* A.2.4). Impact regions are constructed to (i) respect national borders, (ii) be roughly equal in population across regions, and (iii) have approximately homogenous within-region climatic conditions (Extended Data Figure 1).

Projections of national populations and income per capita are derived from the Shared Socioeconomic Pathways (SSPs),[59] a set of scenarios of socioeconomic development over the 21^{st} century in the absence of climate impacts or policy. We utilize population[60] and country-level GDP[61,62] projections for scenarios SSP1, SSP2, SSP3, SSP4, and SSP5.[63] These projections have been used as inputs to IAM-based projections of other social and economic outcomes, such as land cover changes or air pollution, through the SSP research program,[59] although we do not utilize those outputs in our main calculations. However, we do examine the sensitivity of our results to assuming alternative energy price projections that are output from those IAM exercises. National population projections are respectively allocated to 24,378 impact regions based on current satellite-based within-country population distributions[64] (*Supplementary Section* A.3.3) or an alternative, time-varying scenario of within-country population distributions that reflects projected urbanization[65,66] (*Supplementary Section* G.1).

The price trajectories we use to monetize estimated impacts of climate change are constructed based on either of two distinct data sources— present-day statistics from the IEA are used for our main estimates, while price projections from integrated assessment models (IAMs) are used in sensitivity tests. We obtain present-day average electricity generation costs by region of the world from the IEA's *World Energy Outlook 2017* (Figure 6.25); prices for other fuels are obtained from the IEA's *Energy Prices and Taxes Statistics* dataset. Price projections of electricity and other fuels' prices from 5 IAMs were obtained from IIASA's Scenario Explorer database.[67] Price projections from IAMs are only used to examine the sensitivity of our results to alternative pricing assumptions, however it should be noted that they are derived using models that express market equilibria different from the projected changes in energy consumption that we estimate here. Details on how prices

are assigned across countries and over time can be found in Supplementary Section C.

Step 2: Econometric estimation of energy-temperature responses

Using historical data on national annual per capita energy consumption, climate, and income, we flexibly model electricity and other fuels consumption each as a function of daily average temperatures within a year, while accounting for heterogeneity in energy-temperature responses along the dimensions of both income and long-run climate. Importantly, our econometric procedure is designed to recover nonlinear changes in local per capita energy consumption at the grid-cell-by-day level, in response to locally experienced daily temperatures and these other factors. Accounting for such local nonlinearity is crucial in this context, since different locations within a country on the same day, or the same location on different days within a year, may exhibit very different temperatures, which generate divergent energy consumption responses.

We apply methods from prior research that has demonstrated the local effect of climate variables on many outcomes (including energy consumption) may be nonlinear in important ways.[68] These outcome variables are sometimes measured at the same temporal and spatial resolution as that at which these nonlinear effects manifest (e.g. refs. [69,70]). However, in most contexts, nonlinear effects emerge over timescales and spatial scales (e.g., for individual grid cells on single days) that are much finer than the scale at which outcome data are available[30,71,72] (e.g., for entire countries over a year). Yet, despite only observing spatially and temporally aggregated outcomes (i.e., *annual national per capita energy consumption*), it is possible to empirically recover the nonlinear relationships that take place at the spatial and temporal scale at which the climate variables are recorded (i.e., *the effect of daily grid-cell temperature on daily grid-cell per capita energy consumption*), provided that the climate variables are themselves aggregated in a way that preserves nonlinearities.[24,71]

Recovering such high resolution energy consumption-temperature responses is only possible because we observe the temperature on each day in each grid cell. Conceptually, these data enable us to search for the grid cell-level temperature-energy consumption relationship that, if applied to every grid cell for every daily temperature, would generate predicted per capita energy consumption at the country-by-year level that best matches observed consumption (see Extended Data Figure 6). This approach is established in the broader literature; for example ref. [71] estimate nonlinear local effects of daily temperature on crop yields using annual aggregate yields, and the approach is derived in the review by ref. [72]. Here we implement this approach through a country-year level regression of per capita energy consumption on specific population-weighted nonlinear climate variables (described below). A crucial step in implementation is properly constructing weighted aggregates of nonlinear transformations of local daily temperature (*Supplemen-*

tary Section A.2.4).

Specifically, let E_{zjdtc} denote consumption in GJ per capita in grid cell z of country j, on day d of year t, for fuel category c (electricity, other fuels), and let T_{zjdt} denote the temperature at grid cell z on day d. Let $\boldsymbol{T}_{zjdt}$ denote an M-element vector in which each element $(T_{zjdt1}, \ldots, T_{zjdtM})$ is a nonlinear transformation of grid-cell-level daily temperature (e.g., polynomial terms, $T_{zjdt1} = T^1_{zjdt}$, $T_{zjdt2} = T^2_{zjdt}$). We assume per capita fuel category c energy consumption at grid cell z on day d is a function of the grid cell's temperature on that day, where this function, $f_c(\boldsymbol{T}_{zjdt})$, is a linear combination of the nonlinear elements in $\boldsymbol{T}_{zjdt}$:

$$E_{zjdtc} = f_c(\boldsymbol{T}_{zjdt}) = \beta_{c1} T_{zjdt1} + \cdots + \beta_{cM} T_{zjdtM} = \sum_{m=1}^{M} \beta_{cm} T_{zjdtm}, \tag{1}$$

where $\beta_{c1}, \ldots, \beta_{cM}$ are assumed to be constant average coefficients.

Daily grid-cell-level per capita energy consumption (E_{zjdtc}) is unavailable to us, but we observe national annual per capita energy consumption (E_{jtc}), which is the population-weighted average of daily per capita consumption across grid cells in the country, summed over days in the year.[24] Let w_{zj} denote the share of a country j's population that falls into grid cell z. Country j's per capita annual consumption in the year t is thus the weighted average of daily per capita consumption across grid cells in j, aggregated over all 365 days in year t:

$$\begin{aligned} E_{jtc} = \sum_{d \in t} \sum_{z \in j} w_{zj} E_{zjdtc} &= \sum_{d \in t} \sum_{z \in j} w_{zj} \Big[\sum_{m=1}^{M} \beta_{cm} T_{zjdtm} \Big] \\ &= \underbrace{\sum_{m=1}^{M} \beta_{cm} \underbrace{\Big[\sum_{d \in t} \sum_{z \in j} w_{zj} T_{zjdtm} \Big]}_{\widetilde{T}_{jtm}}}_{f_c(\widetilde{\boldsymbol{T}}_{jt})}. \end{aligned} \tag{2}$$

The second line of Equation 2 is obtained by substitution from Equation 1 and interchanging the order of summation, expressing national annual per capita energy consumption as $f_c(\widetilde{\boldsymbol{T}}_{jt})$, where $\widetilde{\boldsymbol{T}}_{jt}$ is an M-element vector in which the m^{th} element, $\widetilde{T}_{jtm}$, is a country-by-year aggregation of the corresponding element from the grid-cell-level daily vector $\boldsymbol{T}_{zjdt}$ (*Supplementary Section* A.2.4). Removing the coefficients $\beta_{c1}, \ldots, \beta_{cM}$ from the summation over grid cells and days is possible given that these coefficients are assumed homogenous within a country and year. Thus, a regression of country-level annual per capita energy consumption (E_{jtc}) on variables that are country-year weighted aggregates of the nonlinear temperature terms $(\widetilde{T}_{jt1}, \ldots, \widetilde{T}_{jtM})$ recovers the same coeffi-

cients, $\beta_{c1}, \ldots, \beta_{cM}$, that describe the primitive grid cell-by-day relationship described by Equation 1. (See Extended Data Figure 6 for a simplified, graphical illustration of this concept.)

In practice, we allow energy-temperature responses to vary by income and long-run climate, estimating the function $f_c(\cdot)$ conditional on these covariates. If this conditional function is homogenous within a country and year, then we can recover a grid cell-by-day relationship, as demonstrated above. To model heterogeneity by income, we use the 15-year moving average of a country j's natural log of per-capita GDP in year t ($\overline{LogGDPPC}_{jt}$). To model heterogeneity by long-run climate we use average annual cooling degree days and heating degree days over the sample period ($\overline{CDD}_j$ and $\overline{HDD}_j$). Annual cooling (heating) degree days are a common measure of exposure to warm (cold) temperatures and are defined as the cumulative deviations of daily average temperatures from a benchmark of 20° C, over all days in the year where the average temperature exceeded (fell below) 20° C. Because these measures do not change substantially over the historical record, we do not rely on long-run temporal variation within the timespan of the sample and instead use the average over the sample period (*Supplementary Section* B.3).

Our estimating equation takes the following form:

$$E_{jtc} = f_c(\widetilde{\boldsymbol{T}}_{jt}|\overline{LogGDPPC}_{jt}, \overline{CDD}_j, \overline{HDD}_j) + g_c(\widetilde{\boldsymbol{P}}_{jt}) + \alpha_{jic} + \delta_{wtc} + \varepsilon_{jtc}. \qquad (3)$$

In our main specifications, $\widetilde{\boldsymbol{T}}_{jt}$ contains linear and quadratic terms for a spline in daily average temperatures (allowing a kink at 20°C), each averaged over grid cells and summed across the year, as shown in Equation 2. Exploiting flexible interactions between the three income and long-run climate covariates ($\overline{LogGDPPC}_{jt}$, $\overline{CDD}_j$, and $\overline{HDD}_j$) and all terms in the temperature vector ($\widetilde{\boldsymbol{T}}_{jt}$), we estimate an energy-temperature response f_c for fuel category c that is conditional on income and long-run climate. Details of this procedure can be found in Supplementary Section B.3. Importantly, the interactions involving the long-run climate covariates are country-by-year aggregations of grid-cell-level interactions, allowing us to recover heterogeneity in the energy-temperature response due to long-run climate at the grid-cell level. In contrast, because our income data are available only at the country-level, we recover heterogeneity in the energy-temperature response due to income only at the country level.

All our econometric specifications control for the effects of precipitation through the function $g_c(\cdot)$, constructed analogously to $f_c(\cdot)$; the vector $\widetilde{\boldsymbol{P}}_{jt}$ contains linear and quadratic terms of daily cumulative precipitation, each averaged over grid cells and summed annually. We also include a full set of country-by-reporting regime intercepts, referred to here as "fixed effects" (α_{jic}), where reporting regimes (i) are time spans within a country where observations for a given fuel category are documented by the IEA to

be comparable (*Supplementary Section* A.1). These fixed effects flexibly account for all permanent differences in energy consumption across country-regimes. In addition, we include world region-by-year fixed effects (δ_{wtc}) for each fuel category, where w indexes world regions based on UN classifications (Oceania, N. America, N. Europe, S. Europe, W. Europe, E. Europe, E. Asia, S.E. Asia, Central America/Caribbean, South America, sub-Saharan Africa, N. Africa/W. Asia, S. Asia). These fixed effects flexibly account for all world region-level trends and shocks in energy consumption. The use of fixed effects is more reliable than trying to individually control explicitly for determinants of energy consumption because it accounts for time-invariant and time-trending factors non-parametrically. We thus exploit random within-country, year-to-year variation in realized daily temperatures to identify a plausibly causal effect of historical temperature distributions on energy consumption, and we use variation in income and long-run climate to predict how the temperature-energy relationship may change in association with these two factors (*Supplementary Section* B.3). It should be noted that because our long-run climate measures ($\overline{CDD}_j$ and $\overline{HDD}_j$) do not vary over time within a country, their direct effect on energy consumption is absorbed in the fixed effects α_{jic}. However, our objects of interest in Equation 3 are the interactions of income and long-run climate with temperature, and not their direct effect on the level of energy consumption. Finally, ε_{jtc} denotes the stochastic error term.

Due to evidence of unit root behavior in the dependent variable, we estimate Equation 3 in first-differences (*Supplementary Section* A.1). Furthermore we employ inverse variance weighting to address differences in data quality across reporting regimes (*Supplementary Section* B.1). Standard errors are clustered by country-fuel category-reporting regime.

While Equation 3 is designed to causally identify the effect of daily temperatures on per capita energy consumption, it does not identify overall levels of per capita energy consumption as these are absorbed in the spatial and temporal fixed effects. We therefore express estimated electricity- or other fuels-temperature responses as predicted consumption relative to a "mild" day with an average temperature of 20°C. The matrices of electricity- and other fuels-temperature responses in Figure 1c summarize the results from estimating Equation 3, while Figures 1a and 1b display responses that are estimated for each decile of the in-sample income distribution, but do not differ by long-run climate (*Supplementary Section* B.2).

Step 3: Projecting the impacts of climate change

To estimate future per capita energy consumption impacts, we first use estimates from Equation 3 along with observable characteristics ($\overline{LogGDPPC}$, $\overline{CDD}$, and $\overline{HDD}$) to predict energy-temperature responses at different points in time for each of 24,378 impact

regions (Extended Data Figure 3). For each impact region r in country j at year t, we use the estimated function $\widehat{f}_c(\cdot)$ from Equation 3, along with 15-year moving averages of the covariates ($\overline{LogGDPPC}_{jt}$,$\overline{CDD}_{rjt}$,$\overline{HDD}_{rjt}$), to predict energy-temperature responses for each fuel category. Responses evolve over time as 15-year moving averages of the covariates change for a given impact region r in country j, thereby reflecting the effects of adaptive behaviors that populations undertake as they become richer and/or are exposed to warmer climates. Because Equation 3 estimates the interaction between temperature and country-level income as well as the interaction between temperature and grid-cell-level climate, our projections reflect changes in income and climate at these two corresponding spatial scales for internal consistency (*Supplementary Section* B.3).

We then apply a set of probabilistic climate change projections to the spatially and temporally heterogeneous energy-temperature responses to compute per capita consumption impacts for each fuel category c and impact region r in country j for each year from 2015 to 2099. The distribution of future daily average temperatures under a given emissions scenario (RCP8.5 or RCP4.5) is obtained from the 33 projections in the SMME (*Supplementary Section* A.2.3).

Let $\widetilde{\boldsymbol{T}}_{rjt}$ represent a vector containing impact region-by-year aggregations of nonlinear grid-cell-level transformations of daily temperature in a future year t, under a warmer climate. In contrast, let $\widetilde{\boldsymbol{T}}_{rjt_0}$ represent the counterfactual temperature vector for the same impact region under a climatology that is the same as that of a historical baseline period t_0 (*Supplementary Section* B.4). These vectors are constructed in exactly the same way as is done for the temperature vectors used in estimating Equation 3, except that we take a weighted aggregation only over grid cells z within the impact region rather than the entire country; e.g. element m of $\widetilde{\boldsymbol{T}}_{rjt}$ is $\widetilde{T}_{rjtm} = \sum_{d \in t} \sum_{z \in r} w_{zr} T_{zjdtm}$, where w_{zr} denotes the share of an impact region r's population that falls into grid cell z (*Supplementary Section* A.2.4). The impact of climate change on fuel category c is expressed as the estimated change in per capita consumption relative to a no-climate-change counterfactual in which the future climatology is the same as in t_0:

$$
\begin{aligned}
ImpactOfClimateChangePerCapita_{crjt} = \quad & \underbrace{\widehat{f}_c(\widetilde{\boldsymbol{T}}_{rjt} \mid \overline{LogGDPPC}_{jt}, \overline{CDD}_{rjt}, \overline{HDD}_{rjt})}_{\substack{\text{Temperature-induced per capita energy consumption under climate change} \\ \text{(with income growth and climate-driven adaptation) (A)}}} \\
- \quad & \underbrace{\widehat{f}_c(\widetilde{\boldsymbol{T}}_{rjt_0} \mid \overline{LogGDPPC}_{jt}, \overline{CDD}_{rjt_0}, \overline{HDD}_{rjt_0})}_{\substack{\text{Temperature-induced per capita energy consumption without climate change} \\ \text{(with income growth) (B)}}} \quad .
\end{aligned}
\tag{4}
$$

The object $ImpactOfClimateChangePerCapita_{crjt}$ represents the change in annual per-capita electricity or other fuels consumption due to a shift in the temperature distribution under climate change, accounting for the evolution of energy-temperature responses as

locations warm and incomes rise. It isolates the *additional* impact of climate change net of other factors (e.g. income) that will change in the future. The two projections A and B are identical in every way, except for the climate. Thus, we evaluate B using future levels of income but use $\widetilde{\boldsymbol{T}}$, $\overline{CDD}$, and $\overline{HDD}$ values from a historical baseline t_0 (*Supplementary Section* B.4). All fixed effects and other controls cancel out and are therefore omitted.

We construct estimates of Equation 4 for all impact regions up to 2099 under emissions scenarios RCP8.5 and RCP4.5, using each of the 33 climate projections in the SMME. Figure 2a maps mean impact estimates across these 33 climate projections at year 2099 under RCP8.5, while 2B and 2C display impacts aggregated to the country and global levels respectively. Confidence intervals around the means are constructed to reflect both climatological and econometric sources of uncertainty. The distribution of impacts across 33 climate projections captures uncertainties in the climate system through to 2099, and we additionally capture uncertainty arising from econometric estimation of Equation 3 using the delta method.[73] Supplementary Section B.5 details the method used to combine both these independent sources of uncertainty.

To highlight the critical importance of income growth and climate-driven adaptation in shaping future energy-temperature responses, we also consider a "no-adaptation" impact projection that ignores these factors (green lines in Figure 2c). To do this, we project

$$\begin{aligned} ImpactOfClimateChangePerCapita_{crjt}^{NoAdaptation} = & \underbrace{\widehat{f}_c(\widetilde{\boldsymbol{T}}_{rjt}|\overline{LogGDPPC}_{jt_0}, \overline{CDD}_{rjt_0}, \overline{HDD}_{rjt_0})}_{\substack{\text{Temperature-induced per capita energy consumption under climate change} \\ \text{(no adaptation)}}} \\ & - \underbrace{\widehat{f}_c(\widetilde{\boldsymbol{T}}_{rjt_0}|\overline{LogGDPPC}_{jt_0}, \overline{CDD}_{rjt_0}, \overline{HDD}_{rjt_0})}_{\substack{\text{Temperature-induced per capita energy consumption without climate change} \\ \text{(no adaptation)}}} , \end{aligned} \tag{5}$$

which captures the change in consumption responses due to future temperature, holding each impact region's income and climate fixed at historical baseline values for all years in the projection.

Step 4: Estimating global energy damage functions

Our fourth step is to pool empirical estimates of climate change impacts constructed using Equation 4 to fit global energy damage functions, which express global energy consumption costs of climate change as a function of the change in global mean surface temperature relative to the 2001-2010 average level (ΔGMST).[4] These damage functions summarize the economic costs of all impacts measured in the detailed empirical analysis, demonstrating how they vary with the change in global mean surface temperature.

Damage functions through 2099 are directly built from estimates of global costs (D_{tlps},

denominated in either EJ or dollars) in each year (t) using 33 climate models (l), two emissions scenarios (p), and a resampling of estimates (s) that captures uncertainty in the estimation of Equation 3. We interpret each of the resulting 33,000 simulation outputs D_{tlps} as a potential realization of damages that result from the spatial distribution of warming in model l, given the overall ΔGMST that is exhibited by that model under the emissions scenario p. Multiple simulations lead to an empirically-derived distribution of potential outcomes that are conditional on the ΔGMST value for the year, climate model, and emissions scenario used to generate that projection. To construct damage functions, we use these outcomes to estimate a conditional distribution of damages[17,18] using ordinary least squares, to obtain expected values, and quantile regressions, to capture uncertainty in damages conditional on ΔGMST.

In our projections of the future, the underlying population distribution and level of per capita income are evolving over time, thereby shaping the sensitivity of energy consumption to warming and through it, global damages. These changes over time require the construction of year-specific damage functions. Thus, we separately estimate a quadratic damage function in each year:

$$D(\Delta GMST, t)_{tlps} = \psi_0^t + \psi_1^t \Delta GMST_{tlp} + \psi_2^t \Delta GMST_{tlp}^2 + \varepsilon_{tlps}, \tag{6}$$

using all simulations within a 5-year window of t, thereby allowing the shape of the function $D(\Delta GMST, t)_{tlps}$ to evolve flexibly and smoothly over the century. Figure 3c displays examples of damage functions at end-of-century, with each point in the scatterplot representing an individual realization of D_{tlps}. The first and second panels demonstrate examples of separate damage functions for electricity and other fuels respectively, where the realizations are denominated in EJ. In these panels, a realization of D_{tlps} is a global aggregation of per-capita consumption impacts projected in every impact region at year t under climate model l, emissions scenario p, and simulation s, i.e. $D_{tlps} = \sum_j \sum_{r \in j} W_{rjt} * ImpactOfClimateChangePerCapita_{crjt,lps}$, for fuel category c (electricity or other fuels), where W_{rjt} denotes the population of impact region r in country j at year t (*Supplementary Section* A.3.3). The third panel displays a damage function for total energy expenditure, denominated in dollars. To monetize the projected impacts of climate change on energy consumption, we apply country-specific real prices for electricity and other fuels to the projected quantity impacts, thus reflecting differential costs across geographies and fuels. Hence, a realization of D_{tlps} in the third panel is $\sum_j \sum_{r \in j} \sum_c W_{rjt} * \rho_{cjt} * ImpactOfClimateChangePerCapita_{crjt,lps}$, where ρ_{cjt} denotes a country-year specific price for fuel category c. Price trajectories up to 2099 are constructed in either of two ways: i) by extrapolating present-day prices under various price growth scenario assumptions or ii) by utilizing price projections developed in existing IAMs (*Supplementary Section* C).

In addition to estimating expected damages, we estimate 19 quantile regressions (for every fifth quantile from the 5^{th} to 95^{th} quantiles) to capture the full distribution of damages conditional on ΔGMST (*Supplementary Section* E.4). Quantile regressions also use a quadratic functional form (Equation 6), but with different coefficients and residuals. The resulting conditional distribution reflects econometric uncertainty in the impact estimates from which damages are constructed, as well as differences in the spatial patterns of warming exhibited across different climate models within the SMME. 5^{th}-95^{th} quantile ranges from this conditional distribution are indicated by shaded areas in Figure 3c.

As described in the next step, we use the estimated dollar-denominated damage functions to compute the net change in global energy expenditures associated with an additional ton of CO_2. Because CO_2 is long-lived in the atmosphere, the US National Academy of Sciences recommends computing SCC values that capture damages through to the year 2300.[6] Because CMIP5 models are not run beyond 2099, the SMME sample ends in 2099. Therefore, it is necessary to develop a separate approach to extend these damage functions beyond 2099. Details of this approach can be found in Supplementary Section D.

Figure 3d depicts damage functions for every 10 years up to end-of-century (orange and black curves, estimated using Equation 6), as well as extended damage functions for every 50 years post-2100 (grey curves).

Step 5: Calculating the partial social cost of carbon

In the final step, we combine a probabilistic, simple climate-carbon cycle model with the set of damage functions described above to compute the partial SCC. The partial SCC at time t_0 is defined as the marginal social cost from elevated energy expenditures imposed by the emission of a marginal ton of CO_2 at t_0 holding all other factors fixed (including the forecast trajectory of baseline greenhouse gas emissions). This is expressed as:

$$Partial\ SCC_{t_0} = \sum_{t=t_0}^{2300} DF_t \frac{d\hat{D}(\Delta GMST, t)}{d\Delta GMST_t} \frac{d\widehat{\Delta GMST}_t}{dCO2_{t_0}}, \tag{7}$$

where $\frac{d\widehat{\Delta GMST}_t}{dCO2_{t_0}}$ is the estimated increase in ΔGMST that occurs at each moment in time along the baseline climate trajectory (e.g. RCP8.5) as a result of a marginal unit of emissions at time t_0, which we approximate with an infinitesimally small pulse of CO2 emissions occurring at time t_0. The values $\frac{d\hat{D}(\Delta GMST,t)}{d\Delta GMST_t}$ are the marginal damages at each moment in time that occur as a result of this small change in future global temperatures; they are computed using the damage functions described in Equation 6. The discount factor, DF_t, converts damages in future year t into a net present value.

To calculate the change in ΔGMST_t due to a marginal pulse of CO_2 in 2020, we

adapt a version of the Finite Amplitude Impulse Response (FAIR) simple climate model that has been developed especially for this type of calculation (*Supplementary Section* E).[25,74] Specifically, we use FAIR to calculate ΔGMST_t trajectories for emissions scenarios RCP4.5 and RCP8.5, both with and without an exogenous impulse of 1 Gt C (equivalent to 3.67 Gt CO2) in the year 2020, an approximation of an infinitesimal emission for which the model numerics are stable. In FAIR, this emissions impulse perturbs the trajectory of atmospheric CO_2 concentrations and ΔGMST_t for 2020-2300, with dynamics that are influenced by the baseline RCP scenario. In each scenario, the trajectory of damages in the "RCP + pulse" simulation is differenced from the baseline RCP simulation to compute $\frac{d\hat{D}(\Delta GMST,t)}{d\Delta GMST_t}\frac{d\widehat{\Delta GMST_t}}{dCO2_{t_0}}$, and the resulting damages are converted into USD per 1t CO_2 and discounted to the present.

Because there are multiple views on how best to discount future damages (see refs. [6,39,40] for reviews and discussions of various options and their implications), we present multiple estimates using both constant discount rates and "Ramsey" discounting.[6] In the case of a constant discount rate r, $DF_t = e^{-r(t-t_0)}$. We use the range of values $r \in \{0.02, 0.025, 0.03, 0.05\}$ to explore the influence of the discount rate. The value $r = 0.02$ is consistent with US Treasury rates over the last two decades,[75,76] while the remaining values are recommended by ref. [1].

In the case of Ramsey discounting, $DF_t = e^{-\sum_{s=t_0}^{t} r_s \mathbf{I}_{s>t_0}}$, where r_s denotes the time-varying discount rate for year s, and $\mathbf{I}_{s>t_0}$ is an indicator variable taking a value of one if year $s > t_0$. Time-varying discount rates are calculated according to the Ramsey equation $r_s = \delta + \eta g_s$, where the parameter δ measures the pure rate of time preference, g_s measures the growth rate of consumption in year s, and η is the elasticity of marginal utility of consumption.[47] We use global per capita income growth from the SSP scenarios to obtain annual values for g_s, and explore a range of parameter values for δ and η based on prior literature[29,39,47,77–83] and guidance from the US National Academy of Sciences.[6] We present estimates using 6 combinations of δ and η values, choosing from $\delta \in \{0\%, 1\%\}$ and $\eta \in \{1, 2, 3\}$. Details of how these combinations were selected can be found in Supplementary Section E.3.

To capture uncertainty in the climate physic represented in FAIR, we generate a distribution of future temperature trajectories by resampling the equilibrium climate sensitivity, the transient climate response, the short thermal adjustment time, and the time scale of rapid carbon uptake by the ocean mixed layer from a joint distribution that we constrain using findings from the literature (*Supplementary Section* E.2). The solid lines in Figures 4a-d indicate trajectories arising from the median values in FAIR's configuration parameters and the shaded areas in Figures 4b-c indicate interquartile ranges calculated through this resampling. The final range of uncertainty in projected damages (shaded area in Figure 4d) combines this uncertainty in climate sensitivity with uncertainty in damages, conditional on the climate sensitivity, by also resampling from quantiles of the damage

function.

Figure 4e and Extended Data Tables 1 and 2 present partial SCC estimates under RCP8.5 and RCP4.5, assuming various discount rates and future energy price scenarios. 5^{th}-95^{th} percentile ranges (in parentheses) account for econometric and climatological uncertainty (*Supplementary Section* E.4). Additional partial SCC estimates demonstrating sensitivity to alternative approaches for estimating post-2100 damages, and alternative socioeconomic scenarios can be found in Supplementary Section F.

Data availability

The authors declare that data for replicating the findings of this study are available at Zenodo: https://doi.org/10.5281/zenodo.5099834.

Code availability

The authors declare that code for replicating the findings of this study are available at GitHub: https://github.com/ClimateImpactLab/energy-code-release-2020/.

Acknowledgments

This project is an output of the Climate Impact Lab consortium that gratefully acknowledges funding from the Carnegie Corporation, Energy Policy Institute of Chicago (EPIC), International Growth Centre, National Science Foundation (#SES1463644), Sloan Foundation, and Tata Center for Development. Tamma Carleton acknowledges funding from the US Environmental Protection Agency Science To Achieve Results Fellowship (#FP91780401). James Rising acknowledges funding from the H2020-MSCA-RISE project GEMCLIME-2020 GA No. 681228.

We thank Laura Alcocer, Thomas Bearpark, Trinetta Chong, Zaya Delgerjargal, Greg Dobbels, Diana Gergel, Radhika Goyal, Simon Greenhill, Iván Higuera-Mendieta, Dylan Hogan, Azhar Hussain, Theodor Kulczycki, Ruixue Li, Brewster Malevich, Maya Norman, Odiche Nwabuikwu, Sébastien Phan, Christina Schwarz, Nishka Sharma, Justin Simcock, Yuqi Song, Emile Tenezakis, Jingyuan Wang, and Jong-kai Yang for research assistance during all stages of this project, and we thank Samantha Anderson, Jack Chang, Megan Landín, and Terin Mayer for project management.

We acknowledge the World Climate Research Programmes Working Group on Coupled Modeling, which is responsible for CMIP, and we thank the climate modeling groups (listed in Extended Data Figure 2b) for producing and making available their model output. For CMIP, the U.S. Department of Energy's Program for Climate Model Diagnosis and Intercomparison provides coordinating support and led development of software

infrastructure in partnership with the Global Organization for Earth System Science Portals.

We thank seminar participants at the UC Berkeley Energy Camp, University of Chicago EPIC Lunch Series and Mansueto Institute Lunch Colloquium, LSE Workshop in Environmental Economics, International Energy Workshop, International Workshop on Empirical Methods in Energy Economics, University of Michigan Sustainability and Development Conference, Berkeley/Harvard/Yale Environmental & Energy Economics Seminar, NBER EEE Summer Institute, UCLA Luskin Center for Innovation Climate Adaptation Research Symposium, and Federal Reserve Bank of Richmond Climate Change Economics Workshop for helpful comments.

Author contributions

AR, SH, MG, RK, TH, AJ, JR, MD, TC conceived and planned the study. JY, KM, MD, RK, AR, AJ, TC prepared historical climate data. JY, KM, MD, RK created and prepared climate projection data. AR, TC, AH, MD, IN, TH prepared energy data. AR, TC, AH, IN, AJ, JR, SH, MG estimated energy-climate response functions. JR and AR computed projected impacts of future climate change. AR, MD, TC, KM, AH, IN, AJ, JR, SH, MG constructed damage functions and computed partial social cost of carbon. AR, SH, MG wrote the main text, AR, TC, AJ, MD, JR, JY, KM wrote the supplementary materials, and all authors edited.

Competing interest declaration

A. Rode, T. Carleton., A. Hultgren, A. Jina, R. Kopp, I. Nath, J. Rising, J. Yuan declare no conflicts of interest. M. Delgado, T. Houser, K. McCusker: Rhodium Group provides independent research and analysis on a range of global economic topics to clients in the public and private sectors. This includes analysis of global energy market trends. While some of those clients could potentially be impacted by the results of this research, both positively and negatively, Rhodium staff contributions to this research were conducted completely independently. M. Greenstone, S Hsiang, R. Kopp: We received no financial or in-kind support for the research conducted in this paper, nor have we received funding or in-kind support from any "interested" parties. As part of a diversified portfolio, we each hold more than $10,000 in stocks and bonds of various companies including those within the energy sector. No other parties have the right to review the paper prior to its circulation. M. Greenstone holds the position of Director at the Energy Policy Institute at the University of Chicago and the Environment and Energy Lab at University of Chicago Labs, and is Faculty Director at the E2e Lab. From July 2015 January 2017, Greenstone was a member of the U.S. Department of Energys Secretary of Energy Advisory Board.

S. Hsiang is the Director of the Global Policy Laboratory at the University of California, Berkeley. R. Kopp previously served as a consultant to Rhodium Group, which provides independent research and analysis on a range of global economic topics to clients in the public and private sectors, including analysis of global energy market trends. Kopp currently serves as Director of the Rutgers Institute of Earth, Ocean, and Atmospheric Sciences. R Kopp provided technical support to and M Greenstone was a co-chair of the US Federal Government Interagency Working Group on Social Cost of Carbon between September 2009 - March 2010. R Kopp was an author of the National Academies of Sciences, Engineering, and Medicine report Valuing Climate Damages Updating Estimation of the Social Cost of Carbon Dioxide published in 2017.

Additional information

Supplementary Information is available for this paper. Correspondence and requests for materials should be addressed to Ashwin Rode. Reprints and permissions information is available at www.nature.com/reprints.

References

[1] Interagency Working Group on Socal Cost of Carbon. Social cost of carbon for regulatory impact analysis - under executive order 12866. Tech. Rep., United States Government (2010).

[2] Revesz, R. L. *et al.* Global warming: Improve economic models of climate change. *Nature News* **508**, 173 (2014).

[3] Pizer, W. *et al.* Using and improving the social cost of carbon. *Science* **346**, 1189–1190 (2014).

[4] Nordhaus, W. D. An optimal transition path for controlling greenhouse gases. *Science* **258**, 1315–1319 (1992).

[5] Greenstone, M., Kopits, E. & Wolverton, A. Developing a social cost of carbon for US regulatory analysis: A methodology and interpretation. *Review of Environmental Economics and Policy* **7**, 23–46 (2013).

[6] National Academies of Sciences, Engineering, and Medicine. *Valuing Climate Damages: Updating Estimation of the Social Cost of Carbon Dioxide* (The National Academies Press, Washington, DC, 2017).

[7] Diaz, D. & Moore, F. Quantifying the economic risks of climate change. *Nature Climate Change* **7**, 774 (2017).

[8] Anthoff, D. & Tol, R. S. The uncertainty about the social cost of carbon: A decomposition analysis using FUND. *Climatic Change* **117**, 515–530 (2013).

[9] Stern, N. Stern review report on the economics of climate change (2006).

[10] Waldhoff, S., Anthoff, D., Rose, S. & Tol, R. S. The marginal damage costs of different greenhouse gases: An application of fund. *Economics* **8** (2014).

[11] Nordhaus, W. D. Estimates of the social cost of carbon: background and results from the rice-2011 model. Tech. Rep., National Bureau of Economic Research (2011).

[12] Pindyck, R. S. Climate change policy: What do the models tell us? *Journal of Economic Literature* **51**, 860–872 (2013).

[13] Burke, M. *et al.* Opportunities for advances in climate change economics. *Science* **352**, 292–293 (2016).

[14] Adler, M. *et al.* Priority for the worse-off and the social cost of carbon. *Nature Climate Change* **7**, 443–449 (2017).

[15] Moore, F. C., Baldos, U., Hertel, T. & Diaz, D. New science of climate change impacts on agriculture implies higher social cost of carbon. *Nature communications* **8**, 1–9 (2017).

[16] Diaz, D. B. Evaluating the Key Drivers of the US Government's Social Cost of Carbon: A Model Diagnostic and Inter-Comparison Study of Climate Impacts in DICE, FUND, and PAGE (2014).

[17] Carleton, T. A. *et al.* Valuing the global mortality consequences of climate change accounting for adaptation costs and benefits. Working Paper 27599, National Bureau of Economic Research (2020). URL http://www.nber.org/papers/w27599.

[18] Hsiang, S. *et al.* Estimating economic damage from climate change in the United States. *Science* **356**, 1362–1369 (2017).

[19] Taylor, K. E., Stouffer, R. J. & Meehl, G. A. An overview of cmip5 and the experiment design. *Bulletin of the American Meteorological Society* **93**, 485 (2012).

[20] Auffhammer, M., Hsiang, S. M., Schlenker, W. & Sobel, A. Using weather data and climate model output in economic analyses of climate change. *Review of Environmental Economics and Policy* **7**, 181–198 (2013).

[21] Kopp, R., Hsiang, S. & Oppenheimer, M. Empirically calibrating damage functions and considering stochasticity when integrated assessment models are used as decision tools. *Impacts World, Potsdam, Germany, May 27-30* (2013).

[22] O'Neill, B. C. *et al.* A new scenario framework for climate change research: the concept of shared socioeconomic pathways. *Climatic Change* **122**, 387–400 (2014).

[23] Rasmussen, D. J. & Kopp, R. E. Appendix A: Physical climate projections. Economic risks of climate change: An American prospectus. *Economic Risks of Climate Change: An American Prospectus* (2015). URL https://cup.columbia.edu/book/economic-risks-of-climate-change/9780231174565. 1510.00313.

[24] Hsiang, S. Climate econometrics. *Annual Review of Resource Economics* **8**, 43–75 (2016).

[25] Smith, C. J. *et al.* Fair v1. 3: a simple emissions-based impulse response and carbon cycle model. *Geoscientific Model Development* **11**, 2273–2297 (2018).

[26] Dell, M., Jones, B. F. & Olken, B. A. Temperature shocks and economic growth: Evidence from the last half century. *American Economic Journal: Macroeconomics* **4**, 66–95 (2012).

[27] Burke, M., Hsiang, S. M. & Miguel, E. Global non-linear effect of temperature on economic production. *Nature* **527**, 235–239 (2015).

[28] Moore, F. C. & Diaz, D. B. Temperature impacts on economic growth warrant stringent mitigation policy. *Nature Climate Change* **5**, 127 (2015).

[29] Ricke, K., Drouet, L., Caldeira, K. & Tavoni, M. Country-level social cost of carbon. *Nature Climate Change* **8**, 895 (2018).

[30] Deschênes, O. & Greenstone, M. Climate change, mortality, and adaptation: Evidence from annual fluctuations in weather in the US. *American Economic Journal: Applied Economics* **3**, 152–185 (2011).

[31] Davis, L. W. & Gertler, P. J. Contribution of air conditioning adoption to future energy use under global warming. *Proceedings of the National Academy of Sciences* 201423558 (2015).

[32] Auffhammer, M., Baylis, P. & Hausman, C. H. Climate change is projected to have severe impacts on the frequency and intensity of peak electricity demand across the united states. *Proceedings of the National Academy of Sciences* 201613193 (2017).

[33] Wenz, L., Levermann, A. & Auffhammer, M. North–south polarization of european electricity consumption under future warming. *Proceedings of the National Academy of Sciences* **114**, E7910–E7918 (2017).

[34] Auffhammer, M. Climate adaptive response estimation: Short and long run impacts of climate change on residential electricity and natural gas consumption using big data. Tech. Rep., National Bureau of Economic Research (2018).

[35] Hadley, S. W., Erickson, D. J., Hernandez, J. L., Broniak, C. T. & Blasing, T. Responses of energy use to climate change: A climate modeling study. *Geophysical research letters* **33** (2006).

[36] Zhou, Y., Eom, J. & Clarke, L. The effect of global climate change, population distribution, and climate mitigation on building energy use in the US and China. *Climatic Change* **119**, 979–992 (2013).

[37] Isaac, M. & Van Vuuren, D. P. Modeling global residential sector energy demand for heating and air conditioning in the context of climate change. *Energy policy* **37**, 507–521 (2009).

[38] Clarke, L. *et al.* Effects of long-term climate change on global building energy expenditures. *Energy Economics* **72**, 667–677 (2018).

[39] Gollier, C. & Hammitt, J. K. The long-run discount rate controversy. *Annu. Rev. Resour. Econ.* **6**, 273–295 (2014).

[40] Bauer, M. & Rudebusch, G. D. The rising cost of climate change: Evidence from the bond market. *Federal Reserve Bank of San Francisco Working Paper Series* (2020).

[41] Sheffield, J., Goteti, G. & Wood, E. F. Development of a 50-year high-resolution global dataset of meteorological forcings for land surface modeling. *Journal of Climate* **19**, 3088–3111 (2006).

[42] International Energy Agency. World energy balances (edition 2017) (2018). URL https://www.oecd-ilibrary.org/content/data/9ddec1c1-en.

[43] Rasmussen, D. J., Meinshausen, M. & Kopp, R. E. Probability-weighted ensembles of US county-level climate projections for climate risk analysis. *J. Appl. Meteor. Climatol.* **55**, 2301–2322 (2016). URL http://journals.ametsoc.org/doi/abs/10.1175/JAMC-D-15-0302.1.

[44] McNeil, M. A. & Letschert, V. E. Modeling diffusion of electrical appliances in the residential sector. *Energy and Buildings* **42**, 783–790 (2010).

[45] Legros, G. *et al.* The energy access situation in developing countries: a review focusing on the least developed countries and sub-saharan africa. *World Health Organization* (2009).

[46] Almond, D., Chen, Y., Greenstone, M. & Li, H. Winter heating or clean air? unintended impacts of china's huai river policy. *American Economic Review* **99**, 184–90 (2009).

[47] Ramsey, F. P. A mathematical theory of saving. *The economic journal* **38**, 543–559 (1928).

[48] Tong, D. *et al.* Committed emissions from existing energy infrastructure jeopardize 1.5 C climate target. *Nature* **572**, 373–377 (2019).

[49] Woodard, D. L., Davis, S. J. & Randerson, J. T. Economic carbon cycle feedbacks may offset additional warming from natural feedbacks. *Proceedings of the National Academy of Sciences* **116**, 759–764 (2019).

[50] Global Administrative Areas. GADM database of global administrative areas, version 2.0. Tech. Rep. (2012). URL www.gadm.org.Accessed25December,2016.

[51] McGrath, G. Natural gas-fired electricity conversion efficiency grows as coal remains stable (2017). Accessed from: https://www.eia.gov/todayinenergy/detail.php?id=32572.

[52] U.S. Environmental Protection Agency. Emission Factors for Greenhouse Gas Inventories (2018). Accessed from: https://www.epa.gov/sites/production/files/2018-03/documents/emission-factors_mar_2018_0.pdf.

[53] Pachauri, R. K. *et al.* *Climate change 2014: synthesis report. Contribution of Working Groups I, II and III to the fifth assessment report of the Intergovernmental Panel on Climate Change* (IPCC, 2014).

[54] Thrasher, B., Maurer, E. P., McKellar, C. & Duffy, P. Technical note: Bias correcting climate model simulated daily temperature extremes with quantile mapping. *Hydrology and Earth System Sciences* **16**, 3309–3314 (2012).

[55] Riahi, K. *et al.* RCP 8.5—A scenario of comparatively high greenhouse gas emissions. *Climatic Change* **109**, 33–57 (2011).

[56] Thomson, A. M. *et al.* RCP 4.5: A pathway for stabilization of radiative forcing by 2100. *Climatic Change* **109**, 77 (2011). URL https://doi.org/10.1007/s10584-011-0151-4.

[57] Van Vuuren, D. P. *et al.* The representative concentration pathways: An overview. *Climatic Change* **109**, 5 (2011).

[58] Tebaldi, C. & Knutti, R. The use of the multi-model ensemble in probabilistic climate projections. *Philosophical Transactions of the Royal Society of London A: Mathematical, Physical and Engineering Sciences* **365**, 2053–2075 (2007). URL http://rsta.royalsocietypublishing.org/content/365/1857/2053.

[59] Riahi, K. *et al.* The shared socioeconomic pathways and their energy, land use, and greenhouse gas emissions implications: an overview. *Global Environmental Change* **42**, 153–168 (2017).

[60] Samir, K. & Lutz, W. The human core of the shared socioeconomic pathways: Population scenarios by age, sex and level of education for all countries to 2100. *Global Environmental Change* (2017).

[61] Cuaresma, J. C. Income projections for climate change research: A framework based on human capital dynamics. *Global Environmental Change* (2017).

[62] Dellink, R., Chateau, J., Lanzi, E. & Magné, B. Long-term economic growth projections in the shared socioeconomic pathways. *Global Environmental Change* (2017).

[63] IIASA Energy Program. Ssp database, version 1.1 [data set]. Tech. Rep., National Bureau of Economic Research (2016). URL https://tntcat.iiasa.ac.at/SspDb. Accessed25December,2016.

[64] Bright, E. A., Coleman, P. R., Rose, A. N. & Urban, M. L. LandScan 2011 (2012). Digital dataset: web.ornl.gov/sci/landscan/index.shtml.

[65] Jiang, L. & O'Neill, B. C. Global urbanization projections for the shared socioeconomic pathways. *Global Environmental Change* **42**, 193–199 (2017).

[66] Jones, B. & O'Neill, B. C. Spatially explicit global population scenarios consistent with the shared socioeconomic pathways. *Environmental Research Letters* **11**, 084003 (2016).

[67] Huppmann, D. *et al.* IAMC 1.5 °C Scenario Explorer and Data hosted by IIASA. Integrated Assessment Modeling Consortium & International Institute for Applied Systems Analysis (2018).

[68] Carleton, T. A. & Hsiang, S. M. Social and economic impacts of climate. *Science* **353**, aad9837 (2016).

[69] Auffhammer, M. & Aroonruengsawat, A. Simulating the impacts of climate change, prices and population on california's residential electricity consumption. *Climatic Change* **109**, 191–210 (2011). URL http://dx.doi.org/10.1007/s10584-011-0299-y.

[70] Graff Zivin, J. & Neidell, M. Temperature and the allocation of time: Implications for climate change. *Journal of Labor Economics* **32**, 1–26 (2014).

[71] Schlenker, W. & Roberts, M. J. Nonlinear temperature effects indicate severe damages to us crop yields under climate change. *Proceedings of the National Academy of sciences* **106**, 15594–15598 (2009).

[72] Hsiang, S. M. & Jina, A. S. The causal effect of environmental catastrophe on long-run economic growth: Evidence from 6,700 cyclones. Tech. Rep., National Bureau of Economic Research (2014).

[73] Wooldridge, J. M. *Econometric analysis of cross section and panel data* (MIT Press, Cambridge and London, 2002).

[74] Millar, R. J., Nicholls, Z. R., Friedlingstein, P. & Allen, M. R. A modified impulse-response representation of the global near-surface air temperature and atmospheric concentration response to carbon dioxide emissions. *Atmospheric Chemistry and Physics* **17**, 7213–7228 (2017).

[75] Board of Governors of the US Federal Reserve System. 10-year treasury inflation-indexed security, constant maturity [dfii10]. Tech. Rep., FRED, Federal Reserve Bank of St. Louis (2020). URL https://fred.stlouisfed.org/series/DFII10.

[76] Carleton, T. & Greenstone, M. Updating the united states government's social cost of carbon. *University of Chicago, Becker Friedman Institute for Economics Working Paper* (2021).

[77] Nordhaus, W. *A question of balance: Weighing the options on global warming policies* (Yale University Press, 2014).

[78] Arrow, K. J. Global climate change: A challenge to policy. *The Economists' Voice* **4** (2007).

[79] Dasgupta, P. The stern review's economics of climate change. *National institute economic review* **199**, 4–7 (2007).

[80] Dasgupta, P. Discounting climate change. *Journal of risk and uncertainty* **37**, 141–169 (2008).

[81] Hall, R. E. Reconciling cyclical movements in the marginal value of time and the marginal product of labor. *Journal of political Economy* **117**, 281–323 (2009).

[82] Weitzman, M. L. A review of the stern review on the economics of climate change. *Journal of economic literature* **45**, 703–724 (2007).

[83] Weitzman, M. L. On modeling and interpreting the economics of catastrophic climate change. *The Review of Economics and Statistics* **91**, 1–19 (2009).

[84] Wood, A. W., Leung, L. R., Sridhar, V. & Lettenmaier, D. Hydrologic implications of dynamical and statistical approaches to downscaling climate model outputs. *Climatic change* **62**, 189–216 (2004).

[85] Meinshausen, M., Raper, S. C. B. & Wigley, T. M. L. Emulating coupled atmosphere-ocean and carbon cycle models with a simpler model, MAGICC6 – part 1: Model description and calibration. *Atmos. Chem. Phys.* **11**, 1417–1456 (2011). URL http://www.atmos-chem-phys.net/11/1417/2011/.

[86] Mitchell, T. D. Pattern scaling: An examination of the accuracy of the technique for describing future climates. *Climatic Change* **60**, 217–242 (2003). URL http://link.springer.com/article/10.1023/A%3A1026035305597.

[87] Lobell, D. B., Schlenker, W. & Costa-Roberts, J. Climate trends and global crop production since 1980. *Science* **333**, 616–620 (2011).

[88] Rahman, M., Rahman, R. & Pearson, L. Quantiles for finite mixtures of normal distributions. *International Journal of Mathematical Education in Science and Technology* **37**, 352–358 (2006).

[89] Kopp, R. E. & Mignone, B. K. The US government's social cost of carbon estimates after their first two years: Pathways for improvement. *Working paper* (2012).

[90] Collins, M., Knutti, R. *et al. Chapter 12: Long-term Climate Change: Projections, Commitments and Irreversibility* (Intergovernmental Panel on Climate Change, 2013). URL http://www.ipcc.ch/report/ar5/wg1/.

[91] Joos, F. *et al.* Carbon dioxide and climate impulse response functions for the computation of greenhouse gas metrics: A multi-model analysis. *Atmospheric Chemistry and Physics* **13**, 2793–2825 (2013).

[92] Geoffroy, O. *et al.* Transient climate response in a two-layer energy-balance model. Part i: Analytical solution and parameter calibration using CMIP5 AOGCM experiments. *Journal of Climate* **26**, 1841–1857 (2013).

[93] Ricke, K. L. & Caldeira, K. Maximum warming occurs about one decade after a carbon dioxide emission. *Environmental Research Letters* **9**, 124002 (2014).

[94] Millar, R. J. *et al.* Model structure in observational constraints on transient climate response. *Climatic Change* **131**, 199–211 (2015).

[95] Mastrandrea, M. D. *et al.* Guidance note for lead authors of the IPCC Fifth Assessment Report on consistent treatment of uncertainties. Tech. Rep., Intergovernmental Panel on Climate Change (2010).

[96] Interagency Working Group on Social Cost of Greenhouse Gases. Technical support document: Technical update of the social cost of carbon for regulatory impact analysis. Tech. Rep., United States Government (2016).

[97] Newell, R. G. & Pizer, W. A. Uncertain discount rates in climate policy analysis. *Energy Policy* **32**, 519–529 (2004).

[98] Millner, A. & Heal, G. Time consistency and time invariance in collective intertemporal choice. *Journal of Economic Theory* **176**, 158–169 (2018).

[99] Li, Y., Pizer, W. A. & Wu, L. Climate change and residential electricity consumption in the yangtze river delta, china. *Proceedings of the National Academy of Sciences* **116**, 472–477 (2019).

[100] Downing, T. E., Greener, R. A. & Eyre, N. The economic impacts of climate change: Assessment of fossil fuel cycles for the ExternE project. Environmental Change Unit, University of Oxford, and Eyre Energy Environment (1995).

[101] Downing, T. E., Eyre, N., Greener, R. & Blackwell, D. Full fuel cycle study: Evaluation of the global warming externality for fossil fuel cycles with and without CO2 abatament and for two reference scenarios. Report to the International Energy Agency greenhouse gas R & D programme, Environmental Change Unit (1996).

[102] Miller, K. & Hodgson, D. Modelling UK energy demand. In *Global Warming and Energy Demand*, 150–161 (Routledge, 2005).

[103] Anthoff, D. & Tol, R. S. The climate framework for uncertainty, negotiation and distribution (FUND): Technical description, version 3.8. *Technical Document* (2014).

Supplementary Information to "Estimating a Social Cost of Carbon for Global Energy Consumption" by Rode et al.

Several of the raw datasets, numerical methods, and intermediate results described in this supplement are also described in the appendix of ref. [17]. We provide this information here for completeness.

Contents

A Data

A.1 Energy consumption data

Data assembly As described in *Methods Step 1*, we obtain data on final consumption of electricity and other fuels from the International Energy Agency's (IEA) *World Energy Balances* dataset. Electricity consumption is taken from the ELECTR variable code, and consumption of other fuels is obtained by aggregating over the following variable codes: COAL (coal and coal products); PEAT (peat and peat products); OILSHALE (oil shale and oil sands); TOTPRODS (oil products); NATGAS (natural gas); SOLWIND (solar/wind/other); GEOTHERM (geothermal); COMRENEW (biofuels and waste); HEAT (heat), and HEATNS (heat production from non-specified combustible fuels). For both electricity and other fuels, we aggregate over the following sectoral codes: TOTIND, which encompasses consumption in the industrial sector, and TOTOTHER, which encompasses consumption in the commercial/public services, residential, agricultural, forestry, fishing, and non-specified sectors. The non-specified sector includes consumption in the other sectors within TOTOTHER if disaggregated figures are not provided for those sectors.

Harmonization of energy consumption data across diverse reporting regimes The IEA extensively documents a range of data quality issues related to its energy consumption data. Data quality issues can arise for a variety of reasons, including lack of data, revisions to data, imputed data, and reporting inconsistencies. The documentation identifies such issues for individual countries over specific years, often explicitly noting "breaks in time series".[1] Our data preparation approach is based on upon reading and categorizing all documentation pertaining to each year of each country in the data.

When carrying out our analyses, we address documented data quality issues in one of two ways– imposing fixed effects that account for mean differences in energy consumption across time spans of observations documented to be incomparable, or dropping of these incomparable observations. Although there are 146 countries in the data, we use the IEA documentation to identify 275 distinct reporting "regimes" for electricity consumption (i.e. time spans within a country where reporting practices are documented to be comparable) and 294 regimes for other fuels consumption. All our regressions contain fixed effects at the country-regime level (i.e. an indicator variable for each country-by-regime), which account for mean differences in energy consumption across reporting regimes. While country-regime fixed effects are a powerful way to deal with known data quality issues, they are not always a sufficient remedy if observations fail to meet even basic standards of comparability. In some cases it is necessary to drop observations altogether. We drop an observation whenever its definition of a fuel or sector category is documented to be at odds with the standard definitions. For instance, we drop observations from Sweden prior

[1] For instance, in the documentation for Denmark, it is noted that "major revisions were made by the Danish administration for the 1990 to 2001 data, which may cause breaks in time series...".

to 1993, as certain road transport fuel consumption was included under the commercial sector during those years, but not during other years for Sweden or any years for other countries. A total of 412 observations are dropped for electricity consumption and 1,117 observations are dropped for other fuels consumption. In our released code base, we provide cleaning scripts depicting precisely the fixed effects imposed and the observations dropped.

Unit root behavior in energy consumption data Despite data preparation measures to guard against quality issues, there continue to exist what appear to be persistent shocks in energy consumption, even within a country-regime. For example, Figure A.1 displays the time series for other fuels consumption in Italy, with each color indicating a distinct regime. Persistent shocks to consumption do not always appear to be tied to a change in regime. Motivated by such patterns, we formally test for a unit root in electricity and other fuels consumption for each of the country-regime time series, using both the augmented Dickey-Fuller and Phillips-Perron tests under various lag lengths (including a time trend in each case). The null hypothesis is that there exists a unit root. Figure A.2 plots the histogram of p-values from the country-regime time series tests. Panel a displays tests on electricity consumption time series while Panel b displays tests on other fuels consumption time series. Each histogram within a panel represents a variant of the unit root test (augmented Dickey-Fuller or Phillips-Perron, each with different lag length). In all variants of the test for both electricity and other fuels consumption, the mass of very high p-values (i.e. close to $p = 1$ and far above the conventional rejection threshold of $p = 0.05$) suggests that it is very difficult to reject a unit root in a large number of time series.[2]

With strong suggestive evidence of unit root behavior in our energy consumption data, we estimate all regressions (detailed in Supplementary Section B) in first differences, as first differences remove confounding sources of spurious correlation that can enter due to unit root behavior.[73]

A.2 Climate data

This section describes the climate data that we use in this analysis as well as some of the methods employed to make these data consistent with the scale and resolution of the energy consumption data. Broadly speaking, we use two classes of climate data, the first being historical data to estimate energy-temperature responses, and the other being future climate data which are used to project the damages of climate change into the future under various emissions scenarios. We begin by describing the historical data, followed by the future projection data, and finally we detail the method we use to spatially and

[2]It should be noted that unit root tests tend to be underpowered. Hence we consider the full distribution of p-values, rather than just how many p-values fall below a conventional rejection threshold such as $p = 0.05$.

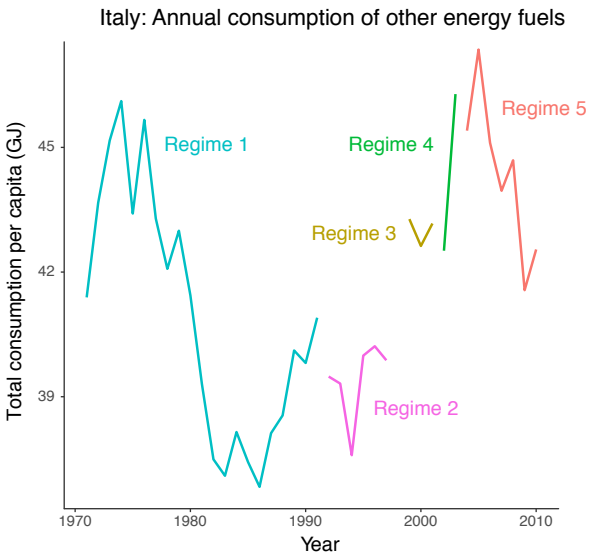

Figure A.1: Per-capita consumption of other fuels in Italy (1971-2012). Each color represents a time span of years where reporting practices are documented by the IEA to be comparable (i.e. a "regime"). Persistent shocks to consumption do not always correspond to known changes in the regime (e.g. in 1989).

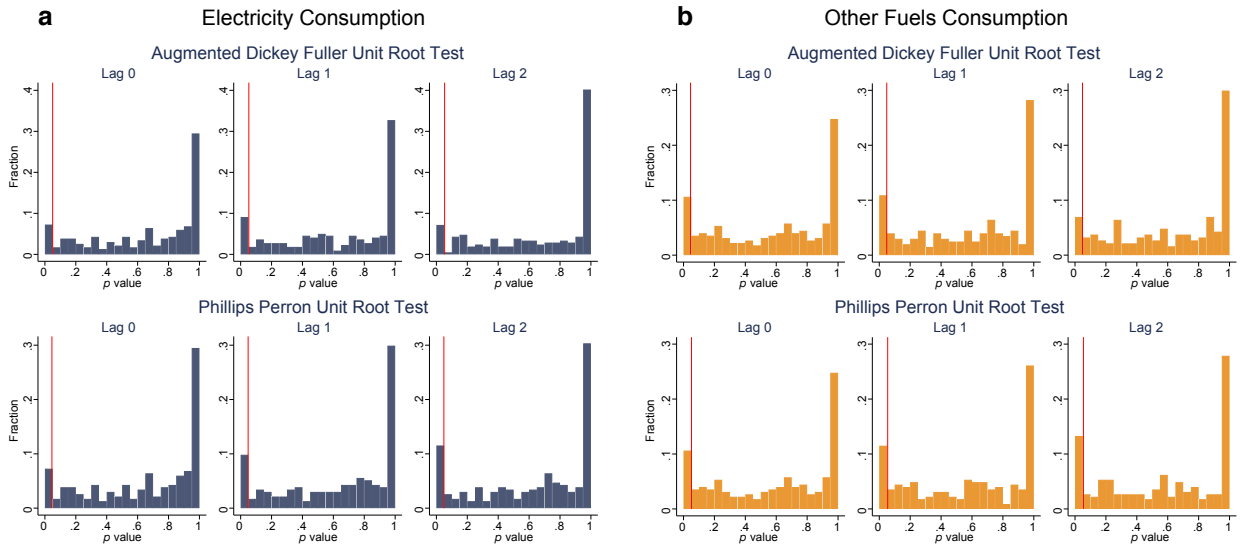

Figure A.2: Unit root tests by country-regime time series. Panel **a** depicts the histogram of p-values from unit root tests on every country-regime time series for electricity consumption; Panel **b** does the same for other fuels consumption. The tests are repeated using different testing procedures (Augmented Dickey-Fuller, Phillips-Perron) and lag length (0,1,2) combinations, in each case including a trend. The existence of a unit root is always the null hypothesis, which fails to be rejected for a substantial number of time series (often with very high p-values), regardless of testing procedure and lag length. Vertical red lines mark p-values of 0.05.

temporally aggregate these outputs to match the lower resolution energy consumption data.

A.2.1 Historical climate data

Data on historical climate exposure is used to estimate the energy-temperature response as well as the heterogeneity in the response by average climatology. For this estimation, we use the Global Meteorological Forcing Dataset, v1 (GMFD).[41] These data provide surface temperature and precipitation information using a combination of both observations and reanalysis. The reanalysis process uses a weather forecasting model to assimilate observational weather data in order to establish a gridded dataset of meteorological variables. The particular reanalysis used is the NCEP/NCAR reanalysis, which is downscaled and bias-corrected using a number of station-based observational datasets to remove biases in monthly temperature and precipitation while retaining daily variability from the NCEP/NCAR reanalysis product.[41][3] Data are available on a $0.25° \times 0.25°$ resolution grid from 1948-2010. The temporal frequency is up to 3-hourly, but the daily data are used for this analysis. We obtain daily average temperatures and monthly average precipitation for all grid cells globally. A primary reason for using GMFD in our regression analysis is that GMFD is used to bias-correct the climate model projections (described below).[4]

A.2.2 Climate projection data

Data on the future evolution of the climate is obtained from a multi-model ensemble of Global Climate Model (GCM) output. However, two important limitations arise when integrating GCM outputs into the current analysis. First, the relatively coarse resolution ($\sim 1°$ of longitude and latitude) of GCMs limits their ability to capture small-scale climate patterns, which renders them unsuitable for climate impact assessment at high spatial resolution. Second, the GCM climate variables exhibit large local bias when compared with observational data.

To address both of these limitations, we use a high-resolution ($0.25°$ X $0.25°$) set of global, bias-corrected climate projections produced by NASA Earth Exchange (NEX): the Global Daily Downscaled Projections (GDDP).[5][5] The NEX-GDDP dataset comprises 21 climate projections, which are downscaled from the output of GCM runs in the Coupled Model Intercomparison Project Phase 5 (CMIP5) archive.[19] The statistical downscaling

[3] These observational datasets are generally available at finer spatial resolutions, but coarser temporal resolutions (e.g., monthly) resolutions than the reanalysis product. Therefore, while the observational datasets are used to downscale the reanalysis in space, they are employed for bias correction on a monthly temporal scale, with submonthly temporal variation provided by the reanalysis.[41]

[4] Because GMFD only contains climate data up to 2010, we are necessarily limited to using energy consumption data only up to 2010 in this analysis.

[5] Climate projections used were from the NEX-GDDP dataset, prepared by the Climate Analytics Group and NASA Ames Research Center using the NASA Earth Exchange, and distributed by the NASA Center for Climate Simulation (NCCS).

algorithm used to generate the NEX-GDDP dataset is the Bias-Correction Spatial Disaggregation (BCSD) method,[54,84] which was developed to address the aforementioned two limitations. This algorithm first compares the GCM outputs with observational data on daily maximum temperature, daily minimum temperature, and daily precipitation during the period 1950-2005. NEX-GDDP uses a climate dataset from GMFD for this purpose.[41] A daily, quantile-specific relation between GCM historical period outputs and historical observations is derived from this comparison. This relation is then used to adjust the GCM outputs in historical and in future time periods so that the systemic bias of the GCM is removed. To disaggregate the bias-corrected GCM outputs to higher resolution, this algorithm interpolates the daily changes relative to climatology in GCM outputs into the spatial resolution of GMFD, and merges the fine-resolution changes with the climatology of the GMFD data.[6]

For each GCM, three different datasets are generated. The first uses historical emissions to simulate the response of the climate to historical forcing from 1850 to 2005. The second and third use projected emissions from Representative Concentration Pathways 4.5 and 8.5 (RCP4.5 and RCP8.5) to simulate emissions under those two emissions scenarios up to 2100. RCP 4.5 represents a "stabilization" scenario in which total radiative forcing is stabilized around 2100;[55,57] RCP8.5 simulates climate change under intensive growth in fossil fuel emissions from 2006 to the end of the 21^{st} century. We use daily average temperature and daily precipitation in the RCP4.5 and RCP8.5 scenarios from this dataset, where the daily average temperature is approximated as the mean of daily maximum and daily minimum temperatures.

A.2.3 SMME and model surrogates

The CMIP5 ensemble of GCMs described above is an "ensemble of opportunity", not a systematic sample of possible futures. Thus, it does not produce a probability distribution of future climate change. Moreover, relative to "simple climate models" designed for probabilistic sampling of the global mean surface temperature (GMST) response to radiative forcing, the CMIP5 ensemble systematically fails to sample tail outcomes.[43,58] To provide an ensemble of climate projections with a probability distribution of GMST responses consistent with that estimated by a probabilistic simple climate model, we use the surrogate model mixed ensemble (SMME) method[43] to assign probabilistic weights to climate projections produced by GCMs and to improve representation of the tails of the distribution missing from the ensemble of GCMs. Generally speaking, the SMME uses (1) a weighting scheme based on a probabilistic projection of global mean surface temperature from a simple climate model (in this case, MAGGIC6)[85] and (2) a form of linear pattern scaling[86] that preserves high-frequency variability to construct model surrogates

[6] Details are available in Appendix A of the NEX-GDDP documentation: https://gdo-dcp.ucllnl.org/downscaled_cmip_projections/techmemo/downscaled_climate.pdf

to fill the tails of probability distribution that are not captured by the GCM ensembles. This method provides us with an additional 12 surrogate models.

The SMME method first divides the unit interval [0,1] into a set of bins. For this analysis, the bins are centered at the 1^{st}, 6^{th}, 11^{th}, 16^{th}, 33^{rd}, 50^{th}, 67^{th}, 82^{nd}, 89^{th}, 94^{th}, and 99^{th} percentiles. Bins are narrower in the tails to ensure samples are created for portions of the GMST probability distribution function that are not captured by CMIP5 models. The bounds and center of each bin are assigned corresponding quantiles of GMST anomalies for 2080-2099 from simple climate model (SCM) output; in the application here and that of ref. [43], this output came from the MAGICC6 model,[85] constrained to match historical temperature observations and the conclusions of the IPCC Fifth Assessment Report regarding equilibrium climate sensitivity. The GMST of CMIP5 models are categorized into bins according to their 2080-2099 GMST anomalies.

If the number of CMIP5 models in a bin is less than 2, surrogate models are generated to raise the total number of models to 2 in that bin. The surrogate models are produced by using the projected annual GMST of the SCM that is consistent with the bin's central quantile to scale the spatial pattern of a selected CMIP5 model, then adding the intercept and residual from the same model. There are two cases of selecting CMIP5 models for pattern and residual. When there is only one CMIP5 model in a bin, an additional model is selected that has a GMST projection close to GMST in the bin and a precipitation projection over the region of interest complementary to the model already in the bin (i.e., if the model in the bin is relatively dry, then a relatively wet pattern is selected, and vice versa). When there is no CMIP5 model, two models are picked with GMST projections close to that of the bin, with one model being relatively wet and one being relatively dry. In the final probabilistic distribution, the total weight of the bin is equally divided among the CMIP5 models and surrogate models in the bin. For instance, if four models are in the bin centered at the 30th percentile, bounded by the 20th – 40th percentiles, each will be assigned a probability of $20\% \div 4 = 5\%$. The resulting distribution of GMST for all members of the SMME is shown in Extended Data Figure 2a, and the weights assigned to each GCM and surrogate under each emissions scenario are shown in Extended Data Figure 2b.

A.2.4 Aggregation of gridded climate data to administrative boundaries

We combine daily, grid-cell level temperature data with annual country-level per capita energy consumption data to empirically recover the nonlinear, daily grid cell-level relationship between temperature and per capita energy consumption. Importantly, in order to recover this daily, grid cell-level relationship, it is necessary that the daily, gridded temperature data are aggregated to the country-year level in a way that reflects temperature extremes experienced in individual grid cells within a country, on individual days within a year. Specifically, nonlinear transformations of temperature must be computed

at the grid-cell-by-day level *before* averaging values across grid cells in a country using population weights, and finally summing over days within a year.

To see how this calculation is operationalized, consider the second-order polynomial specification for temperature used in our main set of results for estimation of Equation 3 in *Methods* (equivalent to Equation B.6 in Supplementary Section B). In this case, we begin with data on average temperatures for each day d of year t at each grid cell z in country j, denoted as T_{zjdt}. These grid-cell-level values must then be aggregated to the level of country j in year t. To do this, we first raise grid-cell-level temperature to the power k, computing $(T_{zjdt})^k$ for $k \in \{1, 2\}$. Let $\boldsymbol{T}_{zjdt}$ denote the grid cell-by-day temperature vector $[(T_{zjdt})^1, (T_{zjdt})^2]$. We then take a spatial average over country j for each element in $\boldsymbol{T}_{zjdt}$, weighting the average by grid-cell-level population.[7] We then sum each element over the 365 days in the year t. The vector of country-by-year temperature variables we use for estimation is thus:

$$\widetilde{\boldsymbol{T}}_{jt} = \sum_{d \in t} \sum_{z \in j} w_{zj} \boldsymbol{T}_{zjdt} = \left[\sum_{d \in t} \sum_{z \in j} w_{zj} (T_{zjdt})^1, \sum_{d \in t} \sum_{z \in j} w_{zj} (T_{zjdt})^2 \right], \tag{A.1}$$

where w_{zj} is the share of j's population that falls into grid cell z, and where superscripts indicate exponents. This procedure recovers grid cell-by-day-level nonlinearities in the energy-temperature (and energy-precipitation) response, because energy consumption is additive across time and space (See Equation 2 in *Methods*).[24]

Instead of following the above procedure, it would be possible, in principle, to simply estimate the effect of average annual country-level temperature and its square on annual country-level per capita energy consumption. Under this approach, temperature values would first be averaged across grid cells in a country and summed over days within a year, before nonlinear transformations are computed, and the vector of country-by-year temperature variables would instead be:

$$\ddot{\boldsymbol{T}}_{jt} = \left[\left(\sum_{d \in t} \sum_{z \in j} w_{zj} T_{zjdt} \right)^1, \left(\sum_{d \in t} \sum_{z \in j} w_{zj} T_{zjdt} \right)^2 \right].$$

While such an approach would be analogous to the analysis of some earlier studies, such as refs. [27,87], it would require assumptions that neglect key findings from existing literature. Specifically, this approach would assume that average per capita energy consumption across a country reflected average temperatures across that country. However, prior work[30–33,69] has demonstrated both that (i) local per capita energy consumption on a given day reflects the local daily temperature rather than temperatures at distant locations within the same country, and (ii) the per capita energy consumption response

[7] Population weights are time-invariant and calculated from the 2010 Gridded Population of the World dataset. Data are available here: https://sedac.ciesin.columbia.edu/data/collection/gpw-v4. We account for fractional grid cells that fall partially within administrative units.

to temperature is highly nonlinear. For example, on a single day in the United States, per capita energy consumption may simultaneously be abnormally high in Phoenix, Arizona, because electricity is heavily used for air conditioning due to high temperatures; low in San Francisco, California, where temperatures are moderate; and high in Chicago, Illinois where it is cold and other fuels are used for heating.

Because local, daily temperatures influence local, daily per capita energy consumption in a nonlinear manner, country-level annual average per capita energy consumption cannot be expressed as a function of $\ddot{\boldsymbol{T}}_{jt}$ in a manner that generalizes across countries that have differing geographic extents (see ref. [24] for additional discussion of this issue). We therefore circumvent this issue by exploiting highly resolved temperature data as in Equation A.1, thus allowing us to estimate local temperature-per capita energy consumption relationships that plausibly generalize across grid cells, regardless of each country's size and shape. Projections of the change in per capita energy consumption (in response to changing temperatures) can then be computed for any aggregation of grid cells, including our 24,378 custom impact regions (Extended Data Figure 1).

In future projections, all daily gridded climate projection data from each of the 33 members of the SMME are aggregated across space and time to the impact region-by-year level based on the approach in Equation A.1. For impact region r in country j, the vector of annual, impact region-by-year temperature variables we use for projections is thus:

$$\widetilde{\boldsymbol{T}}_{rjt} = \sum_{d \in t} \sum_{z \in r} w_{zr} \boldsymbol{T}_{zjdt} = \left[\sum_{d \in t} \sum_{z \in r} w_{zr} (T_{zjdt})^1, \sum_{d \in t} \sum_{z \in r} w_{zr} (T_{zjdt})^2 \right]$$

where w_{zr} is the share of impact region r's population that falls into grid cell z.

A.3 Socioeconomic data and downscaling methodologies

This section provides details of the socioeconomic data used throughout our analysis, which includes historical national incomes, future projections of incomes, and future projections of population counts. Additionally, because we require these variables at high spatial resolution for future projections, we detail the downscaling procedures we use to disaggregate available socioeconomic projections, which are generally provided at relatively low resolution.

A.3.1 Historical income data

Our main specification (Equation 3 in *Methods* and Equation B.6 in Supplementary Section B) estimates heterogeneity in energy-temperature responses as a function of income and long-run average climate in each location. We obtain country-level annual income data from within the International Energy Agency's World Energy Balances dataset; these income data originally are sourced by the IEA from the World Bank. For each country-year, the historical income variable is calculated as the 15-year moving average of the natural log of per-capita GDP.

A.3.2 Income projections

Future projections of national incomes are derived from the Organization for Economic Co-operation and Development (OECD) Env-Growth model[62] and the International Institute for Applied Systems Analysis (IIASA) GDP model,[60] as part of the "socioeconomic conditions" (population, demographics, education, income, and urbanization projections) of the Shared Socioeconomic Pathways (SSPs). The SSPs propose a set of plausible scenarios of socioeconomic development over the 21^{st} century in the absence of climate impacts and policy for use by the Integrated Assessment Modeling (IAM) and Impacts, Adaptation, and Vulnerability (IAV) scientific communities.

While there are many models within the SSP database, only the IIASA GDP model and OECD Env-Growth model provide GDP per capita projections for a wide range of countries. The IIASA GDP model describes incomes that are lower than the OECD Env-Growth model, so we produce results for both of these models to capture uncertainty within each socioeconomic scenario (we compute results for five socioeconomic scenarios: SSP1, SSP2, SSP3, SSP4, and SSP5). To construct annual estimates, we smoothly interpolate between the time series data in the SSP database, which are provided in 5-year increments. For each 5-year period, we calculate the average annual growth rate, and apply this growth rate to produce each year's estimate of GDP per capita.[8]

A.3.3 Population projections and downscaling methodology

Future projections of national populations are derived from the International Institute for Applied Systems Analysis (IIASA)[60] population projections as part of the Shared Socioeconomic Pathways (SSPs).[9] The IIASA SSP population projections provide estimates of population by age cohort, gender, and level of education for 193 countries from 2010 to 2100 in five-year increments. Each projection corresponds to one of the five SSPs, as defined in ref.[22]

[8] OECD estimates of income are provided for 184 countries and IIASA's GDP projections cover 171 countries. For the remaining countries, we apply the average GDP per capita from the available countries for the baseline period, and allow this income to grow at the globally averaged growth rate.

[9] The population data are accessed from the SSP database.[63]

To assemble population projections for each of our 24,378 impact regions (Extended Data Figure 1), we downscale the country-level projections from the SSPs using 2011 high-resolution LandScan estimates of populations.[64] Populations for impact regions in countries or areas not given in the SSP database are held constant at the values estimated by LandScan in 2011. Thus, for any given impact region r in year t, population for scenario v (pop_{rtv}) is estimated as:

$$\widehat{pop}_{rtv} = \begin{cases} pop_{ctv}^{SSP} \left(\frac{pop_{r,2011}^{LandScan}}{\sum_{r \in c} pop_{r,2011}^{LandScan}} \right), & \text{if } r \in C \\ pop_{r,2011}^{LandScan}, & \text{if } r \notin C \end{cases} \tag{A.2}$$

where pop_{ctv}^{SSP} is the SSP population given for country c and year t for scenario v, $pop_{r,2011}^{LandScan}$ is the LandScan estimate for impact region r, and C is the set of 193 countries available in the SSP Database. Note that while this approach distributes country-level projections of population heterogeneously to impact regions within a country, it fixes the relative population distribution within each country at the observed distribution today. In Supplementary Section G.1, we explore how our projected impacts are affected by alternative assumptions on the evolution of within-country population distributions over time.[65,66]

B Estimating energy-temperature responses and projecting impacts of climate change

This section provides details on the estimation of energy-temperature responses and projection of climate change impacts. Section B.1 demonstrates estimation of global average energy-temperature responses, while Section B.2 introduces heterogeneity by income. Sections B.3 and B.4 respectively explain how we estimate and project energy-temperature responses as a function of both income and long-run climate. Finally, Section B.5 details the procedure for characterizing econometric and climatological uncertainty in our estimates of the energy consumption impacts of climate change.

B.1 Global average energy-temperature response

Our energy-temperature responses flexibly model per capita annual electricity and other fuels consumption each as a function of daily average temperatures within a year. Let E_{jtc} denote consumption in GJ per capita in country j, year t, and fuel category c (electricity, other fuels). The temperature and precipitation vectors $\widetilde{\boldsymbol{T}}_{jt}$ and $\widetilde{\boldsymbol{P}}_{jt}$ contain country-by-year aggregations of nonlinear grid-cell-level transformations of daily temperature and precipitation, respectively. These vectors thus summarize the full distribution of daily average weather in country j, year t (*Supplementary Section* A.2.4). The basic econometric specification for a global average energy-temperature response is:

$$E_{jtc} = f_c(\widetilde{\boldsymbol{T}}_{jt}) + g_c(\widetilde{\boldsymbol{P}}_{jt}) + \alpha_{jic} + \delta_{wtc} + \varepsilon_{jtc}. \tag{B.1}$$

Our primary object of interest is the effect of temperature on per capita energy consumption, represented by the response function $f_c(\cdot)$, which differs for electricity and other fuels. In our estimation of Equation B.1, the vector $\widetilde{\boldsymbol{T}}_{jt}$ contains polynomials of daily average temperatures (up to fourth order), each summed across the year, and the vector $\widetilde{\boldsymbol{P}}_{jt}$ contains polynomials of daily cumulative precipitation (up to second order), also each summed annually. We estimate $f_c(\cdot)$ and $g_c(\cdot)$ as *linear* functions of the *nonlinear* elements of $\widetilde{\boldsymbol{T}}_{jt}$ and $\widetilde{\boldsymbol{P}}_{jt}$, respectively. This construction allows us to estimate a linear regression model while preserving the nonlinear relationship between per capita energy consumption and temperature that takes place at the grid-cell-by-day level.[24]

Equation B.1 identifies the energy-temperature response from plausibly random year-to-year variation in temperature within a country. The econometric specification includes a full set of country-by-reporting regime fixed effects (α_{jic}), where reporting regimes (i) are time spans within a country where observations for a given category are documented by the IEA to be comparable (*Supplementary Section* A.1). These fixed effects ensure that we isolate within-location year-to-year variation in temperature and precipitation exposure, which is as good as randomly assigned. In addition, we include world region-

by-year fixed effects (δ_{wtc}) for each category, where w indexes world regions based on UN classifications (Oceania, N. America, N. Europe, S. Europe, W. Europe, E. Europe, E. Asia, S.E. Asia, Central America/Caribbean, South America, sub-Saharan Africa, N. Africa/W. Asia, S. Asia). These fixed effects account for regional time-varying trends or shocks to energy consumption which are unrelated to the climate. Finally ε_{jtc} denotes the stochastic error term; standard errors are clustered by country-category-reporting regime.

Due to evidence of unit root behavior in the dependent variable (*Supplementary Section* A.1), we estimate Equation B.1 and all other regressions in first-differences. Additionally, to address differential data quality across reporting regimes, we employ an inverse variance weighting procedure in all regressions. In particular, we utilize Feasible Generalized Least Squares (FGLS) weights to downweight low credibility country-reporting regimes based on their residual variance.[10] To implement this weighting, we first estimate the regression in first differences. Using the residuals from this regression, we calculate a country-category-reporting regime level weight equal to the inverse of the average value of the squared residuals, where the average is taken across all year observations that fall within a given country-category-reporting regime. We then apply these weights to the regression in a second stage. Observations from all years within a given country-category-reporting regime are given the same weight in the second stage; country-category-reporting regimes with higher average residual variance thus receive lower weight.

Formally, for Equation B.1, each observation in country j, reporting regime i, category c receives a weight $w_{jic} = \frac{1}{Var(\Delta\varepsilon_{jtc\in jic})}$, and the weighted, first-differenced regression specification is:

$$\omega_{jic}\Big[\Delta E_{jtc}\Big] = \omega_{jic}\Big[\Delta f_c(\widetilde{\boldsymbol{T}}_{jt}) + \Delta g_c(\widetilde{\boldsymbol{P}}_{jt}) + \Delta\delta_{wtc} + \Delta\varepsilon_{jtc}\Big], \tag{B.2}$$

where Δ here denotes the first-difference operator.[11] To operationalize Equation B.2, we estimate ω_{jic} with $\widehat{\omega_{jic}} = \frac{1}{\widehat{Var}(\widehat{\Delta\varepsilon_{jtc\in jic}})}$, where $\widehat{\Delta\varepsilon_{jtc}}$ denotes the residual for the country j, year t, category c observation from the unweighted, first-differenced regression, and $\widehat{Var}$ refers to the sample variance.

As discussed in *Methods Step 2*, the estimated electricity- or other fuels-temperature response is expressed as the difference between predicted per capita consumption on a day where the average temperature is T and predicted per capita consumption on a "mild" day with an average temperature of 20°C. The blue curve in Figure B.1 displays the global, population-weighted electricity-temperature response estimated from Equation B.2, while the orange curve displays the other-fuels temperature response.[12] Over the time period

[10] We assume constant residual variance within each country-category-reporting regime.

[11] The fixed effects α_{jic} disappear upon first differencing as they are time-invariant.

[12] These are obtained by estimating Equation B.2 with population weights in addition to inverse-variance weights. Population weighting assigns each country's observations a weight proportional to its average population over the years of the sample. Given that Equation B.2 does not model heterogeneity in the energy-temperature response by income and long-run climate, population weights give us the response

represented by the data (1971-2010), electricity consumption exhibits little sensitivity to temperature on average, globally speaking (blue curve, Figure B.1), while other fuels consumption is seen to increase at cold temperatures (orange curve, Figure B.1). The lack of an electricity-temperature response, particularly on hot days, reflects the fact that during the sample period, most of the global population is too poor to access electricity-intensive protective technologies such as air-conditioning. In contrast, consumption of other fuels is seen to increase on cold days, reflecting the use of these fuels for heating across a broader range of the global population.

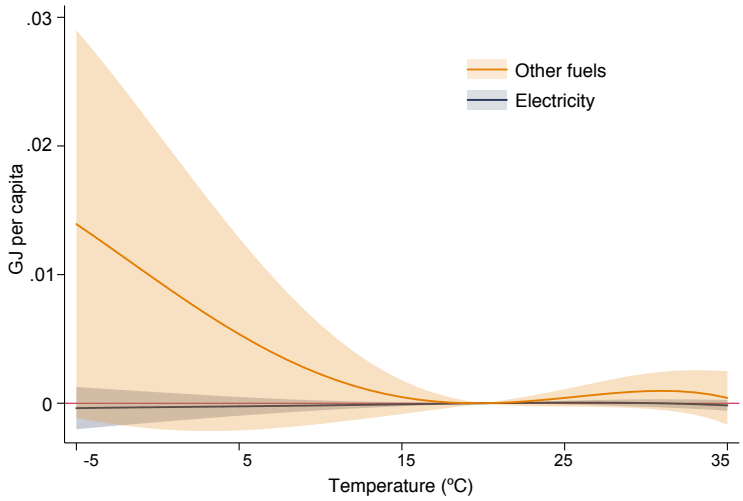

Figure B.1: Population-weighted global average electricity-temperature response (blue) and other fuels-temperature response (orange). Each point on the curve denotes the additional per-capita daily consumption at a daily average temperature denoted on the horizontal axis, relative to a daily average temperature of 20°C. Shaded areas indicate 95% confidence intervals.

B.2 Energy-temperature response heterogeneity by income

The global average energy responses to temperature shown in the previous section are likely to mask substantial heterogeneity by income, as consumption of electricity and other fuels is strongly correlated with wealth. To demonstrate how energy-temperature responses vary by income, we estimate responses for each decile of GDP per-capita as follows:

$$E_{jtc} = f_{cq}(\widetilde{\boldsymbol{T}}_{jt}) + g_c(\widetilde{\boldsymbol{P}}_{jt}) + \phi_{cq} + \alpha_{jic} + \delta_{wtc} + \varepsilon_{jtc}, \tag{B.3}$$

where q indexes the in-sample decile of the 15-year moving average GDP per-capita that country j in year t falls into, and ϕ_{cq} is a fuel category-specific decile fixed effect.[13] As

for the average global person.

[13] Income deciles are calculated for all country-year observations in the sample and are used to define 10 bins of income, which are held fixed through time. Thus the decile boundaries do not change year to year. Fuel category-specific decile fixed effects flexibly account for the direct effect of income on the level of consumption.

with Equation B.1, we take into account nonlinearities in the temperature response, f_{cq}, but do so via a second-order polynomial due to the large number of additional parameters. Thus, the vector $\widetilde{\boldsymbol{T}}_{jt}$ contains linear and quadratic terms of daily average temperatures, each summed across the year (*Supplementary Section* A.2.4). The electricity- and other fuels-temperature responses in main text Figure 1a and 1b are obtained from estimating Equation B.3 in first-differences using inverse variance weighting (as shown in Equation B.2).

B.3 Energy-temperature response heterogeneity by income and long-run climate

All climate impact projections computed throughout our analysis incorporate heterogeneity in the energy-temperature response not only by income, but also by long-run average climate. To represent heterogeneity in the energy-temperature response along the dimensions of both income and long-run climate, we estimate Equation 3 (*Methods*) including flexible interactions between temperature and the following covariates:

1. **Income** measured as the 15-year moving average of a country's natural log of per-capita GDP ($\overline{LogGDPPC}$).[14]
2. **Long-run climate** is measured by average annual values of the following two variables over the time period of the sample:[15]

    - *Heating degree days* ($\overline{HDD}$) are defined as the cumulative deviations of daily average temperatures from a benchmark of 20° C, over all days where the average temperature fell below 20° C. Formally, heating degree days in year t are defined as $\sum_{d\in t} |T_d - 20| * \mathbf{I}_{T_d<20}$, where T_d is the average temperature on day d and $\mathbf{I}_{T_d<20}$ is an indicator variable equal to one if $T_d < 20$.
    - *Cooling degree days* ($\overline{CDD}$) are defined similarly over days where the daily average temperature exceeds 20° C, i.e. cooling degree days in year t are $\sum_{d\in t} |T_d - 20| * \mathbf{I}_{T_d>20}$.

These variables were carefully chosen based on the intersection of prior evidence from the literature, economic theory, and inclusion in standard projections of the global economy developed for integration with physical climate models.[22] Prior literature has emphasized the adaptive significance of income per-capita[31] and average climate.[34] For example,

[14] Because changes in income are unlikely to immediately translate into changes in the energy-temperature response, we take an average over incomes in the current year and 14 previous years (equally weighted). See Supplementary Section G.2 for an exploration of alternative assumptions on the role of income growth.

[15] Because long-run climate is slow moving, it is difficult to rely on temporal variation within the timespan of the sample. We therefore utilize only cross-sectional variation to characterize heterogeneity in the energy-temperature response due to long-run climate.

higher per-capita GDP is associated with more widespread electrification and reliable electricity provision, and entails greater capability to invest in protective measures such as air-conditioning, which can amplify the energy-temperature response as demonstrated in main text Figure 1a. Furthermore, the energy-temperature response may also depend on long-run exposure to extreme temperatures as places with greater previous exposure may differ in their adaptive behaviors.[17]

To illustrate how we model the effects of income and long-run climate on the energy-temperature response, consider a stylized example where per capita energy consumption (E) is a linear function of temperature ($\beta \cdot T$), and the slope β itself depends on $\overline{LogGDPPC}$, $\overline{CDD}$, and $\overline{HDD}$:

$$\beta = \xi_0 + \xi_1 \overline{LogGDPPC} + \xi_2 \overline{CDD} + \xi_3 . \overline{HDD}$$

Then per capita energy consumption would be:

$$E = \beta \cdot T = \underbrace{(\xi_0 + \xi_1 \overline{LogGDPPC} + \xi_2 \overline{CDD} + \xi_3 \overline{HDD}) \cdot T}_{f(\widetilde{\boldsymbol{T}} | \overline{LogGDPPC}, \overline{CDD}, \overline{HDD}) \text{ in Equation 3}} . \tag{B.4}$$

In this example, the parameters ξ_0, ξ_1, ξ_2, and ξ_3 govern how $\overline{LogGDPPC}$, $\overline{CDD}$, and $\overline{HDD}$ shape the energy-temperature response. These parameters can be recovered through a regression containing temperature and its interactions with the three covariates:

$$E = \xi_0 T + \xi_1 (\overline{LogGDPPC} \cdot T) + \xi_2 (\overline{CDD} \cdot T) + \xi_3 (\overline{HDD} \cdot T) + \varepsilon, \tag{B.5}$$

where ε denotes the stochastic error term.

In practice, we estimate a more complex form of $f(\widetilde{\boldsymbol{T}} | \overline{LogGDPPC}, \overline{CDD}, \overline{HDD})$ than Equation B.4, designed to flexibly account for nonlinearities in both the energy-temperature response and how it varies due to each of the covariates. Let $\widetilde{\boldsymbol{T}}_{jt}$ denote the vector containing linear and quadratic terms of daily average temperatures, each summed across the year (*Supplementary Section* A.2.4). To capture the role of income-driven adaptation, we interact a linear spline of $\overline{LogGDPPC}$ with each element of $\widetilde{\boldsymbol{T}}_{jt}$. A knot point of the income spline is set separately for electricity and other fuels consumption, based on the point in the in-sample income distribution at which consumption starts to become responsive to temperature. Figure 1a (main text) suggests that this point is the beginning of the seventh decile for electricity ($\overline{GDPPC} = \$11,258$, 2019 USD PPP) and the beginning of the third decile for other fuels ($\overline{GDPPC} = \$2,849$, 2019 USD PPP). In addition to interactions of income with temperature exposure, we also flexibly control for the direct effect of income on per capita energy consumption through a piecewise linear function of $\overline{LogGDPPC}$ that also allows for step-wise jumps at these points.

To capture the role of climate-driven adaptation, the long-run average climate mea-

sures $\overline{CDD}$ and $\overline{HDD}$ are interacted with the daily temperature vector $\widetilde{\boldsymbol{T}}_{jt}$, but only over specific daily temperature ranges holding adaptive significance. Specifically, we allow long-run exposure to warm temperatures (measured by $\overline{CDD}$) to modulate the energy-temperature response on warm days, where the average temperature is at least 20° C. Conversely, long-run exposure to cool days (measured by $\overline{HDD}$) modulates the energy-temperature response on cool days, where the average temperature is below 20° C. Figure B.2 provides graphical intuition for this split interaction on either side of 20° C. We generate these interaction terms for each grid cell z and day d, before averaging across grid cells within a country j using population weights and finally summing over days within a year t (*Supplementary Section* A.2.4). This procedure recovers grid cell-by-day-level heterogeneity in the energy-temperature response due to long-run climate.[16] Letting T_{zjdt} denote the average temperature on day d of year t, in grid cell z of country j, and $\overline{CDD}_{zj}$ denote the average annual cooling degree days in grid cell z of country j over the time period of the sample, the daily temperature $\times$ $\overline{CDD}$ vector of interactions used in estimation is thus:

$$\left[\widetilde{\boldsymbol{T} \times \overline{CDD}}\right]_{jt} = \left[\sum_{d=1}^{365}\sum_{z\in j} w_{zj}(T^1_{zjdt} - 20)\mathbf{I}_{T_{zjdt}\geq 20}\overline{CDD}_{zj}, \sum_{d=1}^{365}\sum_{z\in j} w_{zj}(T^2_{zjdt} - 20^2)\mathbf{I}_{T_{zjdt}\geq 20}\overline{CDD}_{zj}\right],$$

where w_{zj} is the share of j's population that falls into grid cell z, superscripts indicate polynomial powers, and the variable $\mathbf{I}_{T_{zjdt}\geq 20}$ is an indicator for whether $T_{zjdt} \geq 20$. Similarly, the daily temperature $\times$ $\overline{HDD}$ vector of interactions is:

$$\left[\widetilde{\boldsymbol{T} \times \overline{HDD}}\right]_{jt} = \left[\sum_{d=1}^{365}\sum_{z\in j} w_{zj}(20 - T^1_{zjdt})\mathbf{I}_{T_{zjdt}<20}\overline{HDD}_{zj}, \sum_{d=1}^{365}\sum_{z\in j} w_{zj}(20^2 - T^2_{zjdt})\mathbf{I}_{T_{zjdt}<20}\overline{HDD}_{zj}\right].$$

The form of Equation 3 (*Methods*) that we estimate thus specifies per capita energy consumption in country j, year t, and category c as a function of temperature, and income and climate covariates, as follows:

[16] Unlike long-run climate, our income data are only measured at the country level. It is not possible to similarly generate the interaction between the daily temperature vector and $\overline{LogGDPPC}$ at the grid level, and we can thus only recover country-by-day-level heterogeneity in the energy-temperature response due to income. When constructing impact estimates (*Supplementary Section* B.4), we therefore use country-level income projections, but gridded, high-resolution climate projections.

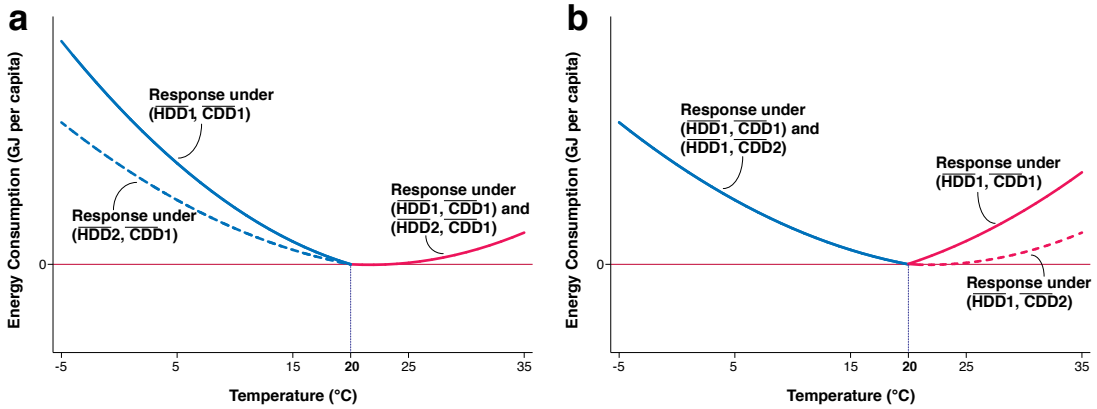

Figure B.2: Modeling adaptation to long-run climate. The schematics above illustrate how we model adaptation to long-run climate separately for two sides of the energy-temperature response (below and above 20° C), through long-run average heating degree day (HDD) and cooling degree day (CDD) measures. Panel **a** illustrates hypothetical responses under two different long-run average HDD values ($\overline{HDD1}$ and $\overline{HDD2}$), holding fixed the long-run average CDD value at $\overline{CDD1}$. Changing the long-run average HDD value from $\overline{HDD1}$ to $\overline{HDD2}$ only alters the response to temperatures less than 20° C. Similarly, Panel **b** illustrates hypothetical responses under two different long-run average CDD values ($\overline{CDD1}$ and $\overline{CDD2}$), holding fixed the long-run average HDD value at $\overline{HDD1}$. Changing the long-run average CDD value from $\overline{CDD1}$ to $\overline{CDD2}$ only alters the response to temperatures $\geq$ 20° C.

$$
\begin{aligned}
E_{jtc} &= f_c(\widetilde{\boldsymbol{T}}_{jt} \mid \overline{LogGDPPC}_{jt}, \overline{CDD}_j, \overline{HDD}_j) + g_c(\widetilde{\boldsymbol{P}}_{jt}) + \alpha_{jic} + \delta_{wtc} + \varepsilon_{jtc} \\
&= \underbrace{\boldsymbol{\beta}_c \cdot \widetilde{\boldsymbol{T}}_{jt}}_{\text{Effect of temperature}} \\
&+ \underbrace{[\boldsymbol{\eta}_{1c} \cdot \widetilde{\boldsymbol{T}}_{jt}](\bar{I}_c - \overline{LogGDPPC}_{jt})\mathbf{I}_{\overline{LogGDPPC}_{jt}<\bar{I}_c} + [\boldsymbol{\eta}_{2c} \cdot \widetilde{\boldsymbol{T}}_{jt}](\overline{LogGDPPC}_{jt} - \bar{I}_c)\mathbf{I}_{\overline{LogGDPPC}_{jt}\geq\bar{I}_c}}_{\text{Effect of income growth on energy-temperature response}} \\
&+ \underbrace{\boldsymbol{\gamma}_c \cdot \left[\boldsymbol{T} \times \widetilde{\overline{CDD}}\right]_{jt}}_{\substack{\text{Effect of climate-driven adaptation} \\ \text{on energy-temperature response} \\ \text{for days} \geq 20^\circ \text{ C}}} + \underbrace{\boldsymbol{\lambda}_c \cdot \left[\boldsymbol{T} \times \widetilde{\overline{HDD}}\right]_{jt}}_{\substack{\text{Effect of climate-driven adaptation} \\ \text{on energy-temperature response} \\ \text{for days} < 20^\circ \text{ C}}} \\
&+ \underbrace{\left[\kappa_{1c}\overline{LogGDPPC}_{jt} + \phi_1\right]\mathbf{I}_{\overline{LogGDPPC}_{jt}<\bar{I}_c} + \left[\kappa_{2c}\overline{LogGDPPC}_{jt} + \phi_2\right]\mathbf{I}_{\overline{LogGDPPC}_{jt}\geq\bar{I}_c}}_{\text{Direct effect of income on per capita energy consumption}} \\
&+ \underbrace{\boldsymbol{\theta}_c \cdot \widetilde{\boldsymbol{P}}_{jt}}_{\text{Precipitation controls}} + \underbrace{\alpha_{jic} + \delta_{wtc}}_{\text{Fixed effects}} + \underbrace{\varepsilon_{jtc}}_{\text{Error term}}, \qquad \text{(B.6)}
\end{aligned}
$$

where $\bar{I}_c$ denotes the income knot point for category c, and $\mathbf{I}_{\overline{LogGDPPC}_{jt}<\bar{I}_c}$ and $\mathbf{I}_{\overline{LogGDPPC}_{jt}\geq\bar{I}_c}$ are indicator variables for whether $\overline{LogGDPPC}$ in country j, year t, is $<$ or $\geq$ the category c income knot point. We estimate this model in first-differences using inverse variance weighting (*Supplementary Section* A.1 and B.1).

Equation B.6 relies on both year-to-year variation in temperature and income within locations and cross-sectional variation in long-run climate between locations. We rely on cross-sectional variation to identify the climate interaction effects because each location has not experienced an alternative long-run climate (within our sample) that could be exploited to identify these effects . As a result, the case for causally interpreting the coefficients capturing climate interactions in Equation B.6 is weaker than for other coeffcients in Equation B.6 and those in Equation B.1. Moreover, while we rely on within-location year-to-year variation in income to identify the effects of income, there may exist unobserved location-specific, time-varying factors affecting energy consumption that are correlated with fluctuations in income (e.g., reliability of electricity supply), posing a potential threat to identification. However, we nonetheless view the estimates from Equation B.6 as informative, since our objects of interest are the interactions of income and climate with temperature, and not their direct effect on the level of energy consumption. Although unobserved factors surely affect the level of energy consumption, their potential influence on its sensitivity to temperature is less direct, particularly after adjustment for income and climate.

The matrices in main text Figure 1c summarize the results of estimating Equation B.6, with each cell in a matrix displaying a predicted energy-temperature response evaluated at a particular point in the income $\times$ long-run climate space within the estimation sample. The cells are ordered vertically by $\overline{LogGDPPC}$ terciles (increasingly rich from bottom to top) and horizontally by $\overline{CDD}$ terciles (increasingly warm climate from left to right). The predicted energy- temperature response function in each cell is evaluated at the mean values of $\overline{LogGDPPC}$, $\overline{CDD}$, and $\overline{HDD}$ within their respective terciles.

We use the estimated parameters from Equation B.6 to extrapolate energy-temperature responses across locations over time based on projected future incomes and climate (this procedure is detailed in *Methods Step 3*). Extended Data Figure 3 demonstrates the overlap in the joint income-climate distributions at 2010 and 2090. Although the future distribution is shifted towards higher incomes, greater cooling degree days, and fewer heating degree days, the substantial overlap in the two distributions allows for credible extrapolation of energy-temperature responses into the future.

B.4 Projecting the energy consumption impacts of climate change

To estimate future per capita energy consumption impacts for each fuel category c and impact region r in country j for each year from 2015 to 2099, we apply a set of probabilistic climate change projections to the spatially and temporally heterogenous energy-temperature responses described above (and detailed in *Methods Step 3*). The distribution of future daily average temperatures under a given emissions scenario (RCP8.5 or RCP4.5) is obtained from the 33 projections in the SMME (*Supplementary Section* A.2.3).

Let $\widetilde{\boldsymbol{T}}_{rjt}$ represent a vector containing impact region-by-year aggregations of nonlinear grid-cell-level transformations of daily temperature in a future year t, under a warmer climate. In contrast, let $\widetilde{\boldsymbol{T}}_{rjt_0}$ represent the counterfactual temperature vector for the same impact region under a climatology that is the same as that of a historical baseline period t_0. These vectors are constructed in exactly the same way as is done for the temperature vectors used in estimating Equation B.6, except that we take a weighted aggregation only over grid cells z within the impact region rather than the entire country (*Methods Step 2*; *Supplementary Section* A.2.4).

The impact of climate change on annual per capita consumption in fuel category c is expressed as the estimated change in consumption relative to a no-climate-change counterfactual in which the future climatology is the same as in t_0. The precise form of Equation 4 (*Methods*) with which we project impacts is thus:

$$
\begin{aligned}
ImpactOfClimateChangePerCapita_{crjt} = \quad & \underbrace{\widehat{f}_c(\widetilde{\boldsymbol{T}}_{rjt} \mid \overline{LogGDPPC}_{jt}, \overline{CDD}_{rjt}, \overline{HDD}_{rjt})}_{\substack{\text{Temperature-induced per capita energy consumption under climate change} \\ \text{(with income growth and climate-driven adaptation)}}} \\
& - \underbrace{\widehat{f}_c(\widetilde{\boldsymbol{T}}_{rjt_0} \mid \overline{LogGDPPC}_{jt}, \overline{CDD}_{rjt_0}, \overline{HDD}_{rjt_0})}_{\substack{\text{Temperature-induced per capita energy consumption without climate change} \\ \text{(with income growth)}}} \\
= \Big[& \widehat{\boldsymbol{\beta}_c} \cdot \widetilde{\boldsymbol{T}}_{rjt} \\
& + [\widehat{\boldsymbol{\eta}_{1c}} \cdot \widetilde{\boldsymbol{T}}_{rjt}](\bar{I}_c - \overline{LogGDPPC}_{jt})\mathbf{I}_{\overline{LogGDPPC}_{jt} < \bar{I}_c} + [\widehat{\boldsymbol{\eta}_{2c}} \cdot \widetilde{\boldsymbol{T}}_{rjt}](\overline{LogGDPPC}_{jt} - \bar{I}_c)\mathbf{I}_{\overline{LogGDPPC}_{jt} \geq \bar{I}_c} \\
& + \underbrace{\widehat{\boldsymbol{\gamma}_c} \cdot \left[\boldsymbol{T} \times \widetilde{\overline{CDD}}\right]_{rjt} + \widehat{\boldsymbol{\lambda}_c} \cdot \left[\boldsymbol{T} \times \widetilde{\overline{HDD}}\right]_{rjt} \Big]}_{\substack{\text{Temperature-induced per capita energy consumption under climate change} \\ \text{(with income growth and climate-driven adaptation)}}} \\
- \Big[& \widehat{\boldsymbol{\beta}_c} \cdot \widetilde{\boldsymbol{T}}_{rjt_0} \\
& + [\widehat{\boldsymbol{\eta}_{1c}} \cdot \widetilde{\boldsymbol{T}}_{rjt_0}](\bar{I}_c - \overline{LogGDPPC}_{jt})\mathbf{I}_{\overline{LogGDPPC}_{jt} < \bar{I}_c} + [\widehat{\boldsymbol{\eta}_{2c}} \cdot \widetilde{\boldsymbol{T}}_{rjt_0}](\overline{LogGDPPC}_{jt} - \bar{I}_c)\mathbf{I}_{\overline{LogGDPPC}_{jt} \geq \bar{I}_c} \\
& + \underbrace{\widehat{\boldsymbol{\gamma}_c} \cdot \left[\boldsymbol{T} \times \widetilde{\overline{CDD}}\right]_{rjt_0} + \widehat{\boldsymbol{\lambda}_c} \cdot \left[\boldsymbol{T} \times \widetilde{\overline{HDD}}\right]_{rjt_0} \Big]}_{\substack{\text{Temperature-induced per capita energy consumption without climate change} \\ \text{(with income growth)}}} \quad ,
\end{aligned}
\tag{B.7}
$$

where the $\widehat{\ }$ denotes estimated objects from Equation B.6, and $\overline{LogGDPPC}_{jt}$, $\overline{CDD}_{rjt}$, and $\overline{HDD}_{rjt}$ denote 15-year moving averages of the covariates for impact region r in country j and future year t.[17] The object $ImpactOfClimateChangePerCapita_{crt}$ rep-

[17] Because impact regions are small in area, with many being smaller than a single grid cell, we generate the multiplicative interactions between the daily temperature and $\overline{CDD}$ directly at the impact region scale. Formally $\left[\boldsymbol{T} \times \widetilde{\overline{CDD}}\right]_{rjt}$ is calculated as

resents the change in annual per-capita electricity or other fuels consumption due to a shift in the temperature distribution under climate change, accounting for the evolution of energy-temperature responses as locations warm and incomes rise. It isolates the *additional* impact of climate change net of other factors (e.g. income) that will change in the future. The no-climate-change counterfactual is constructed to be identical in every way, except for the climate, and is therefore evaluated at the future level of income. However, we do not allow $\overline{CDD}$ and $\overline{HDD}$ values to evolve beyond those of a historical baseline t_0.

We construct estimates of Equation B.7 for all impact regions up to 2099 under emissions scenarios RCP8.5 and RCP4.5, using each of the 33 climate projections in the SMME (Figure 2 in the main text). In addition, to highlight the critical importance of income growth and climate-driven adaptation in shaping future energy-temperature responses, we also display a "no-adaptation" impact projection in which energy-temperature responses $\widehat{f}_c(\cdot)$ are determined solely by an impact region's income, $\overline{CDD}$, and $\overline{HDD}$ values in the baseline t_0 (*Methods* Equation 5).

In implementing all projections, we define the baseline period t_0 as having the climatology of 1981-2005. However, in order to reflect the present-day extent of adaptation, we take the year 2015 as the baseline for income and climate covariates ($\overline{LogGDPPC}$, $\overline{CDD}$, and $\overline{HDD}$).[18] In addition, we normalize impacts of climate change to be zero on average between the years 2001 and 2010.

B.5 Accounting for uncertainty in projected energy consumption impacts of climate change

An important feature of our analysis is to develop estimates of the energy consumption impacts of climate change that reflect the uncertainty inherent in these future projections. This uncertainty arises from two distinct sources– climatological and econometric. The confidence intervals displayed in Figure 2c in the main text, as well as the kernel density plots in Figure 3a and confidence intervals in Figure 3b, represent the combined uncertainty from both these sources.

To account for uncertainty in the climate system, we construct estimates of the energy consumption impacts of future climate change (Equation 4 in *Methods*) for each of 33 distinct climate projections in the surrogate model mixed ensemble.[19] Distributions

$\left[\overline{CDD}_{rjt}\sum_{d=1}^{365}\sum_{z\in r} w_{zj}(T^1_{zjdt}-20)\mathbf{I}_{T_{zjdt}\geq 20}, \overline{CDD}_{rjt}\sum_{d=1}^{365}\sum_{z\in j} w_{zj}(T^2_{zjdt}-20^2)\mathbf{I}_{T_{zjdt}\geq 20}\right]$. The multiplicative interactions involving $\overline{HDD}$ are similarly generated.

[18] Income projections of the SSPs are available in 5-year increments, with 2015 being the most recent historical year available.

[19] Note that while the surrogate model mixed ensemble fully represents the tails of the climate sensitivity distribution (*Methods Step 1*; *Supplementary Section* A.2.3), there remain important sources of climate uncertainty that are not captured in our projections. These include some climate feedbacks that may amplify the increase of global mean surface temperature, as well as some factors affecting local climate that are poorly simulated by GCMs.

of climate change impacts are provided by weighting across the 33 projections using the weights listed in Extended Data Figure 2b. Furthermore, independent of physical uncertainty, an important second source of uncertainty arises from the econometric estimation of Equation B.6. To account for this econometric uncertainty, we apply the delta method[73] to characterize the Gaussian distribution of impacts (*Methods* Equation 4) under each of the 33 climate projections. Finally, to characterize the full distribution of impacts across both climate and econometric uncertainty, we construct the mixture distribution of these 33 Gaussian distributions[20] using Newton's method.[88]

The confidence intervals for the global impact time series shown in Figure 2c and Figure 3b in the main text are derived from quantiles of such mixture distributions. Importantly, the same method to characterize uncertainty can also be applied to impacts for individual impact regions, as illustrated by the kernel density plots for selected impact regions in Figure 3a.

[20] Probability weights for each of the 33 climate projections are used in the construction of the mixture distribution (*Supplementary Section* A.2.3).[43]

C Valuing impacts

To monetize the projected impacts of climate change on energy consumption, we apply geographically-specific real prices for electricity and other fuels to the projected quantity impacts constructed from Equation B.7, thus reflecting differential costs across geographies and fuels.[21] We consider a range of future price scenarios, constructed either from direct extrapolation of present-day price statistics or from price projections generated by integrated assessment models (IAMs).

C.1 Extrapolating present-day prices

For scenarios based on direct extrapolation (e.g., Subpanel I in Figure 4e in the main text), impacts on electricity consumption are valued using an average cost of electricity generation, which the IEA's *World Energy Outlook 2017* provides globally as of 2016 at the country or world region level.[22] Impacts on other fuels consumption are valued using residential and non-residential end-user prices excluding taxes, which the IEA's *Energy Prices and Taxes* dataset provides for coal, oil, and natural gas fuels in 55 countries as of 2012.[23] Countries that lack price data for a given fuel are assigned the global average price for that fuel. To obtain a price for the pooled, multi-fuel "other fuels" category, we weight the prices of the individual fuels according to their shares in a country's overall "other fuels" consumption as of 2012 (the most recent year for which consumption data are available).[24] Thus, each country receives unique prices at which its impacts on other fuels consumption are valued.[25] To extrapolate prices into the future, we consider three annual price growth trajectories: a moderate growth trajectory of 1.4% annual price growth (equal to the historical growth of US real energy prices), a stagnant trajectory of 0% annual price growth, and a high growth trajectory of 3% annual price growth.[26]

[21] All prices are converted to 2019 USD PPP, the unit in which we express damages and partial SCC estimates.

[22] Costs are specified for the following geographies: Japan, European Union, Korea, Brazil, Australia, Mexico, Southeast Asia, Middle East, India, Africa, United States, China, Canada, Russia. When a cost is not available specific to a particular geography we extend these costs based on UN world region classifications: Oceania receives the Australia cost, N., S., and W. Europe receive the EU cost, E. Europe receives the Russia cost, Central America/Caribbean receive the Mexico cost, S. America receives the Brazil cost, N. Africa receives the Middle East cost, and S. Asia receives the India cost.

[23] We take a weighted average of residential and non-residential prices, with a weight of 16% on residential and 84% on non-residential. These weights are determined based on the average share of consumption in these two sectors in the set of 55 countries where a sectoral breakdown is available.

[24] Although our consumption data do cover fuels besides coal, oil, and natural gas (including solar, geothermal, and biofuels), no price data are available for fuels other than coal, oil, and natural gas. We therefore extend the weighted average price to the remaining fuels.

[25] Even countries that are assigned the global average price for the individual fuels will differ in the shares of each fuel in their other fuels consumption mix.

[26] These trajectories apply globally to prices for both electricity and other fuels. The 1.4% growth trajectory is informed by US price data on end-use energy average prices from 1970-2015, taken from the *State Energy Data System* of the U.S. Energy Information Administration. The IEA's *Energy Prices and Taxes* dataset also provides country/fuel historical price time series for OECD as well as developing

C.2 Price projections from IAMs

As a complement to price scenarios extrapolated from present-day prices, we also consider price scenarios based on projections of multiple IAMs. IAMs simulate the entire energy system and determine energy prices by equilibrating supply and demand. We obtain price projections of IAMs from IIASA's Scenario Explorer database.[27] This database contains output from 416 IAM × scenario combinations, of which 155 include price projections for electricity and other fuels as part of their output. To monetize impacts under RCP8.5, we limit ourselves to scenarios that do not posit any policies to mitigate greenhouse gas emissions (e.g. carbon price). There are 5 IAM × scenario combinations that satisfy this requirement. To monetize impacts under RCP4.5, we identify a counterpart scenario for each of these combinations that is broadly consistent with RCP4.5. Table C.1 lists the IAM × scenario combinations whose price projections we utilize for monetizing impacts under RCP8.5 and RCP4.5.

IAM	Scenario for RCP8.5	Scenario for RCP4.5
WITCH-GLOBIOM 4.2	ADVANCE_NoPolicy	ADVANCE_2030_WB2C
REMIND 1.7	ADVANCE_NoPolicy	ADVANCE_2030_WB2C
REMIND 1.7	CEMICS-Ref	CEMICS-2.0-CDR8
MERGE-ETL 6.0	BAU	DAC2_66
REMIND-MAgPIE 1.7-3.0	SMP_REF_Def	SMP_2C_Def

Table C.1: IAMs and scenarios used for monetizing impacts under RCP8.5 and RCP4.5. This table lists IAMs and associated scenarios whose price projections we use to monetize the projected impacts of climate change on energy consumption. IAMs and scenarios were selected from IIASA's Scenario Explorer database,[67] based on availability of future price projections and suitability for RCP8.5 and RCP4.5 emissions trajectories.

Every IAM × scenario reports electricity, oil, coal, natural gas, and biofuels prices for 6 world regions up to 2100.[28] To obtain a price for the "other fuels" category, we weight the prices of the individual fuels according to their shares in a region's overall "other fuels" consumption in each year, where the consumption levels for years up to 2100 are reported by the IAM × scenario.

Panel b of Extended Data Figure 5 presents the time series of total global monetized impacts under RCP8.5 assuming various price trajectories, while the Panel a does the

countries (including China, India, Brazil, and Indonesia). Although these time series are of variable length and not comprehensive across fuels for many countries, they exhibit a median annual price growth of 0.64%, with an interquartile range of -0.46% to 2.13%. Thus a 0%-3% price growth range is broadly consistent with the range of historical price growth in various countries/fuels.

[27] https://data.ene.iiasa.ac.at/iamc-1.5c-explorer/#/workspaces.

[28] The 6 regions are OECD 1990 and EU, Eastern Europe and former Soviet Union, Middle East and Africa, Latin America, Asia, and Rest of the World. Prices are available at 5-year intervals and are linearly interpolated for the intervening years.

same for RCP4.5.[29] Regardless of the emissions scenario or assumed price trajectory, end-of-century damages (i.e. net savings) represent a minute fraction of the US $353 trillion end-of-century global GDP projected under SSP3. For both end-of-century global cost estimates (Extended Data Figure 5) and partial SCC values (RCP8.5, 2% discount rate, see Extended Data Table 1), our 0% and 3% price growth trajectories provide lower and upper bounds, respectively, for the magnitude of estimates. All estimates based on IAM price projections, as well as the 1.4% price growth trajectory, fall within these bounds. For transparency and simplicity, we highlight results under 1.4% price growth in the main text, while reporting SCC central estimate ranges across all price scenarios (Figure 4e, Subpanel II).[30]

[29] The panels display global aggregations of monetized per-capita annual impacts projected in every impact region in a given year.

[30] SCC central estimates and 5^{th}-95^{th} percentile ranges for each price scenario are presented in Extended Data Tables 1 and 2.

D Damage function estimation

As described in *Methods Step 4*, we pool empirical estimates of climate change impacts constructed using Equation B.7 to fit global energy damage functions. These damage functions express global energy consumption costs of climate change as a function of the change in global mean surface temperature relative to the 2001-2010 average level (ΔGMST).[4] Summarizing the economic costs of all impacts measured in the detailed empirical analysis, these functions can be differentiated everywhere, allowing for marginal costs of a CO_2 impulse to be computed for any global climate trajectory. Due to differences in the availability of climate and socioeconomic projections pre- and post-2100, there are some important differences in our approach for calculation of damage functions before and after 2100.

Computing damage functions through 2100 As detailed in *Methods Step 4*, we estimate time-varying damage functions for all years t prior to 2100 directly from the high-resolution climate change impact projections described in Supplementary Section B.4 and converted to dollar values as described in Supplementary Section C. To construct a damage function for year t, we pool all simulated damage estimates (globally summed across 24,378 impact regions and converted to dollar value) within a 5-year window of t and estimate the quadratic damage function shown in Equation 6 (*Methods*).[31] Because the underlying population distribution and level of per capita income are evolving over time, the shape of our estimated damage functions change throughout the 21^{st} century (see Figure 3d in main text).

Computing damage functions after 2100 Data limitations in climate and socioeconomic projections beyond end-of-century necessitate an alternative approach to estimating post-2100 damage functions. Only 6 of the 21 GCMs that we use to build our surrogate model mixed ensemble are run by their respective modeling teams to simulate the climate after the year 2100 for both RCP scenarios, and post-2100 data are not available in the NEX-GDDP downscaled and bias-corrected projections that we use for generating high-resolution impact projections (*Supplementary Section*, A.2.2). Furthermore, the SSPs needed to project future incomes and demographics also end in 2100. Although one approach is to simply end economic cost calculations in 2100,[18] neglecting post-2100 damages is a substantial omission as a large fraction of costs, in net present value, are thought to occur after 2100 at 3% discount rates.[89]

To estimate post 2100-damages, we follow the method in ref. [17] to extrapolate changes in the damage function beyond 2100 using the observed evolution of damages in the last fifteen years of the 21^{st} century. To implement this extrapolation, we pool values D_{tlps} from 2085-2099 and estimate a quadratic model similar to Equation 6 (*Methods*), but

[31] Because damage functions are intended to explicitly model damages conditional on ΔGMST and not to integrate over ΔGMST, we do not utilize climate model weights (Extended Data Figure 2b) in their estimation.

interacting each term linearly with year t.[32] This allows us to estimate a damage surface as a parametric function of time. We then predict extrapolated damage functions for all years after 2100, smoothly transitioning from our flexible climate model-based damage functions prior to 2100.[33]

Figure 3d in the main text illustrates damage functions every 10 years prior to 2100, as well as extrapolated damage functions for the years 2150, 2200, 2250, and 2300. Extrapolated damages continue to become more steeply negative post-2100, as they did pre-2100.[34]

Damage functions without income growth or climate adaptation The damage functions displayed in Figure 3c-d in the main text are based on empirical estimates of climate change impacts constructed using Equation B.7, and thus reflect the effects of income growth and climate adaptation on the energy-temperature response. In Figure D.1, we find that ignoring the effects of income growth and climate adaptation on the energy-temperature response would have substantially underestimated the steepness of the separate damage functions for electricity and other fuels. The steepness of the total energy expenditure damage function would have also been underestimated, but to a lesser extent. This is because ignoring income growth and climate adaptation would reduce projected gains to electricity consumption, but also reduce projected savings of other fuels consumption (see also Figure 2c in main text). Due to these countervailing effects, the total expenditure damage function is less affected than the damage functions by fuel.

Figure D.1 displays damage functions based on "no adaptation" impact estimates constructed using *Methods* Equation 5. As in Figure 3c-d in the main text, damages are slightly quadratic in GMST anomaly, although essentially linear. However, an additional +1° ΔGMST warming at end-of-century (relative to 2001-2010 average) *reduces* annual consumption of electricity by 0.33 EJ[35] (compared to an *increase* of 4.54 EJ in Figure 3c) and reduces the consumption of other fuels by only 2.28 EJ (compared to a reduction of 11.28 EJ in Figure 3c), causing a net reduction in energy expenditures by $108 billion (compared to $176 billion in Figure 3c). The differences between the damage relationships

[32] The specific interaction model we estimate is: $D(\Delta GMST, t)_{tlps} = \nu_0 + \nu_1 \Delta GMST_{tlp} \times t + \nu_2 \Delta GMST^2_{tlp} \times t + \varepsilon_{tlps}$.

[33] Furthemore, we also separately estimate a time-interacted regression for each of 19 quantiles (i.e. every 5^{th} percentile from the 5^{th} to 95^{th}), which we use to predict these quantiles of the damage functions for years after 2100. See *Methods Step 4* for details.

[34] Constructing damage functions using damage estimates denominated as a share of GDP yields essentially equivalent damage functions up to 2100. However, the lack of GDP projections post-2100 prevents us from computing such damage functions post-2100 in a form that can be used to calculate an SCC. Future research should refine the characterization of post-2100 damage functions by incorporating improvements in climate, population, and income projections as they become available.

[35] This reduction occurs because present-day low-income locations in the tropics would not be projected to increase electricity consumption due to warming, if the effects of future income growth and climate adaptation on the electricity-temperature response are ignored. In contrast, present-day high-income locations at high latitudes would still be projected to save electricity as warming reduces the number of extreme cold days (Figure 1 in main text).

in Figure 3c-d in the main text and Figure D.1, underscore the importance of incorporating the effects of income growth and climate adaptation on energy-temperature responses.

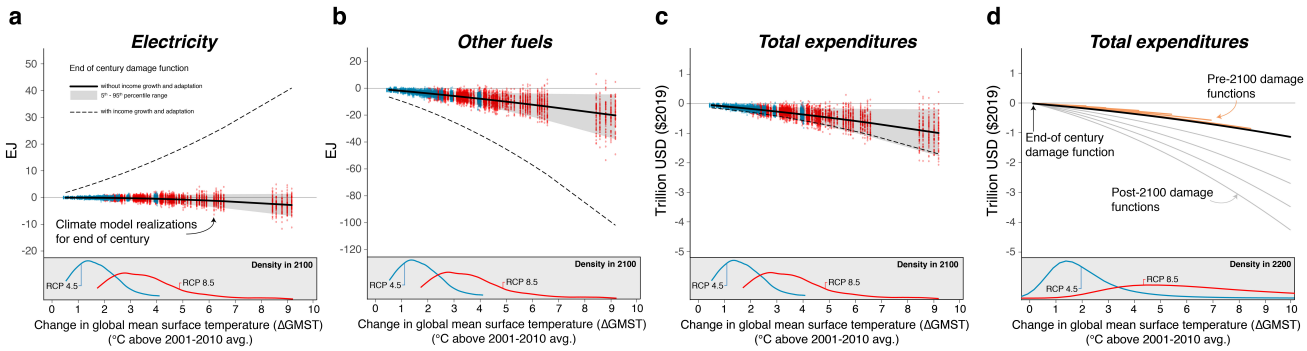

Figure D.1: Global energy damage functions, without income growth or climate adaptation Total global electricity consumption impacts (**a**), other fuels consumption impacts (**b**), and changes in total energy expenditures (**c**) at end-of-century (all assuming no income growth or climate adaptation) are indexed against the global mean surface temperature anomaly (ΔGMST) realized in each climate model simulation (blue dots=RCP 4.5; red dots=RCP 8.5; see *Methods Step 4*). Solid black curves depict the damage functions estimated from these points; shaded areas indicate the range between 5^{th} and 95^{th} quantiles (*Methods Step 4*). To contrast, the dashed black curves depict damage functions that incorporate the effects of income growth and climate adaptation on the energy-temperature response (also depicted in Figure 3c). Probability density functions below display the distribution of ΔGMST anomalies at end of century in each emissions scenario across all 33 climate models and model surrogates. Damage functions that evolve over time (**d**) are estimated up to 2100, and their continuing evolution extrapolated forward to 2300. Orange curves depict damage functions for every 10 years pre-2100; the black curve depicts the end-of-century damage function; grey curves depict damage functions for every 50 years post-2100, all assuming no income growth or climate adaptation.

E Calculation of an energy consumption partial social cost of carbon using a simple climate model

In principle, one could compute an energy partial social cost of carbon (SCC) estimate by perturbing each global climate model (GCM) in the surrogate model mixed ensemble (SMME) with a pulse of CO_2 and projecting energy consumption for each location in both the original and perturbed simulations. However, in practice, such a procedure would prevent the calculation of an SCC for any climate trajectory that did not exactly coincide with one of the 33 models, and would also be prohibitively costly from a computational standpoint. Instead, we rely on a probabilistic, simple climate-carbon cycle model (hereafter, "simple climate model"), in combination with our empirically-derived damage functions, to construct energy partial SCC estimates. We detail this implementation here.

E.1 Set up of the climate module using a simple climate model

A core component of any analysis of the SCC is the climate module used to estimate both the baseline climate and the response of the climate system to a marginal change in greenhouse gas emissions. The Finite Amplitude Impulse Response (FAIR) model[25,74] satisfies key criteria for such a module, including those outlined by the National Academies of Sciences, Engineering, and Medicine.[6] In particular, the National Academies recommends that the climate module be transparent, simple, and "consistent with the current, peer-reviewed scientific understanding of the relationships over time between CO_2 emissions, atmospheric CO_2 concentrations, and CO_2-induced global mean surface temperature change, including their uncertainty" [6, p. 88]. For this last criterion, the authors recommend that the module be "assessed on the basis of its response to long-term forcing trajectories (specifically, trajectories designed to assess equilibrium climate sensitivity, transient climate response and transient climate response to emissions, as well as historical and high- and low-emissions scenarios) and its response to a pulse of CO_2 emissions." The authors specifically point to the FAIR model as an example of a model that is structurally capable of meeting all these criteria.

The FAIR model is defined by five equations that represent the evolution of global mean variables over time t. Global mean surface temperature $GMST$ is the sum of two temperature variables, T_0 and T_1, representing the slow and fast climate system response to forcing F:

$$\frac{dT_i}{dt} = \frac{q_i F - T_i}{d_i}, i \in \{0, 1\}, \tag{E.1}$$

where the q_i values collectively define the equilibrium climate sensitivity (ECS), and where the d_i values (the thermal adjustment times) along with q_i define the transient climate response (TCR). The ECS is the sensitivity of the climate (as measured by GMST increases) to a doubling of atmospheric CO_2, relative to some initial state. The TCR is

the average temperature response to a doubling of CO_2 in which the CO_2 increases by 1% each year. The ECS is larger than the TCR, as it captures the time taken for the climate system to fully adjust to increased CO_2.

The CO_2 concentration above the pre-industrial baseline, R, is the sum of four fractions, R_j, representing different uptake timescales:

$$\frac{dR_j}{dt} = a_j E - \frac{R_j}{\alpha_j \tau_j}, j \in \{0, 1, 2, 3\} \tag{E.2}$$

where E is the CO_2 emissions rate, a_j values represent the fraction of emissions that enter each atmospheric fraction, τ_j values represent the base uptake time scale for each fraction, and where α_j is a state-dependent coefficient that reflects feedbacks from temperature onto uptake timescales. The remaining three equations describe forcing F as a function of R and of exogenous non-CO_2 forcing, and α as a function of global mean surface temperature and atmospheric CO_2 concentrations.[25,74]

We obtain the latest release of the FAIR model, which was version 1.3.2 at the time of computation, from its online repository.[36] As described below in Section E.2, we develop a methodology to generate energy partial SCC estimates that capture uncertainty in climate sensitivity by varying four core parameters in FAIR: the equilibrium climate sensitivity (ECS), the transient climate response (TCR), the short thermal adjustment time (d_2), and the time scale of rapid carbon uptake by the ocean mixed layer (τ_3). By varying these four parameters across thousands of Monte Carlo simulations, we are able to capture uncertainty in the short and long term response of temperature and the carbon cycle to changes in emissions. The median values across our uncertainty distributions (described in detail below) for each core model parameter are as follows: ECS is 2.72°C per CO_2 doubling, TCR is 1.58°C per CO_2 doubling, d_2 is 3.66 years, and τ_3 is 4.03 years. Throughout our implementation, all other parameters in FAIR are held fixed at their default values.

The two scenarios considered in this analysis, RCP4.5 and RCP8.5, represent two widely divergent emissions and climatic pathways, especially in years beyond 2050. Following the method used in previous estimates of the SCC,[6] we include projections starting in the current period (here defined as 2020) through the year 2300. Due to the long residence times of CO_2 in the atmosphere and the changes in global mean surface temperature associated with CO_2 emissions, SCC estimates can vary significantly depending on the definition of this window, especially when low discount rates are applied. To illustrate the large differences across RCP scenarios, Figure E.1 shows fossil CO_2 emissions, CO_2 concentrations, total radiative forcing (the difference between incoming solar radiation and outgoing terrestrial radiation), and temperature as anomalies from FAIR's reference state, which is year 1765, for the median climate parameters listed above and under each

[36] https://github.com/OMS-NetZero/FAIR/tree/v1.3.2.

emissions scenario.

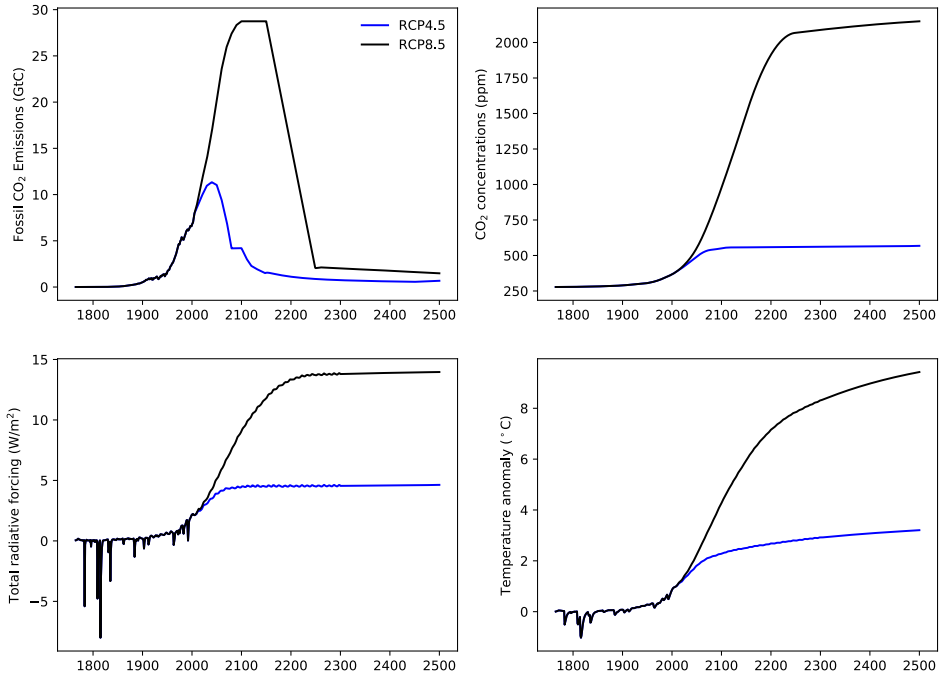

Figure E.1: Behavior of key variables in the FAIR simple climate model under median climate parameters: Each panel shows the temporal trajectory of key variables in FAIR that are used in our calculation of the social cost of carbon. The trajectories shown arise under FAIR run with median climate parameter values calculated from our uncertainty distributions for the equilibrium climate sensitivity, transient climate response, short thermal adjustment time, and time scale of rapid carbon uptake by the ocean mixed layer. The values are shown as anomalies from the year 1765, FAIR's reference state.

In order to estimate the marginal effect of CO_2 emissions, we add two additional scenarios to the "control scenarios" of RCP4.5 and RCP8.5. Each additional scenario adds a 1 GtC (3.67 Gt CO_2) pulse of fossil CO_2 emissions in 2020 to each of the control scenarios described above. The FAIR model is then run again for these pulse scenarios, resulting in a new time series of concentrations, forcing, and temperature anomalies. The difference between the control and pulse scenarios, including climate uncertainty (discussed below), is shown in the main text Figure 4A-D; as described below and in *Methods Step 5*, this difference is used to construct energy partial SCC estimates.

E.2 Methodology for capturing uncertainty in climate sensitivity within the simple climate model FAIR

The analysis described above relies solely on the simple climate model FAIR with key climate parameters set to median values that are computed from their uncertainty distributions. However, a complete study of the energy partial SCC should represent the

uncertainty in key model parameters, including the joint probability distribution of the ECS and TCR. We now discuss the development of such uncertainty distributions and the representation of climate uncertainties in FAIR.

To represent climate uncertainties, we vary TCR, ECS, d_2, and τ_3 such that our climate uncertainties conform to those of the literature. These four parameters represent the behavior of the short and long timescales of response of temperature and the carbon cycle. For TCR and ECS, we draw upon constraints from the IPCC Fifth Assessment Report (AR5);[90] for d_2 and τ_3 we follow ref.,[25,74] based on refs.[91] and.[92]

In general, we produce initial distributions of these parameters based on constraints from the literature. However, a key difference between our approach and those in the existing literature is that we explicitly model the tails of the climate sensitivity uncertainty distributions. The AR5 synthesis generally regards the 5–95% ranges of variables in the CMIP5 models as representing the "likely" range (central at least 66% probable range) due to structural uncertainty. Previous studies based on CMIP5 results[91,93] and those using the CMIP5 5–95% range of TCR and ECS as 5-95% input ranges to their models[25,74] thus show results that characterize only the central 66% of possibilities. Here we explicitly model the tails of the input and output distributions by generating TCR and ECS distributions with likely ranges as specified by the AR5 report. To preserve the expected correlation between TCR and ECS, rather than sampling ECS directly, we follow refs.[25,94] and instead sample the realized warming fraction (RWF, the ratio of TCR/ECS), which is nearly independent of TCR. We subsequently filter the parameter sets to ensure consistency with expectations regarding the initial pulse adjustment timescale (the time it takes the climate system to reach a warming peak following a pulse emission of CO_2).

Below we outline the sources used to construct the distributions of each parameter.

- **TCR:** Ref.[90] concludes that "TCR is *likely* in the range 1°C to 2.5°C... is positive and extremely unlikely greater than 3°C" (p. 1112). In IPCC terminology,[95] *likely* refers to a probability of at least 66%, *very likely* to a probability of at least 90%, and *extremely likely* to a probability of at least 95%. Thus we construct a log-normal distribution for TCR with a 17th to 83rd percentile range of 1.0-2.5 °C.

- **RWF:** An RWF likely range of 0.45 to 0.75 is approximately consistent with the ECS likely range of 1.5 – 4.5°C.[90] We construct a normal distribution for RWF following this central 66% likelihood range, and sample this distribution, along with TCR, to construct the ECS distribution as TCR/RWF.

- **ECS:** Ref.[90] concludes that "ECS is positive, *extremely unlikely* less than 1°C (high confidence), and *very unlikely* greater than 6°C (medium confidence)" (p. 1111) and *likely* between 1.5 and 4.5°C. To construct our sampling distribution, we randomly draw samples from the TCR and RWF distributions, and obtain ECS

samples by calculating TCR/RWF. The constructed ECS samples follow a log-normal distribution with a 17^{th}-83^{rd} percentile range of 1.60-4.65 °C.

- ***d_2*:** The AR5 does not assess the range of d_2. We construct our distribution of d_2 as a log-normal distribution with a 5-95^{th} percentile range of 1.6-8.4 years.[25,74]

- ***τ_3*:** Ref.[91] summarized τ_3 in three comprehensive Earth System Models (HADGEM2-ES, MPI-ESM, NCARCSM1.4), seven Earth System Models of Intermediate Complexity (EMICs), and four box-type models (ACC2, Bern-SAR, MAGICC, TOTEM). Using the mean (4.03) and standard deviation (1.79) of these values, we construct a normal distribution for τ_3.

After defining these distributions, we generate a 100,000-member ensemble of parameter sets via Monte Carlo sampling. As τ_3 should be larger than 0, we sample from a truncated normal distribution, and discard parameter sets in which $\tau_3 < 0$ or $> 2 \times 4.03$ to keep the mean of τ_3 in parameter sets consistent with the multi-model mean in ref.[91] About 2.4% of parameter sets are filtered by this constraint. Similarly, RWF must be less than 1. We therefore truncate its distribution at 1, which is the 99.4^{th} percentile, and truncate at the 0.06^{th} percentile to keep symmetry (which also removes unrealistic RWF values near and less than 0 that cause unrealistic, large and/or negative ECS values). About 1.2% of parameter sets are filtered by this constraint. After applying the τ_3 and RWF filters, which have a small overlap, we are left with 96,408 parameter samples. Using these remaining parameter samples, we evaluate model performance according to several criteria.

Our criteria for evaluating model performance are described in detail below, and summarized in Table E.1 and Figure E.2.

Initial pulse-adjustment timescale (IPT) The National Academies highlights the IPT as a measure that is important for SCC computations, yet does not provide a clear, consistent definition.[6] It "measures the initial adjustment timescale of the temperature response to a pulse emission of CO_2" and is "the time over which temperatures converge to their peak value in response to the pulse." [6, p. 88]. This could either be the time to an initial peak, or the ultimate maximum temperature change over the duration of a simulation, which also depends on simulation length. Here we catalogue multiple versions of a potential IPT metric, comparing with previous literature where appropriate.

To assess the IPT, we set CO_2 concentrations to 2010 levels (389 ppm) and hold them constant throughout the simulation. To provide an emissions baseline to which a pulse will be added, we numerically solve the CO_2 emissions pathway in FAIR to meet the CO_2 concentration pathway for each parameter sample. We then construct a pulse experiment, in which 100 GtC of CO_2 is injected instantaneously in the year 2015. The difference in temperature between the pulse and control run measures the temperature

response to a CO_2 pulse. To quantify the time to initial peak, we define the IPT as the time at which the time derivative of the temperature response first becomes negative (noting that, in many simulations, feedbacks between temperature and the carbon cycle mean that the temperature rises again after the initial peak and decline, and reaches the maximum temperature later. Therefore, the time to initial peak is not necessarily the same as the time to maximum temperature). The resulting IPT has a median of 9.0 years, with a central 90% probability range of 0–24.0 years. We drop parameter sets that lead to simulations in which the first negative time derivative of temperature occurs after 100 years post-pulse, indicative of temperatures that only increase throughout the experiment (in contrast to the simulations with an initial post-pulse decrease in temperature that begins increasing again after a time). This results in a filtering out of 112 additional parameter samples on top of the τ_3 and RWF filters, yielding a total number of post-filtering simulations of 96,306 for examination in the remaining discussion.

We also evaluate other potential metrics: the time to maximum temperature considering the full 500 year simulation, the time to maximum temperature considering just the 100 years post-pulse, and the time to maximum temperature considering 100 years post-pulse but excluding simulations reaching max at year 100. We find central 90% probable ranges of 4.0–485 (median 19.0), 4.0–100 (median 12.0), and 3.0–23.0 (median 9.0), respectively. The results of ref.[91] and other subsequent analysis[93] indicate that a peak in warming in response to a pulse emission occurs within about a decade after emission. In particular, ref.[93] estimate a central 90% range for time to peak warming of 6.6–30.7 years, with a median of 10.1 years, and 2% of simulations reaching maximum at the end of their 100-year simulations. Ref.,[93] however, do not sample from continuous distributions of ECS and TCR, but rather use narrower discrete distributions of parameters based on individual CMIP5 GCMs; thus, we expect their range to be narrower than that in our analysis. Considering the first 100-years of simulation, our median time to peak warming is comparable to ref.,[93] but spans a wider range of outcomes, as expected, with 24% of simulations reaching their peak at 100 years post-pulse (44% reach peak warming at simulation's end in year 2500).

Transient climate response to emissions (TCRE) The TCRE measures the ratio of transient warming to cumulative carbon emissions at the time of CO_2 doubling in a simulation with a 1% /year increase (year 70). TCRE is between 0.8 and 2.5°C per 1000 GtC with at least 66% probability.[90] To assess TCRE, we set up an experiment that increases CO_2 concentrations at 1%/year until CO_2 concentrations double in year 70. Again, for each parameter sample, we numerically solve the CO_2 emissions pathway in FAIR to meet the CO_2 concentration pathway. The resulting TCRE exhibits a likely range of 0.88–2.34°C per 1000 GtC, which is consistent with the central 66% probable range assessed by AR5.

Longevity of pulse warming Coupled climate-carbon cycle experiments indicate

that a majority (about 70% in the multimodel mean) of peak warming persists 500 years after emissions.[91] In our IPT experiments, the central 66% probable range is 72.9 – 137.6 percent of initial peak warming persists after 500 years.

Representative Concentration Pathway (RCP) experiments We assess the warming in the RCP experiments relative to those in the CMIP5 multi-model ensemble, noting that we compare the central 66% probability ranges from our ensemble to those of the CMIP5 5th–95th percentile range (Table E.1).

The final reduced sample set constitutes 96,306 samples as noted above, and the diagnostic metrics are essentially unchanged from the pre-filtering distributions (see Table E.1). Based on this post-filtering evaluation, we conclude that the resulting distribution is adequately consistent with our target constraints and the recommendations of the National Academies of Sciences, Engineering, and Medicine.[6] We apply the retained parameter sets to FAIR to produce climate projections that represent climactic uncertainties and are further used in calculating the SCC uncertainty, as described in the next section. The interquartile range of the final SCC values across the entire distribution of parameter sets are shown in Figure 4E in the main text.

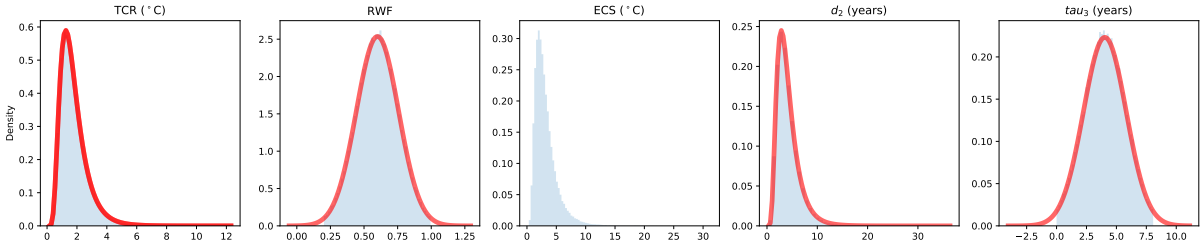

Figure E.2: Distributions of key FAIR parameters for climate sensitivity uncertainty both before and after applying constraints: Each panel indicates the distribution of a key parameter in the FAIR simple climate model, both before (red curve) and after (blue shading) the imposition of constraints described in the text. Distributions shown from left to right are: transient climate response (TCR); realized warming fraction (RWF) used to define ECS (=TCR / RWF); equilibrium climate sensitivity (ECS) shown only after applying constraints due to unrealistic values in the initial distribution occurring as RWF$\rightarrow$ 0; short thermal adjustment time (d_2); time scale of rapid carbon uptake by the ocean mixed layer (τ_3).

Parameter	*Distribution from literature*	*Pre-IPT distribution*	*Post-IPT distribution*	Distribution	*Source*
TCR (C)	[1.00, 2.50]	[1.00, 2.49]	[1.00, 2.50]	Lognormal	AR5
RWF	[0.45, 0.75]	[0.45, 0.75]	N/A	Normal	NAS (2017)
ECS (C)	[1.5, 4.5]	[1.60, 4.65]	[1.61, 4.61]	Lognormal	AR5
d_2 (years)	(1.6, 8.4)	(1.6, 8.4)	(1.6, 8.3)	Lognormal	[25,74]
τ_3 (years)	[91] point estimates	4.04 (1.07, 6.96)	4.04 (1.25, 6.79)	Normal	[91]
Key metrics					
TCRE (C/TtC)	[0.8, 2.5]	N/A	[0.88, 2.34]	Normal	AR5
Time to T_{max} (years)	(6.6, 30.7)	(4.0, 100.0)*	(4.0, 100.0)*	N/A	[93]
RCP 4.5 GMST					
$2046-2065$	1.4 [0.9, 2.0]	N/A	1.38 [0.73, 1.98] (0.51, 2.88)	Normal	AR5
$2081-2100$	1.8 [1.1, 2.6]	N/A	1.81 [0.93, 2.60] (0.65, 3.88)	Normal	AR5
$2181-2200$	2.3 [1.4, 3.1]	N/A	2.37 [1.13, 3.46] (0.78, 5.41)	Normal	AR5
$2281-2300$	2.5 [1.5, 3.5]	N/A	2.73 [1.24, 4.01] (0.85, 6.45)	Normal	AR5
RCP 8.5 GMST					
$2046-2065$	2.0 [1.4, 2.6]	N/A	2.05 [1.09, 2.90] (0.77, 4.20)	Normal	AR5
$2081-2100$	3.7 [2.6, 4.8]	N/A	3.71 [1.96, 5.31] (1.39, 7.73)	Normal	AR5
$2181-2200$	6.5 [3.3, 9.8]	N/A	7.34 [3.82, 10.60] (2.69, 15.35)	Normal	AR5
$2281-2300$	7.8 [3.0, 12.6]	N/A	8.86 [4.48, 12.84] (3.11, 18.84)	Normal	AR5

Table E.1: Comparisons of the distributions of key FAIR parameter values: This table compares the distributions of key FAIR parameter values that pass the initial pulse-adjustment timescale (IPT) constraint against the relevant distributions from the literature (included in the IPT constraint is filtering of τ_3 and RWF as specified in the text). Distributions shown are: transient climate response (TCR); realized warming fraction (RWF); equilibrium climate sensitivity (ECS); short thermal adjustment time (d_2); time scale of rapid carbon uptake by the ocean mixed layer (τ_3); transient climate response to emissions (TCRE); and the change in global mean surface temperature (GMST) from the reference period 1986-2005 at various points in the projections. Note that RWF is only used to create our ECS distribution, and so the post-IPT distribution of RWF is not reported. Distributions reported are determined by the reference values from the literature, so that different parameters have different descriptions of their associated distributions: 5 to 95% ranges are given in ( ), 17 to 83% ranges (*likely* ranges for AR5) are given in [ ], and means are given without ( ) or [ ].

* We only consider the first 100 years post-pulse.[93]

Finally, we assess the reasonableness of the "handoff" between the SMME models, with which the damage function is estimated (Equation 6 in *Methods*), and FAIR, with which future damages due to a pulse of CO_2 are calculated using the difference in temperature between the pulse and control runs. A comparison of climate sensitivity uncertainty across these two climate projections is important, as the climate sensitivity uncertainty captured in the empirically-based projections of energy damages derives from the SMME, while the uncertainty we proliferate through to the SCC relies on the simple climate model FAIR. Figure E.3 shows the distribution of GMST changes relative to 2001-2010 (ΔGMST) over time, according to the SMME (top row) and the simple climate model FAIR (bottom row). SMME data are available until the year 2100; thus, the two rows show a direct comparison between FAIR and the SMME models for these years, showing a strong amount of overlap in both RCP4.5 and RPC8.5 distributions of warming and indicating the handoff is reasonable (as would be expected based on the construction of the SMME).

E.3 Converting temperature scenarios to an energy expenditure partial SCC

We convert the temperature scenarios developed in the climate module into estimates of energy-related damages using the global damage functions described in *Methods Step 4* and in Supplementary Section D. These damage functions characterize energy expenditure impacts as a function of ΔGMST (changes in GMST relative to 2001-2010). The coefficients on these quadratic damage functions are constructed for each year from 2015 to 2300, as described in *Methods Step 4* and Supplementary Section D. We then generate annual estimates of temperature-related energy expenditure changes by applying the ΔGMST values from both the control FAIR scenarios (RCP4.5 and RCP8.5), as well as pulse scenarios, to the empirically derived damage functions. After computing energy expenditure changes associated with each scenario, we subtract each control scenario from the corresponding pulse scenario and divide by the pulse amount to estimate the marginal effect of the pulse.

Figure E.4 depicts the marginal effect of the pulse under both the RCP4.5 and RCP8.5 control scenarios. A CO_2 pulse emitted today perturbs the future trajectory of atmospheric CO_2 concentrations nonlinearly, affected by the half life of CO_2 in the atmosphere as it is stored and released in the oceans and biosphere (Figure E.4A-B). This results in future ΔGMST that deviates from the control scenario, which in turn causes a stream of energy damages in future years (Figure E.4C-D).[37] Annual damages, discounted using

[37] All time series in Figure E.4 represent the difference between a pulse scenario and control scenario. The background CO_2 concentration has a large effect on the ability of the land and ocean to absorb the marginal CO_2 pulse, hence less of the pulse is absorbed by the land and ocean in a high CO_2 background (RCP8.5) than in a low CO_2 background (RCP4.5) leading to more CO_2 remaining in the atmosphere

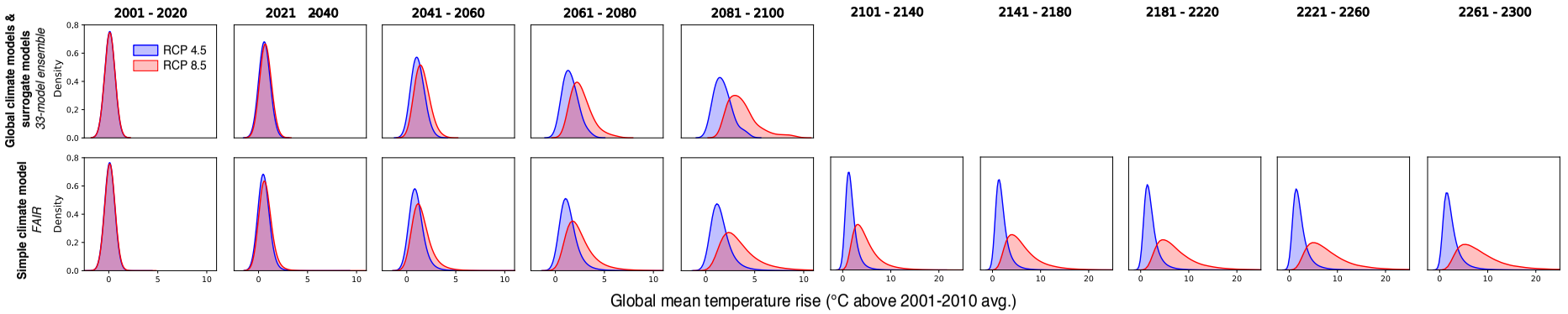

Figure E.3: Distribution of changes in global mean surface temperature from an ensemble of global climate models and surrogate models and from the simple climate model FAIR: Top row: Distribution of changes in global mean surface temperature relative to 2001-2010 average (ΔGMST) from 2001 to 2100, according to an ensemble of 33 GCMs and surrogate models that form the surrogate/model mixed ensemble (SMME). Second row: Distribution of ΔGMST from 2001 to 2300, according to 96,306 of simulation runs of the simple climate model FAIR.

either constant or Ramsey discount rates, are then summed through time to create a net present value, following Equation 7 in *Methods*. This final value is the net present value of the energy expenditure impacts caused by a marginal emission of CO_2.

Constant discount rates of 2.5%, 3%, and 5% discount rates are recommended in refs. [6,96]. However, we also include a 2% discount rate because it conservatively reflects changes in global capital markets over the last several decades;[76] the average 10-year Treasury Inflation-Indexed Security value over the available record of this index (2003-present) is just 1.01%.[75]

In addition to constant discount rates of 2%, 2.5%, 3%, and 5%, we also present results under Ramsey discounting as recommended in ref. [6].[38] In this case, we calculate a global discount rate, r_s, for each year s according the Ramsey equation $r_s = \delta + \eta g_s$, where the parameter δ measures the pure rate of time preference, g_s measures the growth rate of consumption in year s, and η is the elasticity of marginal utility of consumption. We use global per capita income growth from the SSP scenarios to obtain annual values for g_s,[39] and use 6 combinations of δ and α values, choosing from $\delta \in \{0\%, 1\%\}$ and $\eta \in \{1, 2, 3\}$. This set of values is broadly accepted in the literature, and a subset of these values can satisfy the recommendation in ref. [6] that they "produce certainty-equivalent discount rates consistent, over the next several decades, with consumption rates of interest. Achieving both objectives is not necessarily guaranteed, since the Ramsey formula is a normative formulation of discounting that may or may not match any observed interest rates when sensible values for δ, η, and g are applied.

A value of $\delta = 0\%$ implies that individuals with equal income but at different moments in time are treated equally, while a value of 1% means that damages experienced later in time are down-weighted by 1% per year, after adjusting for income. Many authors throughout economics have argued that a value of zero (or very near zero) is the only ethically reasonable choice, and such ethical judgement is required since this formulation of discounting is normative.[39][40] However, some authors nonetheless advocate a non-zero value on the grounds that a non-zero value is required to ensure the total value for the overall discount rate r is a specific value.[77] A value of 1% has been used in many contexts,[29] so we consider it as well.

in a high CO_2 world (Figure E.4B). However, a high background CO_2 also means the change in CO_2 concentration results in a relatively smaller change in radiative forcing, as radiative forcing from the marginal CO_2 pulse is proportional to the natural logarithm of the ratio of the pulse concentration change to background CO_2 concentration. This compensating effect means there is a smaller change in the temperature anomaly in a high CO_2 background (RCP8.5) than in a low CO_2 background (RCP4.5)[91] (Figure E.4C).

[38] Future work should also explore the implications of other more complex discounting procedures, such as declining discount rates.[97,98]

[39] The SSPs do not provide projections of income growth post-2100. We therefore assume that in each SSP, the annual growth rate in every year post-2100 is equal to the average annual growth rate from 2085-2099 in that SSP.

[40] Ramsey himself deemed it "ethically indefensible" to use a positive value of δ for social discounting.[47]

Based on the literature, we examine cases where the elasticity of marginal utility of consumption, η, takes values of 1, 2 or 3. Unlike δ, these values have an empirical basis in macroeconomics, with estimates generally centered around 2 and mostly falling between 1 and 3.[78–83]

A final consideration in the recommendations of ref. [6] is checking whether the values we use "produce certainty-equivalent discount rates consistent, over the next several decades, with consumption rates of interest. Examining the SSPs, which determine the global GDP growth rate we would use to compute the Ramsey discount rate, the average growth rate is 2.5% per year for 2020-2040 and 2.2% per year for 2020-2050 (since the next several decades does not precisely define what interval to consider). These values produce discount rates that generally align with a range of consumption interest rates of 2.2%-8.5%. Values around 3%-5% are likely to be more plausible for the consumption rate of interest than values near the top of this range, although as mentioned earlier, there is not a theoretical guarantee that these values should align. Nonetheless, there exist high, medium, and low values within this set that would satisfy Recommendation 6-2 in ref. [6].

E.4 Uncertainty in the energy partial SCC

We characterize uncertainty in the energy partial SCC in three ways: accounting for climate sensitivity uncertainty only, damage function uncertainty only, and full uncertainty (both climate and damage function, reported in main text Figure 4E). Here we briefly describe how these values are generated.

Energy partial SCC estimates accounting for both climate sensitivity and damage function uncertainty As described in *Methods Step 4*, damage functions are computed using estimates of the global monetized damages in each year generated from 33 climate models, two emissions scenarios, and a resampling of damage estimates that captures uncertainty in the estimation of Equation 3 (*Methods*). These multiple simulations (we draw 100 realizations of global damages for each climate model, emissions scenario, SSP trajectory, and year) give us an empirically-derived distribution of potential economic outcomes that are conditional on the ΔGMST value for the year, emissions scenario, and climate model used to generate that projection. To account for uncertainty in a single year's damage function, we pool these realizations for the associated 5-year window (see *Methods Step 4* and Supplementary Section D). We then run quantile regressions to fit quantile-specific damage functions for 19 quantiles (i.e. every 5^{th} percentile from the 5^{th} to 95^{th}). As in the mean damage function estimation, extrapolation past the year 2100 is accomplished using a time interaction model (*Supplementary Section* D). In this extrapolation, we allow each quantile to evolve over time heterogeneously, based on the observed changes over time that we estimate at the end of the 21^{st} century.

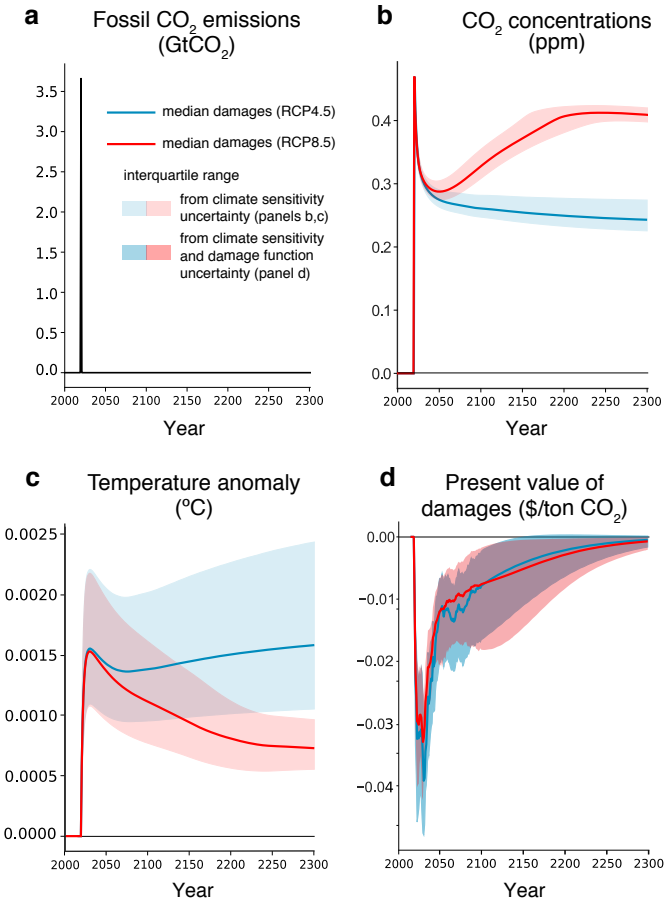

Figure E.4: The effects of a CO_2 pulse in the RCP4.5 and RCP8.5 emissions scenarios, using the FAIR simple climate model.[25,74] Effects in RCP4.5 are depicted in blue, while effects in RCP8.5 are depicted in red. Solid lines use the default configuration, shaded area is the interquartile range of projections, sampling from a constrained joint distribution of climate parameters (b-c) and also damage function quantiles (d). **(a)** A 1GtC pulse released in 2020. **(b)** The effect on atmospheric CO_2 concentrations, relative to the control scenario. **(c)** The impact on global mean surface temperature anomalies (ΔGMST). **(d)** The change in the discounted flow of energy expenditures estimated with the empirically-derived damage functions in Figure 3D (1.4% annual price growth, 2% annual discount rate). Integration of this flow is the partial social cost of carbon for energy expenditure under the given control scenario — RCP4.5 or RCP8.5 (Table E.2).

We run each quantile-specific damage function through each of the 96,306 sets of FAIR parameters and up-weight runs in order to reflect probability mass in the damage function uncertainty space. This process reflects a joint sampling from the full space of damage function uncertainty and climate sensitivity uncertainty. The relevant SCC 5^{th}-95^{th} percentile ranges are resolved from the resulting distribution of energy partial SCCs.

Energy partial SCC estimates accounting for climate sensitivity uncertainty only: To isolate uncertainty in the energy partial SCC that derives from climate sensitivity uncertainty, we run the mean damage function through each of the 96,306 sets of FAIR parameters. The corresponding SCC 5^{th}-95^{th} percentile range is resolved from the resulting distribution of energy partial SCCs.

Energy partial SCC estimates accounting for damage function uncertainty only: To isolate uncertainty in the energy partial SCC that derives from uncertainty in the damage function, we run the set of quantile-year damage functions through FAIR with each climate parameter fixed at its median value (as is done in the central energy partial SCC estimates) and up-weight runs in order to reflect probability mass in the damage function uncertainty space. The corresponding SCC 5^{th}-95^{th} percentile range is resolved from the resulting distribution of energy partial SCCs.

Table E.2 reproduces SCC estimates from Figure 4e, Subpanel I (main text) and Extended Data Table 2, with interquartile ranges separately showing the influence of climate sensitivity and damage function uncertainty.

Discount rate:	Constant $\delta = 2\%$	Constant $\delta = 2.5\%$	Constant $\delta = 3\%$	Constant $\delta = 5\%$	Ramsey $\delta = 0\%, \eta = 1$	Ramsey $\delta = 0\%, \eta = 2$	Ramsey $\delta = 0\%, \eta = 3$	Ramsey $\delta = 1\%, \eta = 1$	Ramsey $\delta = 1\%, \eta = 2$	Ramsey $\delta = 1\%, \eta = 3$
RCP 8.5	-2.27	-1.61	-1.25	-0.69	-13.93	-6.00	-2.93	-3.35	-1.90	-1.20
Climate sensitivity uncertainty	[-7.98,-0.79]	[-4.58,-0.65]	[-2.89,-0.55]	[-0.98,-0.34]	[-77.87,-2.40]	[-30.99,-1.27]	[-13.43,-0.77]	[-14.66,-0.94]	[-7.07,-0.63]	[-3.72,-0.46]
Damage function uncertainty	[-5.20,0.56]	[-3.35,0.09]	[-2.37,-0.12]	[-1.04,-0.30]	[-39.96,10.61]	[-16.58,3.98]	[-7.63,1.52]	[-8.53,1.58]	[-4.46,0.56]	[-2.57,0.14]
Full uncertainty	[-9.42,0.84]	[-5.64,0.24]	[-3.70,-0.04]	[-1.27,-0.22]	[-81.41,13.56]	[-33.28,5.17]	[-14.87,2.02]	[-16.46,2.13]	[-8.20,0.81]	[-4.45,0.25]
RCP 4.5	-1.73	-1.43	-1.21	-0.76	-4.16	-2.46	-1.60	-1.97	-1.38	-1.01
Climate sensitivity uncertainty	[-6.24,-0.68]	[-3.97,-0.61]	[-2.81,-0.54]	[-1.25,-0.36]	[-53.54,0.03]	[-21.43,-0.42]	[-9.52,-0.46]	[-10.56,-0.62]	[-5.39,-0.52]	[-3.07,-0.42]
Damage function uncertainty	[-4.51,0.36]	[-3.07,-0.07]	[-2.28,-0.26]	[-1.12,-0.36]	[-29.42,11.22]	[-12.63,3.99]	[-6.08,1.40]	[-6.90,1.41]	[-3.81,0.41]	[-2.31,0.03]
Full uncertainty	[-8.49,0.50]	[-5.31,0.00]	[-3.67,-0.17]	[-1.50,-0.27]	[-71.19,14.08]	[-28.86,4.99]	[-12.93,1.76]	[-14.37,1.77]	[-7.32,0.54]	[-4.11,0.09]

Table E.2: Social cost of energy consumption due to climate change. This table displays estimates of a social cost of carbon for excess energy expenditures under high (RCP8.5) and moderate (RCP4.5) emissions scenarios and the 1.4% annual price growth scenario. All estimates are computed using the socioeconomic scenario SSP3. Costs are discounted to the present using either a constant annual discount rate (2%, 2.5%, 3%, or 5%) or Ramsey discount rates under various values of the pure rate of time preference, δ, and elasticity of marginal utility of consumption, η (*Methods Step 5*). Brackets indicate 5^{th}-95^{th} percentile ranges that reflect climate sensitivity uncertainty, damage function uncertainty, or both (i.e. full uncertainty).

F Sensitivity of the energy consumption partial social cost of carbon

The partial SCC estimates shown in the main text and in Table E.2 depend upon a set of future price scenarios, damage function extrapolation beyond 2100, and are reported for a particular socioeconomic scenario (SSP3). In Extended Data Tables 1 and 2, we provide a range of additional partial SCC estimates under alternative future price scenarios. In this section, we provide estimates under alternative extrapolation approaches for the damage function, and multiple different socioeconomic scenarios. In all cases, we show estimates under multiple discount rates and baseline emissions trajectories.

F.1 Alternative approach to estimating post-2100 damages

We explore the importance of post-2100 extrapolation of the damage function (*Supplementary Section* D) by using an alternative approach to estimating post-2100 damages, in which we calculate partial SCC estimates using a damage function held fixed at its end-of-century shape for all years 2100-2300. With this alternative approach, most estimates of the energy consumption partial SCC remain between -$3 and -$1 (1.4% price growth scenario), indicating that extrapolation of the damage function has negligible impact on our partial SCC estimates, due in part to the important role of discounting (Table F.1).

F.2 Alternative socioeconomic scenarios

In the main text, we display climate change impact projections and estimates of the partial social cost of carbon under the socioeconomic scenario SSP3. Each SSP scenario models a different possible pathway of economic development, population growth, and demographics. Here, we show estimates of the energy consumption partial social cost of carbon under alternative scenarios (SSP1, SSP2, SSP4, and SSP5, alongside SSP3). Results from these alternative scenarios are generally similar in magnitude to those from SSP3.

	Constant				Ramsey					
Discount Rate	2%	2.5%	3%	5%	$\delta = 0\%$ $\eta = 1$	$\delta = 0\%$ $\eta = 2$	$\delta = 0\%$ $\eta = 3$	$\delta = 1\%$ $\eta = 1$	$\delta = 1\%$ $\eta = 2$	$\delta = 1\%$ $\eta = 3$
					1.4% price growth					
RCP 8.5	-1.79	-1.40	-1.15	-0.69	-5.87	-3.12	-1.84	-2.22	-1.45	-1.01
RCP 4.5	-1.83	-1.48	-1.24	-0.76	-5.28	-2.91	-1.79	-2.18	-1.47	-1.05
					0% price growth					
RCP 8.5	-0.93	-0.78	-0.68	-0.47	-2.18	-1.28	-0.84	-1.04	-0.74	-0.56
RCP 4.5	-1.00	-0.86	-0.76	-0.53	-2.06	-1.27	-0.87	-1.08	-0.79	-0.61
					3% price growth					
RCP 8.5	-4.55	-3.24	-2.45	-1.16	-20.39	-10.01	-5.40	-6.33	-3.76	-2.39
RCP 4.5	-4.36	-3.21	-2.49	-1.26	-17.64	-8.85	-4.91	-5.82	-3.56	-2.33
					MERGE-ETL 6.0 prices					
RCP 8.5	-1.18	-0.91	-0.74	-0.42	-3.97	-2.10	-1.23	-1.48	-0.95	-0.65
RCP 4.5	-1.34	-1.03	-0.84	-0.48	-4.65	-2.42	-1.40	-1.69	-1.08	-0.74
					REMIND 1.7 (ADVANCE) prices					
RCP 8.5	-5.10	-3.92	-3.16	-1.77	-17.36	-9.18	-5.36	-6.43	-4.13	-2.82
RCP 4.5	-5.52	-4.26	-3.45	-1.95	-19.03	-9.96	-5.79	-6.95	-4.46	-3.05
					REMIND 1.7 (CEMICS) prices					
RCP 8.5	-4.94	-3.78	-3.04	-1.68	-16.99	-8.96	-5.21	-6.25	-4.00	-2.72
RCP 4.5	-5.37	-4.12	-3.32	-1.85	-18.80	-9.79	-5.66	-6.80	-4.34	-2.95
					REMIND-MAgPIE 1.7-3.0 prices					
RCP 8.5	-4.86	-3.74	-3.02	-1.70	-16.45	-8.71	-5.09	-6.11	-3.93	-2.69
RCP 4.5	-5.31	-4.10	-3.33	-1.89	-18.02	-9.47	-5.52	-6.64	-4.28	-2.93
					WITCH-GLOBIOM 4.2 prices					
RCP 8.5	-4.95	-3.71	-2.93	-1.56	-18.46	-9.53	-5.42	-6.45	-4.04	-2.70
RCP 4.5	-5.06	-3.82	-3.03	-1.65	-18.94	-9.71	-5.52	-6.57	-4.13	-2.77

Table F.1: Social cost of energy consumption due to climate change under alternative approach to estimating post-2100 damages. This table displays estimates of a partial Social Cost of Carbon for excess energy expenditures under the socioeconomic scenario SSP3. Costs are discounted to the present using either a constant annual discount rate (2%, 2.5%, 3%, or 5%) or Ramsey discount rates under various values of the pure rate of time preference, δ, and elasticity of marginal utility of consumption, η (*Methods Step 5*). In contrast to the estimates in Figure 4e (main text) and Extended Data Tables 1 and 2, these estimates are calculated using a damage function held fixed at its end-of-century shape for all years 2100-2300.

	Constant				Ramsey					
Discount Rate	2%	2.5%	3%	5%	$\delta = 0\%$ $\eta = 1$	$\delta = 0\%$ $\eta = 2$	$\delta = 0\%$ $\eta = 3$	$\delta = 1\%$ $\eta = 1$	$\delta = 1\%$ $\eta = 2$	$\delta = 1\%$ $\eta = 3$
						SSP1				
RCP 4.5	-1.71	-1.45	-1.25	-0.79	-1.50	-0.76	-0.47	-1.10	-0.62	-0.41
						SSP2				
RCP 8.5	-1.35	-1.16	-1.01	-0.68	-1.46	-0.80	-0.53	-1.02	-0.65	-0.46
RCP 4.5	-1.45	-1.32	-1.18	-0.78	-1.29	-0.92	-0.61	-1.16	-0.75	-0.52
						SSP3				
RCP 8.5	-2.27	-1.61	-1.25	-0.69	-13.93	-6.00	-2.93	-3.35	-1.90	-1.20
RCP 4.5	-1.73	-1.43	-1.21	-0.76	-4.16	-2.46	-1.60	-1.97	-1.38	-1.01
						SSP4				
RCP 8.5	-2.16	-1.57	-1.23	-0.70	-7.88	-2.54	-1.11	-2.27	-1.11	-0.67
RCP 4.5	-1.90	-1.52	-1.28	-0.78	-3.96	-1.75	-0.97	-1.79	-1.05	-0.69
						SSP5				
RCP 8.5	-1.35	-1.23	-1.12	-0.80	-1.03	-0.61	-0.41	-0.88	-0.53	-0.37

Table F.2: Social cost of energy consumption due to climate change under alternative socioeconomic scenarios. This table displays estimates of a partial Social Cost of Carbon for excess energy expenditures under various socioeconomic scenarios, for the 1.4% price annual growth trajectory. For each RCP, we selected the four SSPs which, in their marker scenarios, had end-of-century CO_2 concentrations and radiative forcing changes most similar to that RCP. This resulted in our selecting SSPs 1-4 for RCP 4.5 and SSPs 2-4 for RCP 8.5. Costs are discounted to the present using either a constant annual discount rate (2%, 2.5%, 3%, or 5%) or Ramsey discount rates under various values of the pure rate of time preference, δ, and elasticity of marginal utility of consumption, η (*Methods Step 5*).

G Robustness and sensitivity checks

In this section, we explore how alternative assumptions about population distributions, income growth and climate-driven adaptation affect our projected impacts. In addition, we conduct a robustness check to address issues of data quality.

G.1 Alternative assumptions on future within-country population distributions

To construct global measures of the projected impacts of climate change, we aggregate projected per capita impacts across all 24,378 impact regions using each region's projected future population. In our main results, these impact region-level population projections are obtained by allocating projected national populations under the SSP scenarios based on current satellite-based within-country population distributions (*Supplementary Section* A.3.3). Here, we conduct a sensitivity analysis in which we use an alternative, time-varying allocation of national populations developed in ref. [66] that reflects projected urbanization.[65] Figure G.1 displays the time series of global per-capita electricity and other-fuels consumption impacts under the within-country population distributions from ref. [66]. Impacts are seen to be extremely similar to our main estimates. This is likely due to high spatial correlation of temperature within country borders and minimal covariance between temperature exposure and changing population dynamics within countries.

G.2 Alternative assumptions on the role of income growth and climate-driven adaptation

In our main results, we use the estimated coefficients from Equation B.6 in combination with high-resolution data on future incomes ($\overline{LogGDPPC}$) and climates ($\overline{HDD}$, $\overline{CDD}$) to extrapolate energy-temperature responses over time, thus capturing future changes in the responses due to income growth and climate-driven adaptation (*Supplementary Section* B.3). In conducting this extrapolation, it is necessary to make an assumption regarding the rates at which energy-temperature responses evolve with changing incomes and climates. As discussed previously, our projections rely on 15-year moving averages of $\overline{LogGDPPC}$, $\overline{HDD}$, and $\overline{CDD}$ (*Supplementary Section*, B.3).

Here, we conduct a sensitivity analysis where the speed at which energy-temperature responses change with income and climate covariates is deterministically reduced by half. This exercise is used to understand how the impacts of future climate change differ if energy-temperature responses evolve more slowly with income and climate than is estimated in the historical data.[41]

[41] Note that in our econometric estimation of Equation B.6, income is modeled as a 15-year moving average, while climate is treated as a time-invariant average over the entire sample (*Supplementary*

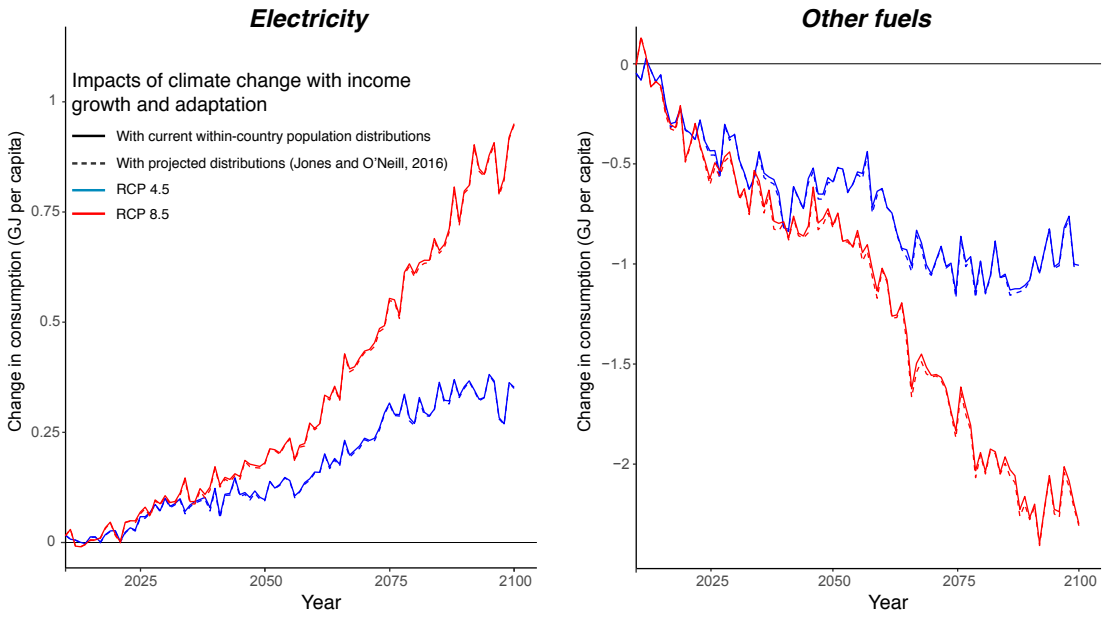

Figure G.1: Projected impacts of climate change under time-varying within-country population distributions. The dashed lines present the time series of average global energy consumption impacts of climate change (in GJ per capita), in which future national populations are allocated spatially within a country based on projections developed in ref. [66]. To contrast, the solid lines present impacts in which future national populations are allocated spatially based on current satellite-based within-country population distributions (*Supplementary Section* A.3.3). All impacts are calculated under the SSP3 socioeconomic scenario using climate projections from a single climate model (CCSM4).

In the main projection, income grows for each impact region r according to $GDPPC_{rt} = \rho_{jt} GDPPC_{r,t-1}$, where j indicates the country that region r falls into, and ρ_{jt} is a country- and year-specific growth rate given exogenously by the SSP scenarios. The moving average values of heating degree days for region r used in the main projection are specified by $\overline{HDD}_{rt} = \overline{HDD}_{r,t-1} + \Delta\overline{HDD}_{rt}$, and moving averages of cooling degree days are specified similarly. In this "slow adaptation" alternative approach, we replace income growth with $GDPPC_{rt} = \left(\frac{\rho_{jt}-1}{2} + 1\right) GDPPC_{r,t-1}$ after the year 2015, and we reduce linear change in heating degree days by replacing it with $\overline{HDD}_{rt} = \overline{HDD}_{r,t-1} + \frac{\Delta\overline{HDD}_{rt}}{2}$. The linear change in cooling degree days is similarly replaced. Note that both the main and slow-adaptation analyses generate identical incomes, heating degree days, and cooling degree days (and hence, energy-temperature responses) in 2015.

Figure G.2 displays the time series of global per-capita electricity and other-fuels consumption impacts under a slow-adaptation scenario. Impacts under slow-adaptation are seen to be considerable lower in magnitude than our main estimates.

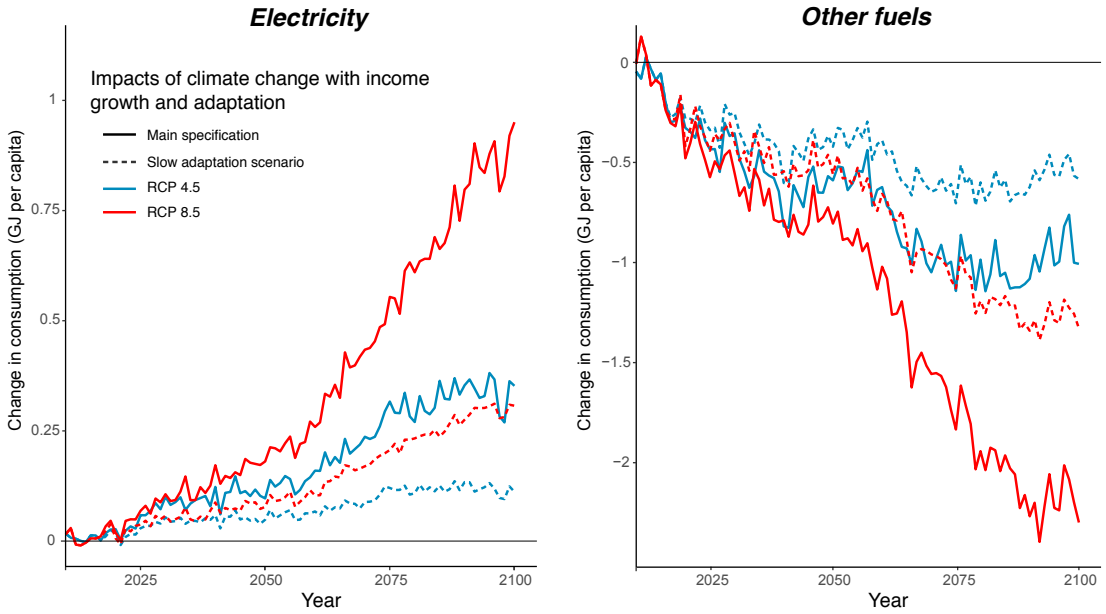

Figure G.2: Projected impacts of climate change under a slow-adaptation scenario. The dashed lines present the time series of average global energy consumption impacts of climate change (in GJ per capita) under a slow-adaptation scenario, where the speed at which energy-temperature responses change with income and climate covariates is reduced by half. To contrast, the solid lines present projected impacts based on the estimates of the main model (Equation B.6). All impacts are calculated under the SSP3 socioeconomic scenario using climate projections from a single climate model (CCSM4).

Section, B.3), due to limited in-sample variation in the average climate. Thus, the decision of how quickly the energy-temperature response evolves with climate in the future is less informed by historical data than is the case for income.

G.3 Data quality

The IEA data on energy consumption are of differential quality across countries as well as years within a country, and issues of quality and comparability are extensively noted in the documentation. All our specifications account for data quality and comparability concerns through inverse variance weighting, imposition of country-regime fixed effects, and dropping observations that fail to meet basic standards of comparability (*Supplementary Sections* A.1 and B.1). To further ensure that data quality issues do not pose a threat to our core findings, here we conduct a robustness check in which we re-estimate Equation B.6 after dropping additional observations in which the energy consumption data is obtained by imputation.[42] If the energy consumption data in such cases are themselves estimated as a function of income and climate variables, it is possible that our results simply reflect this imputation procedure rather than a real causal relationship. Figure G.3 displays the matrices of energy-temperature responses when estimating Equation B.6 including and not including observations with imputed energy consumption data (dark and light response curves respectively).[43] The predicted responses are similar, thus our results do not seem to be an artifact of imputed energy consumption data.

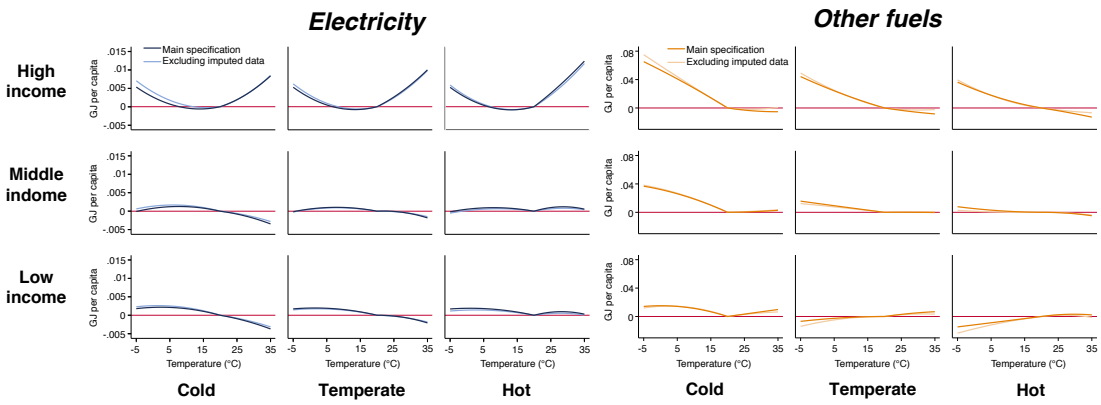

Figure G.3: Energy-temperature response as a function of income and climate: Robustness to imputed data. This figure displays the results from an econometric specification that models heterogeneity in the energy-temperature response due to both income and long-run climate (Equation B.6). The dark response curves are identical to those from Figure 1c (main text), while the light response curves are estimated using a subset of the data in which observations with imputed energy consumption data are dropped. Each cell within a matrix represents predicted energy-temperature responses at a point in the income × long-run climate covariate space within the full sample. Cells are ordered vertically by income terciles (increasing income from bottom to top) and horizontally by terciles of annual cooling degree-days (increasingly warm climate from left to right) (*Supplementary Section* B.3).

[42] The documentation notes instances where the energy consumption data are derived solely from estimates by either the IEA or country government. For electricity consumption 145 additional country-years are dropped, while for other fuels consumption 465 additional country-years are dropped.

[43] The dark curves are identical to those from the matrices in Figure 1c (main text).

H Comparisons to other studies

In this section, we consider prior econometric and process model-based estimates of climate change impacts on energy consumption, and compare them to their nearest counterparts from among our estimates. Although not perfectly comparable in their scope or their intent, we generally find that estimates from prior studies are qualitatively consistent with those from this analysis (Table H.1).

Ref. [33] estimates the effect of temperature on electricity consumption using daily data from European countries, and use these estimates to project the impacts of climate change under one of the 33 climate projections (i.e. GFDL-ESM2M) in our SMME. Their analysis encompasses electricity consumption in all sectors, including transportation (which we exclude).[44] Moreover, they do not account for the effect of income differences or climate-driven adaptation on the electricity-temperature response. Nonetheless, their end-of-century impact projections under RCP8.5 for major European countries are comparable in magnitude and direction to ours (Table H.1A). Ref. [32] similarly estimate the effect of temperature on electricity electricity consumption using daily data from the US, and use these estimates to calculate a mean impact across the across climate projections in the CMIP5 ensemble (*Supplementary Section* A.2.2). While their analysis also includes the transportation sector (which we exclude) and does not account for the effect of income differences or climate-driven adaptation on the electricity-temperature response, their estimates are qualitatively consistent with ours (Table H.1B).

Ref. [31] estimate the effect of temperature on residential electricity consumption using billing data from Mexico, and use the estimates to calculate a mean impact across 25 climate projections.[45] Importantly they account for the effect of income growth and climate-driven adaptation via increased air-conditioning adoption. Although their analysis is limited to the residential sector (excluding commercial, industrial, and agricultural consumption, which we include), their end-of-century impact projections under RCP8.5 for Mexico (in percentage terms) are qualitatively similar to ours (Table H.1C).

Using the NEMS energy model, ref. [18] project the impact of climate change on total energy expenditures in the United States, accounting for the direct effects of warming along with price, supply-side, and macroeconomic feedbacks. Calculating a mean impact across the full set of climate projections in the SMME, they project a 12.1% increase in annual energy expenditures at end-of-century (relative to 2012) due to climate change under RCP8.5, while we project a 4.1% decrease (Table H.1D) under a 0% price growth scenario.[46] However, the two studies have important differences in scope and approach.

[44] As of 2013, transportation accounted for less than 3% of electricity consumption in the EU. See https://www.eea.europa.eu/ds_resolveuid/8d7f4a83fc3a4936be07b8d40c24352c.

[45] These climate projections are drawn from 25 climate models that have partnered with Climate Wizard, an online tool developed by the Nature Conservancy.

[46] Because ref. [18] assume a stationary economy with no population growth, we use our per-capita estimates under a 0% price growth scenario as the point of comparison.

Most fundamentally, the analysis in ref. [18] is limited to the residential and commercial sectors (excluding industrial and agricultural consumption, both of which we include)[47] and also does not account for the effect of income differences or climate-driven adaptation on energy-temperature responses. The exclusion of industrial consumption likely contributes to the positive estimate in ref. [18]. Industrial consumption accounts for approximately half of non-transport end-use energy consumption both in the US and globally.[48] Recent evidence suggests that unlike residential and commercial consumption, industrial electricity consumption does not exhibit responsiveness to temperature,[99] and to our knowledge, no existing study specifically examines industrial end-use consumption of other fuels. Although the energy consumption data used in our analysis lacks consistent sectoral breakdowns across all fuels, countries, and years, future research should examine the effects of temperature on energy consumption by fuel and end-use sector across diverse socioeconomic settings and climate zones.[49]

Ref. [38] use a process model-based approach to project the impact of climate change on global cooling and heating expenditures under the SSP2 socioeconomic scenario. Using one of the 33 climate projections (i.e. CESM1-BGC) in our SMME, they project that at end-of-century, climate change under RCP8.5 will lead to a net increase in global expenditures representing 0.3% of 2100 global GDP (Table H.1E). For the same socioeconomic scenario, climate projection, and RCP, we project a similarly modest change in global expenditures, despite using a purely econometric approach. Although the magnitudes are similar, it should be noted that the two studies do not purport to estimate the same object. While the authors explicitly model changes to cooling and heating demands, our estimates encompass changes from all end uses, not necessarily limited to cooling and heating. Another important distinction is that the estimates in ref. [38] are specific to the endogenously determined price trajectories of the GCAM energy model.

Ref. [99] estimate an electricity consumption damage function for Shanghai, China. To compare our findings, we follow their approach and estimate a similar damage function for Shanghai based on climate projections in the CMIP5 ensemble (*Supplementary Section* A.2.2). In particular, we index the projected percent increase in Shanghai's electricity consumption to the global mean surface temperature increase in each realization, and estimate a linear damage function using pooled realizations from 2080 to 2099 (*Methods Step 4*).[50] Although their analysis is limited to the residential sector (excluding commer-

[47] While NEMS does model industrial energy consumption, it does not model the direct effect of warming on industrial consumption. Thus the impact projections in ref. [18] reflect changes to industrial consumption only via general equilibrium effects arising from climate-driven changes in residential and commercial consumption.

[48] Data available from U.S. EIA *Monthly Energy Review* and IEA *World Energy Balances* dataset.

[49] Ref. [18] does not contain a breakdown by fuel.

[50] Based on the procedure described in *Methods Step 4*, we build such a damage function from estimates of Shanghai's projected increase in electricity consumption (D_{tlps}, denominated as percent of 2015 consumption) in each year (t) using 21 climate models (l), two emissions scenarios (p), and a resampling of estimates (s) that captures uncertainty in the estimation of Equation 3 (*Methods*). The linear damage

cial, industrial, and agricultural consumption, which we include), we obtain qualitatively similar estimates for the percentage increase in Shanghai's consumption per 1°C increase in global mean surface temperature (Table H.1F).

function we estimate through ordinary least squares is: $D(\Delta GMST, t)_{tlps} = \psi_0 + \psi_1 \Delta GMST_{tlp} + \varepsilon_{tlps}$, using all realizations from 2080-2099 as done in ref. [99].

Geography	Study Estimate	Our Estimate
	A. Wenz et al., 2017	
	Change in annual per-capita electricity consumption at end-of-century under RCP8.5, as percent of 2012 consumption.	
France	0.9%	0.8%
Germany	-0.8%	-0.5%
Greece	7.3%	3.5%
Italy	1.3%	1.9%
Spain	5.2%	3.6%
United Kingdom	-1.7%	-0.9%
	Notes: Both estimates are based on climate projections from the GFDL-ESM2M climate model. Wenz et al.'s estimates include electricity consumption in the transportation sector, which we exclude.	
	B. Auffhammer et al., 2017	
	Change in annual electricity consumption at 2090 under RCP8.5, as percent of 2012 consumption.	
United States	7.9%	2.3%
	Notes: Both estimates represent mean impacts across climate projections in the CMIP5 ensemble (*Supplementary Section* A.2.2). Auffhammer et al.'s estimates include electricity consumption in the transportation sector, which we exclude.	
	C. Davis and Gertler, 2015	
	Change in annual electricity consumption at end-of-century under RCP8.5, as percent of 2010 consumption.	
Mexico	83.1%	44.6%
	Notes: Our estimates represent mean impacts across all climate projections in the SMME (*Supplementary Section* A.2.3), while Davis and Gertler's estimates represent mean impacts across 25 climate models that have partnered with Climate Wizard, an online tool developed by the Nature Conservancy. Davis and Gertler's estimates only encompass electricty consumption in the residential sector, whereas ours also include commercial, industrial, and agricultural end-uses.	
	D. Hsiang et al., 2017	
	Change in annual per-capita energy expenditure at 2090 under RCP8.5, as percent of 2012 expenditure.	
United States	12.1%	-4.1%
	Notes: Both estimates represent mean impacts across all climate projections in the SMME (*Supplementary Section* A.2.3). Hsiang et al.'s estimates are for the period 2080-2099 and do not include energy consumption in the industrial sector, which we include. Our estimates determine future expenditures under the 0% price growth scenario, while those of Hsiang et al. use prices determined endogenously through the NEMS (AEO 2013) energy model.	

Continued on next page.

Continued from previous page.

Geography	Study Estimate	Our Estimate
	E. Clarke et al., 2018	
	Change in total annual energy expenditures at end-of-century under RCP8.5 and SSP2 socioeconomic scenario, as percent of 2100 global GDP.	
Global	0.3%	-0.00005%
	Notes: Both estimates are based on climate projections from the CESM1-BGC climate model. Clarke et al.'s estimates explicitly model changes to cooling and heating demands, while our estimates encompass changes from all end uses, not limited to cooling and heating. Our estimates determine future expenditures under the 1.4% price growth scenario, while those of Clarke et al. use prices determined endogenously through the GCAM energy model.	
	F. Li et al., 2019	
	Change in annual electricity consumption at end-of-century per 1°C increase in global mean surface temperature, as percent of 2015 consumption.	
Shanghai, China	9.2%	12.8%
	Notes: Both estimates are based on climate projections in the CMIP5 ensemble (*Supplementary Section* A.2.2). In both studies, the projected percent increase in Shanghai's electricity consumption is indexed to the global mean surface temperature increase in each realization, and a linear damage function is estimated pooling realizations from 2080 to 2099 (*Methods Step 4*). Li et al.'s estimates only encompass electricty consumption in the residential sector, whereas ours also include commercial, industrial, and agricultural end-uses.	

Table H.1: Comparison of our climate change impact projections with those of other studies. This table compares our projected impacts of climate change on energy consumption (right column) with those of previous studies that focus on specific geographical regions and fuels (middle column). Our projected impacts are derived from the main model (Equation B.6). Caveats to comparability are noted below each study comparison.

I Comparison to regional estimates from the FUND integrated assessment model

Figure I.1 compares our estimates of energy expenditure damages at 2099 with those of the FUND integrated assessment model for each of the 16 world regions defined by FUND. For each region, we display our damage estimates reflecting income growth and adaptation (Equation 4 in *Methods*, Figure 3a), income growth but not adaptation[51], and neither income growth nor adaptation (Equation 5 in *Methods*). In all cases, we aggregate damages over all impact regions within the FUND region. For most regions, the magnitude and direction of FUND's damage estimates contrast starkly with ours, regardless of how we model the consequences of income growth and adaptation on the energy-temperature response.[52] In particular, FUND projects dramatically larger increases in energy consumption due to climate change across many middle and low income regions, such as China, North Africa, Southeast Asia and Sub-Saharan Africa. These contrasts are consistent with concerns regarding FUND's limited empirical basis for calibration — e.g. FUND's parameters for the income elasticity of cooling and heating energy demand are calibrated using data from a single wealthy country — the UK.[100–103] We estimate that replacing FUND's energy expenditure damage function with those estimated here (Figure 3c-d), while retaining all other features of FUND's climate and economic modeling, dramatically reduces FUND's partial SCC estimate from \$10 to -\$0.20 per ton of CO_2 (high emissions scenario, 3% discount rate).

When contrasting our estimates with those FUND, it is also important to note a conceptual difference in the objects calculated by models such as FUND versus those derived from reduced-form econometric estimates. While FUND specifically models the impact of climate change on cooling and heating energy demand, our econometric estimates capture a total behavioral response of end-use energy consumption to climate change, including not only heating and cooling channels but also, for instance, changes to consumption due to climate-driven changes in economic output.[27] Future research should further explore the specific channels through which energy consumption patterns are altered under a changing climate.

[51] The impact projection in this case reflects the effect of income growth on the temperature sensitivity of energy consumption, but not the effect of climate adaptation. Formally, the calculation is $\widehat{f}_c(\widetilde{\boldsymbol{T}}_{rjt} \mid \overline{LogGDPPC}_{jt}, \overline{CDD}_{rjt_0}, \overline{HDD}_{rjt_0}) - \widehat{f}_c(\widetilde{\boldsymbol{T}}_{rjt_0} \mid \overline{LogGDPPC}_{jt}, \overline{CDD}_{rjt_0}, \overline{HDD}_{rjt_0})$.

[52] Although Figure I.1 displays our estimates of energy expenditure damages under a 1.4% annual price growth scenario, Extended Data Figure 5 and Table 1 indicate that the overall discrepancy between our results and those of FUND would be significantly larger under most other price growth scenarios.

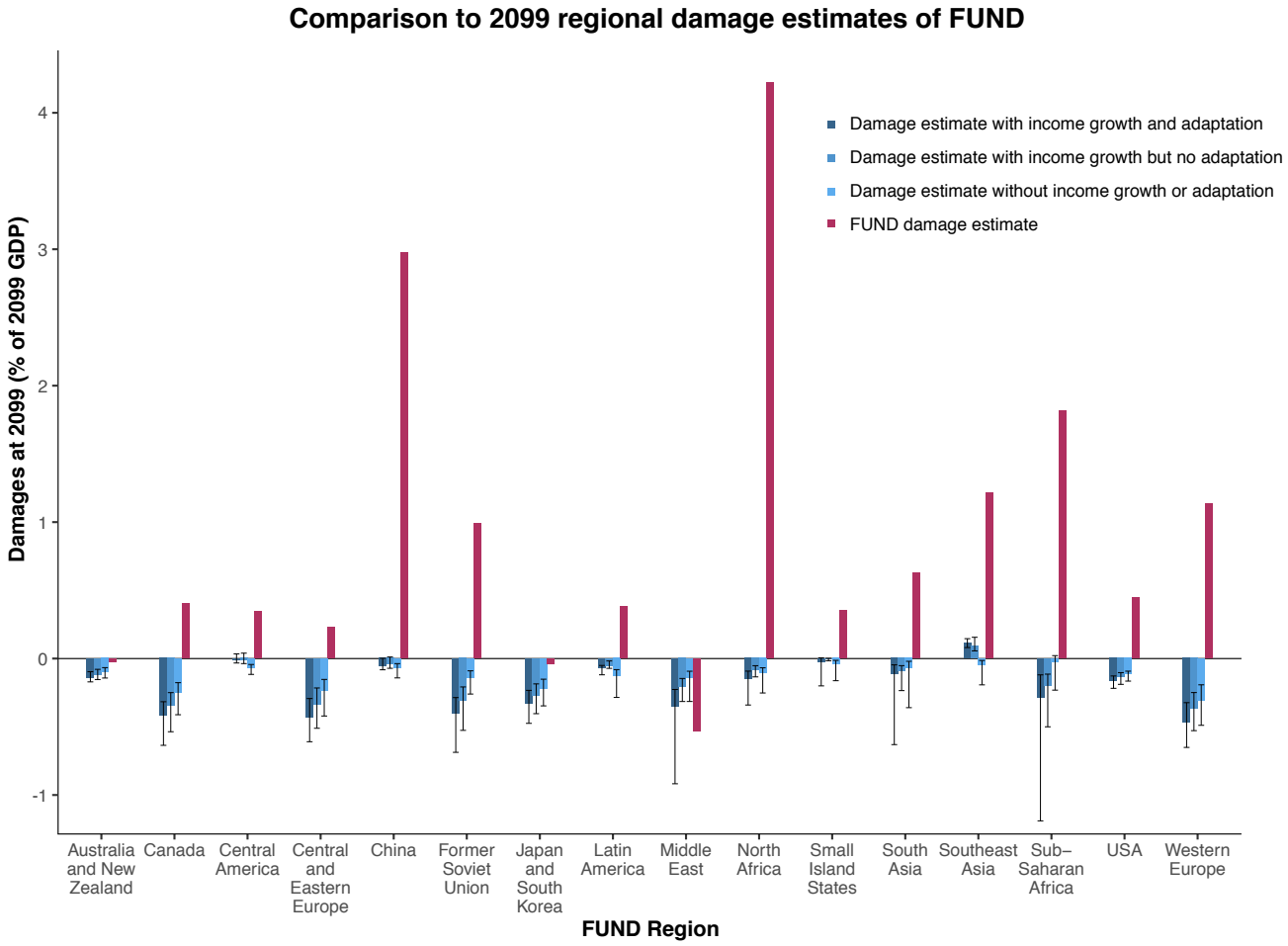

Figure I.1: Comparison to regional estimates from FUND. Figure I.1 compares our energy expenditure damage estimates at 2099 under a high emissions scenario (RCP8.5), the SSP3 socioeconomic scenario, and the 1.4% annual price growth scenario to those of FUND under its "business-as-usual" scenario, for each of the 16 world regions defined by FUND. Damages are expressed as a fraction of 2099 regional GDP. We depict our main estimates reflecting income growth and adaptation (leftmost bar per region), income growth but no climate adaptation (second bar from left), and no income growth or climate adaptation (third bar from left), all of which represent an aggregation of damages across impact regions within a FUND region and a mean across 33 climate models and model surrogates. Intervals indicate 5^{th}-95^{th} percentiles of projected distributions, accounting for climate model and econometric uncertainty (*Supplementary Section* B.5).